A Theoretical Study on the Marangoni Instability

Toshio FUNADA

October, 1989

Wakayama National College of Technology

A Theoretical Study on the Marangoni Instability

Contents

Main parts of the present thesis are based upon the following papers.

Chapter 2:

T. Funada: Marangoni Instability of Thin Liquid Sheet.
J. Phys. Soc. Jpn. 55 (1986) pp. 2191-2202.

Chapter 3:

T. Funada and M. Kotani: A Numerical Study of Nonlinear Diffusion Equation Governing Surface Deformation in the Marangoni Convection.
J. Phys. Soc. Jpn. 55 (1986) pp. 3857-3862.

T. Funada: Nonlinear Surface Waves Driven by the Marangoni Instability in a Heat Transfer System.
J. Phys. Soc. Jpn. 56 (1987) pp. 2031-2038.

Chapter 4:

M. Sakata and T. Funada: Effects of the Surface Deformation on Marangoni Instability in Chemical Reaction.
J. Phys. Soc. Jpn. 50 (1981) pp. 696-702.

T. Funada and M. Sakata: Marangoni Instability Due to Chemical Absorption with an Irreversible Reaction.
J. Phys. Soc. Jpn. 57 (1988) pp. 476-489.

Abstract

Since the 1970's, much interest has grown up in the Marangoni effect, because it may cause fluid-flows even in a weak gravity field, such as in a space laboratory. To understand micro-scale mechanisms for which capillary effects become important is now required to develop new engineering devices and applications. In this sense, the phenomena due to the Marangoni effect and the relating mechanisms propose new subjects which are to be significant in science and engineering. Since the 19-th century when the Marangoni effect was recognized correctly as the surface tension gradient, many investigations have been made extensively. However, this effect still yields formidable problems in carrying out experiments and analysis to clarify its mechanism and to develop its applications. In the present thesis, a theoretical approach to the Marangoni effect is made from the standpoint of fluid mechanics. Rather elementary but fundamental problems of the Marangoni instability, in which effects of free surface deformations play an important role, are discussed here. Prior to the main parts of the thesis, the investigations made so far on the Marangoni effect are reviewed briefly in Chapter 1. The main parts consist of the following three chapters:

Chapter 2. Marangoni instability of thin liquid sheet

The Marangoni instability of a thin liquid sheet driven by

the surface tension gradient (due to variations of temperature or of concentration) is studied by means of a linear theory. It is found that the critical Marangoni number for the steady mode can be expressed as a simple function of the wavenumber when two boundaries of the sheet are flat. When the surface deformations are taken into account, another type of instability may occur at small wavenumbers for small values of the Biot number. An effect of deviation of the surface tension coefficient from the mean value at the free surfaces and the resulting surface pattern at small wavenumbers are also discussed. Furthermore, an eigenvalue relation for the unsteady mode is examined in comparison with that for the steady mode.

Chapter 3. Nonlinear surface waves driven by the Marangoni instability in a heat transfer system

Nonlinear surface waves of long wavelength driven by the Marangoni instability are investigated theoretically for a heat transfer system, in which temperature of a thin liquid layer causes variations of the surface tension coefficient. For two examples considered there, the surface waves are governed, respectively, by a nonlinear evolution equation of diffusion type and the Kuramoto-Sivashinsky equation. It is shown for the first example that the steady solution, which is expressed by the cnoidal function, can be realized if a condition prescribed by values of parameters involved is satisfied at an initial instant. This result is confirmed by solving the initial value problem

numerically, where damping and explosive types of solutions are also obtained. For the second example, it is shown that the surface waves include two types of shock wave solutions.

Chapter 4. Marangoni instability due to chemical absorption with an irreversible reaction

The Marangoni instability due to a chemical absorption is studied theoretically by taking into account the mass transfer of gas, solute and product resulting from an irreversible reaction. It is found that the critical Marangoni number for an inactive product and the corresponding critical wavenumber change in a complicated manner depending on various parameters involved. Furthermore, it is found that an active solute also leads to the Marangoni instability, where roles of the gas are discussed as well. The Marangoni effect due to the product and that due to the solute are coupled so as to reinforce each other. Effects of the surface deformation give rise to another type of instability in the limit of zero wavenumber.

Chapter 1. Historical Review on the Marangoni Instability

§ 1. Earlier Work on the Marangoni Effect

Surface tension gradient along an interface of fluids is now called the Marangoni effect after Carlo Marangoni who first proposed a clear model for such surface phenomena. For this Marangoni effect, we can trace a long history of investigations: Heyde (1686)[1] observed fragments of camphor moving on the surface of olive oil; Romieu (1748)[1] observed the same motion of camphor on the surface of water; Carradori (1794)[1] observed that reaction of camphor particles against the spreading force of a camphor film causes the particles to dance, whereas if a camphor particle is held still, the underlying fluid can be visibly set into motion. Thomson (1855),[1,2] who observed that the surface tension is not the same in different liquids, made the first correct explanation for evaporative convections such as the well-known tears of strong wine and the spreading of a drop of alcohol on the surface of water: he rightly inferred that the surface tension gradient does occur in such a way that one portion of high tension (more watery one) attracts another portion of low tension (more alcoholic one). Marangoni (1871),[1-3] who was aware of Carradori's work but not of Thomson's, formulated a rather complete theory for flows driven by the surface tension gradient due to variations of temperature and of composition. Associated with the Marangoni effect, other surface mechanisms were found in the

experiments made by Plateau (1869);[1] he noted first the surface viscosity and elasticity peculiar to liquids, which arise as the resistance of fluid against deformation. From the work of Plateau, Marangoni (1872)[1] recognized the role of surface contamination, then Gibbs (1878)[1] studied it more precisely; hence the name "Plateau-Marangoni-Gibbs effect" was also introduced: it causes tangential stress along interfaces of liquids. Further details of early work and the subsequent development in the study of the surface phenomena were cited extensively in a review "The Marangoni effects" by Scriven and Sternling (1960),[4] in which we can find various relevant phenomena, such as emulsions in liquids, flows in crystal growth, liquid-liquid extractions, motion of protoplasm, transport of bacteria, surface fractionation, absorption and distillation, foam stability, surface engine, and others. We should also refer to a review "Evaporative convection" by Berg, Acrivos and Boudart (1966).[5] The remarkable investigations on the interface mechanisms were then made by Oldroyd (1955),[6] Scriven (1960),[7] and others, in which the surface viscosity and the surface dilational viscosity (called the Gibbs effect) are discussed as well: for Newtonian surface fluids, refer to the theory by Scriven.

At the opening of this century, Bénard (1900, 1901)[2,8] observed the hexagonal cell pattern of convections in a horizontal spermaceti layer, which was of thickness 0.5-1 [mm] and was vertically bounded below by a heated metal plate and above by a free surface. Rayleigh (1916)[9] considered that the convections were

caused by buoyancy. He showed, using linear stability theory, that for a horizontal fluid layer with two free boundaries, a quiescent state of the layer becomes unstable and cellular convections can occur if the Rayleigh number (i.e., the temperature difference imposed on the layer) exceeds a critical value, at which the corresponding critical wavenumber gives the cell size; the qualitative agreement in the cell size between his results and Bénard's experiments stimulated further to investigate the buoyancy-driven instability (refer to Chandrasekhar (1961)[10]). Block (1956)[11] found, however, that such hexagonal cell pattern occurs actually when a liquid layer is very shallow and even when it is cooled from below, and that the cells disappear when the free surface is covered by an insoluble monolayer. Pearson (1958)[12] showed theoretically that the surface tension gradient due to variations of temperature or of concentration (the Marangoni effect) can be responsible for convections in a liquid layer with a free surface: two typical cases considered for the lower boundary of the layer are that the heat flux is prescribed by (I) conducting (isothermal) condition and by (II) insulating condition. The results in the case (I) revealed that the convections observed by Bénard were certainly due to the surface tension gradient rather than due to the buoyancy, because the Marangoni number estimated from Bénard's data was larger than the critical (though the Rayleigh number estimated was less than the critical) and that the cell size gave the critical wavenumber predicted. On the basis of Pearson's model, Scriven and Sternling (1964)[13]

studied effects of the surface deformation on the steady Marangoni convections. They showed that an upflow occurs beneath the depression of the free surface and a downflow occurs beneath the elevation: this flow pattern is just the same as that found by Bénard in his experiments, but is converse to that in buoyancy-driven convections shown by Jeffreys (1951).[14] To clarify what sort of cellular pattern was preferred in the Marangoni convections observed, Scanlon and Segel (1967)[15] made a nonlinear analysis for a fluid layer with semi-infinite depth. They showed for the case of infinite Prandtl number that hexagonal cells are stable for a range of Marangoni number from just below the critical to 64 times the critical; for the larger Marangoni number (up to 196 times the critical), roll cells, as well as the hexagons, become stable.

On the other hand, to explain the origin of interfacial turbulence and of spontaneous agitation arising at fluid interfaces, Sternling and Scriven (1959)[16] studied the Marangoni instability due to mass transfer. They adopted as a typical model two immiscible liquid layers with semi-infinite depth, at the interface of which both the surface shear and dilational viscosities were also taken into account. Their results contain various factors pertaining to instability, such as the viscosities of bulk fluids, the diffusivities of compositions and the direction of the mass transfer across the interface: one of the most typical results is the oscillatory Marangoni instability due to the surface viscosities (for details, see their paper). Then, extending the model

of Sternling and Scriven, Ruckenstein and Berbente (1964)[17] showed that a chemical reaction, even if small amount, affects the stability condition in a very different manner as compared with the instability in physical mass transfer. Brian, Vivian and Matiatos (1967)[18] found experimentally that the rate of mass transfer increases over the values estimated by penetration theories and is much activated by the Marangoni convections due to chemical reactions. Although there exist many investigations made later for mass transfer systems, the details are omitted here, because very complicated mechanisms of instability arise at the gas-liquid interface and at the liquid-liquid interface respectively, where other effects may also be concerned (for effects of electric force, see a review by Melcher and Taylor (1969)[19]). In this respect, Sherwood, Pigford and Wilke (1975)[20] suggested in their textbook that 'a great deal needs to be done before interfacial turbulence becomes well understood and the theory developed to the point where it is useful in engineering design.'

§ 2. Recent Development in the Study on the Marangoni Convection for Heat Transfer Systems

Following the eminent work noted above, more realistic theoretical models based on actual phenomena have been proposed actively, and well-controlled experiments have been made to obtain the data of high accuracy. In this connection, we should note that the Rayleigh-Bénard convections have also been studied ex-

tensively (both theoretically and experimentally), which has much stimulated the study of Marangoni convections. To review the recent development briefly, we focus our attention mainly to the Marangoni convection due to variations of temperature.

Since gravity of the earth may affect the convections observed in the usual experiments, Nield (1964)[21] took into account both the Marangoni effect and the buoyancy for the stability of a horizontal fluid layer. He showed that the two agencies causing instability reinforce each other and are tightly coupled so as to make the cell size approximately the same as the one observed by experiments. Smith (1966)[22] studied the Marangoni instability for two immiscible horizontal fluid layers with finite depth whose interface is deformable; he showed that the depth ratio affects the onset of convection and the resulting flow pattern, where the gravity waves have a stabilizing effect on the convection when the gravity acts downward. Koschmieder (1967)[23] made experiments for a shallow layer of silicone oil on a circular plate heated from below, in which concentric circular rolls appeared and then broke into hexagonal cells; this tendency was found rather clearly when the layer was contiguous above to an air layer, which showed qualitative agreement with the results by Nield. Taking similar apparatus to that used by Koschmieder, Hoard, Robertson and Acrivos (1970)[24] found that the cell pattern in a layer of silicone oil was concentric circular rolls when the layer was covered by a glass lid, while hexagons when it was in contact with a thin air layer; moreover, for Aroclor of

much variable viscosity, both the patterns of regular hexagons and of rolls were found for the free and rigid upper conditions: note that the experiments were made with taking account of the theoretical results for buoyancy-driven convections by Palm (1960),[25] Schlüter, Lortz and Busse (1965),[26] Busse (1967),[27] and Krishnamurti (1968).[28] Furthermore, Palmer and Berg (1971)[29] made experiments for a layer of silicone oil heated from below and bounded above by a very thin air layer, and they found that the data obtained gave excellent agreement with Nield's prediction: this appears to be the first quantitative confirmation of the results from the linear stability theory for the convections due to the Marangoni effect. Then, Kayser and Berg (1973)[30] studied free surface deformations accompanying convections in shallow liquid pools heated from below by a straight nichrome wire: their experiments demonstrated that as thickness of the layer increases, the surface pattern transition can occur from the pattern shown by Scriven and Sternling (1964)[13] to that shown by Jeffreys (1951).[14] This transition was also confirmed by their numerical simulation. In addition to the results for heat transfer systems, we should pay attention to results obtained for mass transfer systems. Berg and Acrivos (1965)[31] extended Pearson's analysis to consider effects of insoluble surfactants, and they predicted that even trace amounts of such materials would exert an extreme stabilizing influence on the system. Palmer and Berg (1972)[32] took into account the contamination of surfactant solutions for Nield's model, the roles

of which in stabilizing convections were found to be in qualitative agreement with the experimental results due to Palmer and Berg (1973).[33]

In the 1970's, much attention arose in the Marangoni effect, since low-gravity environments were realized in spacecrafts. The dramatic experiments for the onset of convections were made in Apollo 14 where the acceleration due to gravity was evaluated as 10^{-6}g (see the report by Grodzka and Bannister (1972)[34]). It was confirmed that the surface tension gradient alone can drive cellular convections of visible magnitude. The convections observed were affected, however, by the radial thermal conduction which occurred along the bottom plate and in the sidewall of the circular container. Subsequently, with a more improved apparatus, the experiments were made in a weaker gravity field of 10^{-8}g in Apollo 17, so that the polygonal cells were surely observed and that their size was found to be just the one predicted by Pearson's theory (see Grodzka and Bannister (1975)[35]). These results much excited the investigations on the Marangoni convection, and they now seem to propose new subjects: evidently, one of them is what occurs in low-gravity environments such as the human has not recognized so far, in which there may arise fascinating topics for science and engineering. On the other hand, recent subjects in engineering are micro-scale mechanisms for which capillary effects become dominant, and they have to be understood to achieve various applications: one of the typical examples is crystal growth to make up electronic large-scale-

integrated-circuits. Therefore, it seems that the Marangoni effect and the relating mechanisms give new subjects with fruitful future.

There exist, however, many formidable problems for the Marangoni effect, pertaining to the very complicated surface mechanisms and to the method of analytical approach. Here we consider some of them. In the case of Marangoni convections, the stability problem is not self-adjoint and that the Marangoni number as an eigenvalue is contained in the boundary conditions at interfaces of fluids. Thus, it is not obvious whether the principle of the exchange of stabilities may be applied or not. Scriven and Sternling (1964)[13] showed that an oscillatory Marangoni instability may occur due to the surface viscosity. Vidal and Acrivos (1966)[36] found numerically that for Pearson's model of case (I), the neutral state of Marangoni convections is stationary rather than oscillatory. Similar results were found by Takashima (1970)[37] for Rayleigh-Marangoni convections. McConaghy and Finlayson (1969)[38] found that an oscillatory Marangoni instability may occur in a rotating fluid layer. Takashima (1981)[39] showed numerically that the Marangoni number for the oscillatory mode becomes negative values of large magnitude. Sakata and Funada (1981)[40] found numerically that for a chemical absorption system, an oscillatory Marangoni instability may occur if the frequency is very large, which leads to negative critical Marangoni numbers of large magnitude. McTaggart (1983)[41] showed that an oscillatory Marangoni in-

stability may occur under the condition such that the thermal Marangoni number is positive and that the solutal Marangoni number is negative: this is a new type of instability which may stem from combined Marangoni effects.

Because of the difficulties mentioned above, problems of nonlinear Marangoni convections have been solved only for a few cases. Kraska and Sani (1979)[42] analyzed numerically the Rayleigh-Marangoni convection for a horizontal layer of Newtonian fluid of infinite horizontal extent resting on a heated, rigid surface of high thermal conductivity, where a free surface deformation was also taken into account. The phase diagram for the cell pattern transition was obtained for six disturbances of the same critical wavenumber, for which the important results are as follows: the range of the Marangoni number where hexagonal cells become stable is rather narrow as against that obtained by Scanlon and Segel; this tendency becomes remarkable as effects of the surface deformation dominate. Rosenblat, Davis and Homsy (1982)[43] studied the Rayleigh-Marangoni convections in cylindrical containers, using stress-free conditions at the cylindrical wall. Sivashinsky (1982)[44] showed for Pearson's model of case (II) (in which the critical Marangoni number is given as 48 in the limit of zero wavenumber) that finite amplitude of convections with large cells are governed by a nonlinear diffusion equation, and he discussed it in comparison with the Kuramoto-Sivashinsky equation that has chaotic solutions. Cloot and Lebon (1984)[45] made a nonlinear analysis for the Rayleigh-Marangoni

convection, and showed supercritical and subcritical zones of instability where hexagonal cells are allowable. Riahi (1987)[46] also found for the Rayleigh-Marangoni convection that hexagonal cells are preferred. Now, for the results cited above, the confirmation by experiments is eagerly expected. Since the 1970's, various aspects of Marangoni convections have been studied, which we can find in the proceedings edited by Sørensen (1979),[47] in the textbook "Low-Gravity Fluid Dynamics" by Myshkis et al. (1987),[48] and in a recent review due to Davis (1987).[49]

References

1) cited in L. E. Scriven and C. V. Sternling: Nature 187 (1960) 186.

2) cited in J. C. Berg, A. Acrivos and M. Boudart: Adv. Chem. Engng. 6 (1966) 61.

3) cited in C. Tomlinson: Phil. Mag. 27 (1864) 528, Phil. Mag. 38 (1869) 409.

4) L. E. Scriven and C. V. Sternling: Nature 187 (1960) 186.

5) J. C. Berg, A. Acrivos and M. Boudart: Adv. Chem. Engng. 6 (1966) 61.

6) J. G. Oldroyd: Proc. Roy. Soc. A, 232 (1955) 567.

7) L. E. Scriven: Chem. Engng. Sci. 12 (1960) 98.

8) cited in S. Chandrasekhar: Hydrodynamic and Hydromagnetic Stability (Oxford Univ. Press, 1961).

9) Lord Rayleigh : Phil. Mag. 32 (1916) 529.

10) S. Chandrasekhar: Hydrodynamic and Hydromagnetic Stability (Oxford Univ. Press, 1961).

11) M. J. Block: Nature 178 (1956) 650.

12) J. R. A. Pearson: J. Fluid Mech. 4 (1958) 489.

13) L. E. Scriven and C. V. Sternling: J. Fluid Mech. 19 (1964) 321.

14) H. Jeffreys: Quart. J. Mech. 4 (1951) 283.

15) J. W. Scanlon and L. A. Segel: J. Fluid Mech. 30 (1967) 149.

16) C. V. Sternling and L. E. Scriven: AIChE J. 5 (1959) 514.

17) E. Ruckenstein and C. Berbente: Chem. Engng. Sci. 19 (1964) 329.

18) P. L. T. Brian, J. E. Vivian and D. C. Matiatos: AIChE J. 13 (1967) 28.

19) J. R. Melcher and G. I. Taylor: Ann. Rev. Fluid Mech. 1 (1969) 111.

20) T. K. Sherwood, R. L. Pigford and C. R. Wilke: Mass Transfer (McGraw-Hill, 1975)

21) D. A. Nield: J. Fluid Mech. 19 (1964) 341.

22) K. A. Smith: J. Fluid Mech. 24 (1966) 401.

23) E. L. Koschmieder: J. Fluid Mech. 30 (1967) 9.

24) C. Q. Hoard, C. R. Robertson and A. Acrivos: Int. J. Heat Mass Transfer 13 (1970) 849.

25) E. Palm: J. Fluid Mech. 8 (1960) 183.

26) A. Schlüter, D. Lortz and F. H. Busse: J. Fluid Mech. 23 (1965) 129.

27) F. H. Busse: J. Fluid Mech. 30 (1967) 625.

28) R. Krishnamurti: J. Fluid Mech. 33 (1968) 445, 457.

29) H. J. Palmer and J. C. Berg: J. Fluid Mech. 47 (1971) 779.

30) W. V. Kayser and J. C. Berg: J. Fluid Mech. 57 (1973) 739.

31) J. C. Berg and A. Acrivos: Chem. Engng. Sci. 20 (1965) 737.

32) H. J. Palmer and J. C. Berg: J. Fluid Mech. 51 (1972) 385.

33) H. J. Palmer and J. C. Berg: AIChE J. 19 (1973) 1082.

34) P. G. Grodzka and T. C. Bannister: Science 176 (1972) 506.

35) P. G. Grodzka and T. C. Bannister: Science 187 (1975) 165.

36) A. Vidal and A. Acrivos: Phys. Fluids 9 (1966) 615.

37) M. Takashima: J. Phys. Soc. Jpn. 28 (1970) 810.

38) G. A. McConaghy and B. A. Finlayson: J. Fluid Mech. 39 (1969) 49.

39) M. Takashima: J. Phys. Soc. Jpn. 50 (1981) 2745, 2751.

40) M. Sakata and T. Funada: Memoirs of the Wakayama Technical College (1981) Vol. 16, 17 [in Japanese].

41) C. L. McTaggart: J. Fluid Mech. 134 (1983) 301.

42) J. R. Kraska and R. L. Sani: Int. J. Heat Mass Transfer 22 (1979) 535.

43) S. Rosenblat, S. H. Davis and G. M. Homsy: J. Fluid Mech. 120 (1982) 91.

44) G. I. Sivashinsky: Physica 4D (1982) 227.

45) A. Cloot and G. Lebon: J. Fluid Mech. 145 (1984) 447.

46) N. Riahi: J. Phys. Soc. Jpn. 56 (1987) 3515.

47) T. S. Sørensen, ed.: Dynamics and Instability of Fluid Interfaces (Springer-Verlag, 1979).

48) A. D. Myshkis, V. G. Babskii, N. D. Kopachevskii, L. A. Slobozhanin and A. D. Tyuptsov: Low-Gravity Fluid Mechanics (Springer-Verlag, 1987).

49) S. H. Davis: Ann. Rev. Fluid Mech. 19 (1987) 403.

Chapter 2. Marangoni Instability of Thin Liquid Sheet

§ 1. Introduction

Since the remarkable investigations made by Pearson[1] and by Sternling and Scriven,[2] much attention has been paid to the Marangoni instability, which is reviewed extensively in refs. 3 and 4. Quite recently, a growing interest has arisen in the Marangoni effect as a possible mechanism to drive a flow even in a weak gravitational field, such as in a space laboratory.[5] From a practical point of view, especially in chemical engineering, the typical configurations treated so far are classified into two types: one is a liquid layer between a gas phase and a solid wall and the other two immiscible liquid layers between two solid walls. The surface tension gradient may occur at the gas-liquid interface for the former, while at the liquid-liquid interface for the latter. When a surface deformation does exist, not only the surface tension gradient but also the surface tension itself may have a significant effect on the Marangoni convection.[6] There seems to be, however, no detailed investigations on the stability problem of a liquid sheet between two gas phases, which is rather a prototype of the Marangoni effect in the sense that Carlo Marangoni studied the effect on a soap bubble in the 19-th century. This is the subject of this chapter.

Here we consider the linear stability of a thin liquid sheet sandwiched in between two still gas phases. We assume that heat

and mass transfers arise in the sheet due to convection and diffusion and that they are prescribed at the two free surfaces by the conditions of the type of Newton's cooling law. Thus the Marangoni effect due to variations of temperature and/or of concentration may act on each free surface. This effect is concerned with so many factors derived from the material property at the free surface[7,8] that various effects may appear in a very thin surface layer. The attention in this chapter, however, is confined to the simplest case, in which only the momentum flux of viscous liquid, the surface tension and its variation are taken into account at each free surface. The effects of temperature and of concentration can be treated in a very similar manner, thus we consider both along with. Since the surface tension gradient may act on a free surface even when it is flat, the problem for both flat free surfaces is most elementary, which is called here Case(i). The problem is then extended for Case(ii) so as to include effects of the surface deformations, for which we adopt a mean value of the surface tension coefficient at the two surfaces. Formulation of the problem for Cases(i) and (ii) is made in §2, where an eigenvalue relation is derived for parameters involved, and then results for the steady mode are discussed in §3. In §4, a deviation of the surface tension coefficient from the mean value is taken into account, which is referred to as Case(iii). For Cases(ii) and (iii), a surface pattern resulting from the surface deformations and an induced flow in the limit of small wavenumbers are examined in §5.

Furthermore, a temporal evolution of disturbances in the vicinity of the steady disturbed state for Cases(i) and (ii) is examined in Appendix.

§ 2. Formulation of the Problem

Suppose a viscous liquid sheet with thickness 2d, which is sandwiched in between two still gas phases. Let us take a system of Cartesian coordinates with the y-axis in the direction of thickness and the x- and z-axes in the center plane of the sheet. We thus label one gas phase at the upper side of the sheet (y>d) as 'I' and the other at the lower side (y<-d) as 'II'. Basic equations for this sheet consist of the equation of continuity, the equation of motion and the convection-diffusion equation for temperature or concentration:[1)]

$$\nabla \cdot \mathbf{v} = 0, \tag{2.1}$$

$$\frac{\partial \mathbf{v}}{\partial t} + (\mathbf{v}\cdot\nabla)\mathbf{v} = -\frac{1}{\rho}\nabla p + \nu \nabla^2 \mathbf{v}, \tag{2.2}$$

$$\frac{\partial X}{\partial t} + (\mathbf{v}\cdot\nabla)X = D\nabla^2 X, \tag{2.3}$$

where $\mathbf{v}=(u,v,w)$ is the velocity, p is the pressure, X stands for the temperature T or the concentration C, $\nabla \equiv (\partial/\partial x, \partial/\partial y, \partial/\partial z)$, and t is the time. To simplify the analysis, the density ρ, the viscosity μ ($\equiv \rho\nu$) and the thermometric conductivity ($D=D_T$) or the diffusivity ($D=D_C$) are taken to be constant.

Let us consider an undisturbed rest state with flat free

surfaces at $y=\pm d$. Equations (2.1) and (2.2) have equilibrium solutions given by $v=0$ and $p=$constant. When the temperature of the gas phase I is different from that of II or when the mass transfer occurs across the free surfaces, the temperature or the concentration has an equilibrium distribution $X\equiv\bar{X}(y)$ in the sheet. It is assumed here that $\bar{X}(y)$ is prescribed by boundary conditions of the type of Newton's cooling law:

$$\frac{d\bar{X}}{dy} = -\Gamma_I(\bar{X} - X_I) \qquad \text{at } y=d, \qquad (2.4a)$$

$$\frac{d\bar{X}}{dy} = \Gamma_{II}(\bar{X} - X_{II}) \qquad \text{at } y=-d, \qquad (2.4b)$$

where Γ_I is the transfer coefficient across the upper surface and X_I is the value of X in the gas phase I at a point far from the sheet, while for the lower surface, Γ_{II} and X_{II} are defined likewise. It is also assumed that the difference between Γ_I and Γ_{II} is sufficiently small, so that the transfer coefficients are set as $\Gamma_I=\Gamma_{II}\equiv\Gamma$, say. We thus obtain the following solution $\bar{X}(y)$ from (2.3) and (2.4):

$$\bar{X}(y) = ay + b, \qquad (2.5)$$

where

$$a = \frac{\Gamma}{1+\Gamma d}\,\frac{X_I - X_{II}}{2}, \qquad b = \frac{X_I + X_{II}}{2}. \qquad (2.6a,b)$$

Here we should note that if Γ is zero, a disappears, giving rise to a uniform distribution of $\bar{X}(y)$.

Upon this equilibrium state, small disturbances which are denoted with prime are superimposed. The disturbances of tem-

perature or of concentration may cause variations of the surface tension coefficient. When the surface deformations h'_I and h'_{II} are taken into account, the surface tension itself may also act on each surface. In view of these effects on the surfaces, we consider the case for which the surface tension coefficients σ_I (at the upper deformed surface given by $y=d+h'_I$) and σ_{II} (at the lower deformed surface given by $y=-d+h'_{II}$) are expressed as

$$\sigma_I = \sigma(b) + \beta ad + \beta(X' + ah'_I), \tag{2.7}$$

$$\sigma_{II} = \sigma(b) - \beta ad + \beta(X' + ah'_{II}), \tag{2.8}$$

where $\sigma(b)$ denotes their mean value in the undisturbed state, and β ($\equiv \partial\sigma/\partial X$) is taken as a constant; βad stands for the deviation due to the distribution of $\bar{X}(y)$, and $\beta ah'_I$ and $\beta ah'_{II}$ are the variations of $\bar{X}(y)$ caused by the surface deformations. For small disturbances, the surface tension is estimated by the first two terms in the right-hand-side of (2.7) and by those of (2.8), while it may be estimated approximately by $\sigma(b)$ if the deviation is small (either a in (2.6a) is very small, or the sheet is sufficiently thin). According to (2.7) and (2.8), on the other hand, the surface tension gradient at each surface is expressed as

$$\nabla_I \sigma_I = \beta \nabla_I (X' + ah'_I) \qquad \text{at } y=d+h'_I, \tag{2.9a}$$

$$\nabla_{II} \sigma_{II} = \beta \nabla_{II} (X' + ah'_{II}) \qquad \text{at } y=-d+h'_{II}, \tag{2.9b}$$

where ∇_I and ∇_{II} stand for the gradient operators taken along the respective deformed surfaces. Because of the disturbance X'

in (2.9a,b), the surface tension gradient can act on both of the surfaces even if they are flat. Thus, we classify the problem into the following three cases: in Case(i) both the surfaces are flat, in Case(ii) the surface deformations exist and the surface tension coefficients are estimated under the condition $|\beta a d| \ll \sigma$ (b), and in Case(iii) the surface deformations exist and the surface tension coefficients are given by (2.7) and (2.8). In this section, we formulate the problem for Cases(i) and (ii), while the complicated general Case(iii) will be considered in § 4.

From (2.1)-(2.3), the linearized equations for the disturbances are now given as

$$\nabla \cdot \mathbf{v}' = 0, \tag{2.10}$$

$$\frac{\partial \mathbf{v}'}{\partial t} = -\frac{1}{\rho}\nabla p' + \nu \nabla^2 \mathbf{v}', \tag{2.11}$$

$$\frac{\partial X'}{\partial t} + a v' = D \nabla^2 X'. \tag{2.12}$$

The boundary conditions at each surface consist of the kinematic condition, the tangential stress balance, the normal stress balance and the condition of the type of Newton's cooling law: they are expressed, at the upper surface (y=d), as

$$\frac{\partial h'_I}{\partial t} = v', \tag{2.13}$$

$$\mu \left(\frac{\partial v'}{\partial x} + \frac{\partial u'}{\partial y} \right) = \beta \left(\frac{\partial X'}{\partial x} + a \frac{\partial h'_I}{\partial x} \right), \tag{2.14}$$

$$\mu\left(\frac{\partial v'}{\partial z}+\frac{\partial w'}{\partial y}\right)=\beta\left(\frac{\partial X'}{\partial z}+a\frac{\partial h'_{I}}{\partial z}\right), \tag{2.15}$$

$$p'-2\mu\frac{\partial v'}{\partial y}=-\sigma(b)\left(\frac{\partial^2 h'_{I}}{\partial x^2}+\frac{\partial^2 h'_{I}}{\partial z^2}\right), \tag{2.16}$$

$$\frac{\partial X'}{\partial y}=-\Gamma(X'+ah'_{I}), \tag{2.17}$$

and, at the lower surface (y=−d), as

$$\frac{\partial h'_{II}}{\partial t}=v', \tag{2.18}$$

$$\mu\left(\frac{\partial v'}{\partial x}+\frac{\partial u'}{\partial y}\right)=-\beta\left(\frac{\partial X'}{\partial x}+a\frac{\partial h'_{II}}{\partial x}\right), \tag{2.19}$$

$$\mu\left(\frac{\partial v'}{\partial z}+\frac{\partial w'}{\partial y}\right)=-\beta\left(\frac{\partial X'}{\partial z}+a\frac{\partial h'_{II}}{\partial z}\right), \tag{2.20}$$

$$p'-2\mu\frac{\partial v'}{\partial y}=\sigma(b)\left(\frac{\partial^2 h'_{II}}{\partial x^2}+\frac{\partial^2 h'_{II}}{\partial z^2}\right), \tag{2.21}$$

$$\frac{\partial X'}{\partial y}=\Gamma(X'+ah'_{II}). \tag{2.22}$$

To normalize the system of equations (2.10)−(2.22), representative scales for the sheet are taken as follows: d for the length, d^2/D for the time, D/d for the velocity, $\mu D/d^2$ for the pressure and ad for the temperature or the concentration. Since there arise no confusions, we shall use henceforth the same symbols for the nondimensional variables and disturbances. Then, u', w' and p' are eliminated from the boundary conditions by using (2.10) and (2.11), so that the stability problem against the small disturbances can be denoted in terms of v', X', h'_{I} and h'_{II}.

Let us now seek the solution of the following form:

$$[v', X', h'_I, h'_{II}] = [f(y), g(y), s_I, s_{II}]\exp(ik\cdot x + \lambda t), \tag{2.23}$$

where $k=(k_x, 0, k_z)$ is the wavenumber vector of magnitude k, and λ is the complex growth rate. Using (2.23), we get the equations for f and g:

$$(\pounds - \frac{\lambda}{P_r})\pounds f = 0, \tag{2.24}$$

$$(\pounds - \lambda)g = f, \tag{2.25}$$

where $\pounds = d^2/dy^2 - k^2$, and $P_r = \nu/D$ is the Prandtl number. Then, we get the boundary conditions at y=1:

$$\lambda s_I = f, \tag{2.26}$$

$$(\pounds + 2k^2)f = M_R k^2 (g + s_I), \tag{2.27}$$

$$(\pounds - 2k^2 - \frac{\lambda}{P_r})\frac{df}{dy} = \frac{k^4}{N_C} s_I, \tag{2.28}$$

$$\frac{dg}{dy} = -\gamma (g + s_I), \tag{2.29}$$

and the boundary conditions at y=-1:

$$\lambda s_{II} = f, \tag{2.30}$$

$$(\pounds + 2k^2)f = - M_R k^2 (g + s_{II}), \tag{2.31}$$

$$(\pounds - 2k^2 - \frac{\lambda}{P_r})\frac{df}{dy} = - \frac{k^4}{N_C} s_{II}, \tag{2.32}$$

$$\frac{dg}{dy} = \gamma (g + s_{II}), \tag{2.33}$$

where the parameters are defined as

$$M_R = \frac{\beta a d^2}{\mu D} \qquad \text{Marangoni number,}$$

$$\gamma = \Gamma d \qquad \text{Biot number,} \qquad (2.34)$$

$$N_C = \frac{\mu D}{\sigma(b) d} \qquad \text{Crispation number.}$$

For the system of equations (2.24)-(2.33), let us consider the problem of the steady mode ($\lambda=0$), which is independent of the Prandtl number. (The unsteady mode will be examined in Appendix.) The steady solutions of f and g are obtained as

$$f(y) = [A_1 Y + A_2 + y(A_3 + A_4 Y)]\cosh(ky), \qquad (2.35)$$

$$g(y) = [A_5 Y + A_6 + \frac{y}{2k}(A_1 + A_2 Y) + \frac{y}{4k} A_3 (yY - \frac{1}{k}) + \frac{y}{4k} A_4 (y - \frac{Y}{k})]\cosh(ky), \qquad (2.36)$$

where $Y=\tanh(ky)$, and $A_1 \sim A_6$ are integration constants. The boundary conditions (2.26) and (2.30) for $\lambda=0$ lead to

$$A_3 = - A_1 Z , \qquad A_4 = - A_2 Z^* , \qquad (2.37a,b)$$

with $Z=\tanh(k)$ and $Z^*=1/Z$. Using (2.28), (2.32) (for $\lambda=0$) and (2.37a,b), the surface deformations are expressed as

$$s_I = - \frac{2N_C}{k}(A_1 Z - A_2)\frac{1}{\sinh(k)} , \qquad (2.38)$$

$$s_{II} = \frac{2N_C}{k}(A_1 Z + A_2)\frac{1}{\sinh(k)} , \qquad (2.39)$$

whence we see that the flat surfaces in Case(i) are given formally by setting $N_C=0$. Then, from (2.29) and (2.33), the con-

stants A_5 and A_6 in (2.36) are expressed as

$$A_5 = \frac{-1}{\gamma + kZ^*}\left\{A_1\left[\frac{1}{4} + (1+\gamma)\left(\frac{1}{4k^2} + \frac{2Z^*-Z}{4k}\right)\right] + \frac{\gamma(s_I - s_{II})}{2\sinh(k)}\right\}, \quad (2.40a)$$

$$A_6 = \frac{-1}{\gamma + kZ}\left\{A_2\left[\frac{1}{4} + (1+\gamma)\left(\frac{1}{4k^2} + \frac{2Z-Z^*}{4k}\right)\right] + \frac{\gamma(s_I + s_{II})}{2\cosh(k)}\right\}. \quad (2.40b)$$

Substituting (2.35) and (2.36) into the boundary conditions (2.27) and (2.31), and using (2.37)-(2.40), one obtains the following simultaneous equations for A_1 and A_2:

$$M_R Z F_4 A_1 = -8F_1 A_2 , \quad (2.41a)$$

$$8F_1^* A_1 = -M_R Z^* F_4^* A_2 , \quad (2.41b)$$

where

$$\begin{aligned} F_1 &\equiv F_1(k,Z) = k + \gamma Z, & F_1^* &\equiv F_1(k,Z^*), \\ F_2 &\equiv F_2(k,Z) = k(1 - Z^2), & F_2^* &\equiv F_2(k,Z^*), \\ F_3 &\equiv F_3(k,Z) = \left(2 - \frac{Z}{k}\right)F_2(k,Z) - \frac{Z^2}{k}, & F_3^* &\equiv F_3(k,Z^*), \\ F_4 &\equiv F_4(k,Z) = F_3(k,Z) - 8N_C F_2(k,Z), & F_4^* &\equiv F_4(k,Z^*). \end{aligned} \quad (2.42)$$

A set of equations (2.41a,b) can be solved straightforwardly, so that the eigenvalue relation for the steady mode is expressed as $M_R = F(k, \gamma, N_C)$, which describes a neutrally stable state for the small disturbances.

§ 3. Eigenvalue of the Steady Mode

The explicit form of the eigenvalue M_R in Case(ii) (including Case(i) as a special case) is given by

$$M_R = F(k, \gamma, N_C) = \pm 8\sqrt{\frac{F_1 F_1^*}{F_4 F_4^*}} , \quad (3.1)$$

where the double sign ± should be chosen subject to the following fact. For the definition of M_R in (2.34), it is known that for temperature or for concentration of organic substances, β is negative,[8] so that M_R is taken to be positive (or negative) when the gradient of the equilibrium solution $\bar{X}(y)$, a given by (2.6a), is negative (or positive), while for concentration of inorganic substances, β is positive, so that the sign of M_R agrees with that of a. Therefore, it is found that the surface tension gradient may give rise to an instability of the sheet for both signs of the Marangoni number. This makes a marked contrast to the case of a liquid layer between a gas phase and a solid wall in which the eigenvalue is always positive for the steady mode (see refs. 1, 6 and 9).

Let us examine the eigenvalue in detail as a function of the wavenumber. First, the asymptotic form of (3.1) for $k \to \infty$ is given by

$$M_R = \pm 8k(k + \gamma) \qquad \text{Cases (i) and (ii),} \qquad (3.2)$$

while for $k \to 0$ it is given by

$$M_R = \pm \frac{3}{k^2}\sqrt{15\gamma(\gamma + 1)} \qquad (\gamma \neq 0) \qquad (3.3)$$

Case (i),

$$M_R = \pm \frac{3\sqrt{15}}{k} \qquad (\gamma = 0) \qquad (3.4)$$

$$M_R = \pm \sqrt{\frac{3\gamma(\gamma + 1)}{N_C(1 - 3N_C)}} \qquad (\gamma \neq 0) \qquad (3.5)$$

Case (ii),

$$M_R = \pm \sqrt{\frac{3k^2}{N_C(1 - 3N_C)}} \qquad (\gamma = 0) \qquad (3.6)$$

where (3.3) can be derived by putting $N_C=0$; the small order terms disregarded in (3.3) and (3.5) lead, for $\gamma=0$, to (3.4) and (3.6) respectively. In (3.3) and (3.4) with the positive sign, values of M_R become very large for small k, whereas in (3.5) and (3.6), they become finite at k=0 (e.g., M_R given by (3.6) is found to be zero: the disturbances of zero wavenumber drive always an instability). This gives a remarkable difference between Cases(i) and (ii). Although the equations (3.5) and (3.6) hold for the range $0<N_C<1/3$, they must be treated carefully under the condition for Case(ii) that $|\beta ad| \ll \sigma$ (b): this means here that $N_C|M_R| \ll 1$ or $N_C \ll N_A$, where N_A ($\equiv 1/[3(\gamma^2+\gamma+1)]$) is the solution of N_C to a set of equations $N_C|M_R|=1$ and (3.5). Thus, the condition $N_C \ll N_A \leqq 1/3$ will restrict possible values of N_C especially when γ becomes large for which N_A becomes small. Next, we consider extrema of the eigenvalue with respect to k. Since the equation $\partial M_R/\partial k=0$ derived from (3.1) can be regarded as a quadratic equation for γ, one solution is obtained as

$$\gamma = G(k, N_C) = -B_2 + \sqrt{B_2^2 - k(k - 2B_1)}, \tag{3.7}$$

with

$$\begin{aligned} B_1 &= F_4F_4^*/\frac{\partial}{\partial k}(F_4F_4^*), \\ B_2 &= \frac{1}{2}[(Z + Z^*)(k - B_1) + (Z - Z^*)^2 kB_1], \end{aligned} \tag{3.8}$$

whereas the other solution, being always negative, is meaningless because the Biot number must be positive (or zero for a particular case). Using (3.7), the extrema are now expressed as $M_R=$

$F(k, G(k, N_C), N_C) \equiv M_E$, say. Although M_E can take both signs, we choose here only the positive sign unless otherwise stated (note that the neutral curves are symmetric with respect to $M_R=0$).

The neutral stability curves for Case(i), which are given, on setting $N_C=0$, by (3.1) with the positive sign, are drawn by the heavy solid lines in the (k, M_R) plane of Fig.1 for various values of γ. The extrema (the minima) given by $M_E=F(k, G(k, 0), 0)$ are also drawn in Fig.1 by the light solid line. We find from this that the critical Marangoni number, which is defined as the lowest value of M_R with respect to k, is just given by M_E for each γ. We call hereafter this type of instability Type(A). It is then found that the corresponding critical wavenumber ranges between 0.941 and 1.615, because the Biot number given by $\gamma = G(k, 0)$ changes monotonically from zero to infinity in that range (see Fig.3 for the details). Therefore the critical Marangoni number for Case(i) is found to be given by the simple function $M_E=F(k, G(k, 0), 0)$, which increases from 21.86 to infinity as γ $(=G(k, 0))$ increases.

The neutral curves for Case(ii) given by $M_R=F(k, \gamma, N_C)$ are shown in Fig.2(a,b) together with the extrema $M_E=F(k, G(k, N_C), N_C)$. It turns out from Fig.2(a,b) that effects of the surface deformations arise remarkably for the disturbances of small wavenumbers. This leads to another type of instability, say Type(B), and gives another candidate of critical Marangoni number which is given, at $k=0$, by (3.5) with the positive sign. Figure 2(a) shows that the critical Marangoni number is given for small γ by values of Type

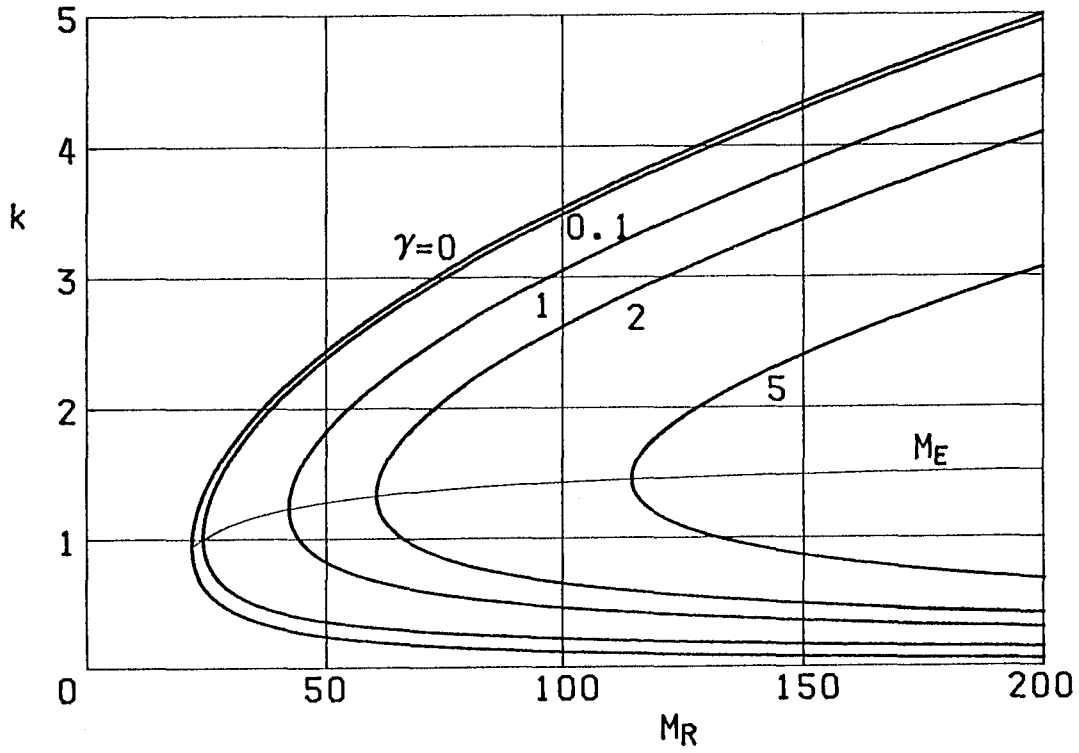

Fig. 1. Neutral curves for Case(i) (N_C=0) for various values of γ: eigenvalues of M_R are drawn by the heavy solid lines, while minima M_E=F(k,G(k,0),0) by the light solid line.

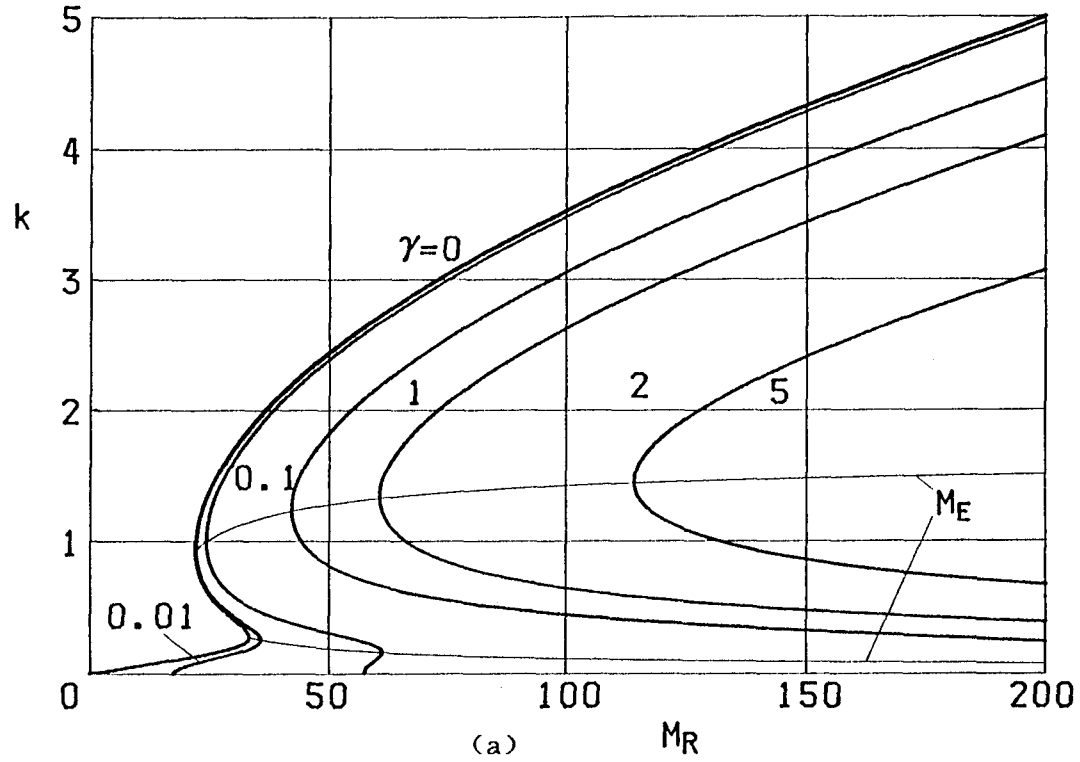

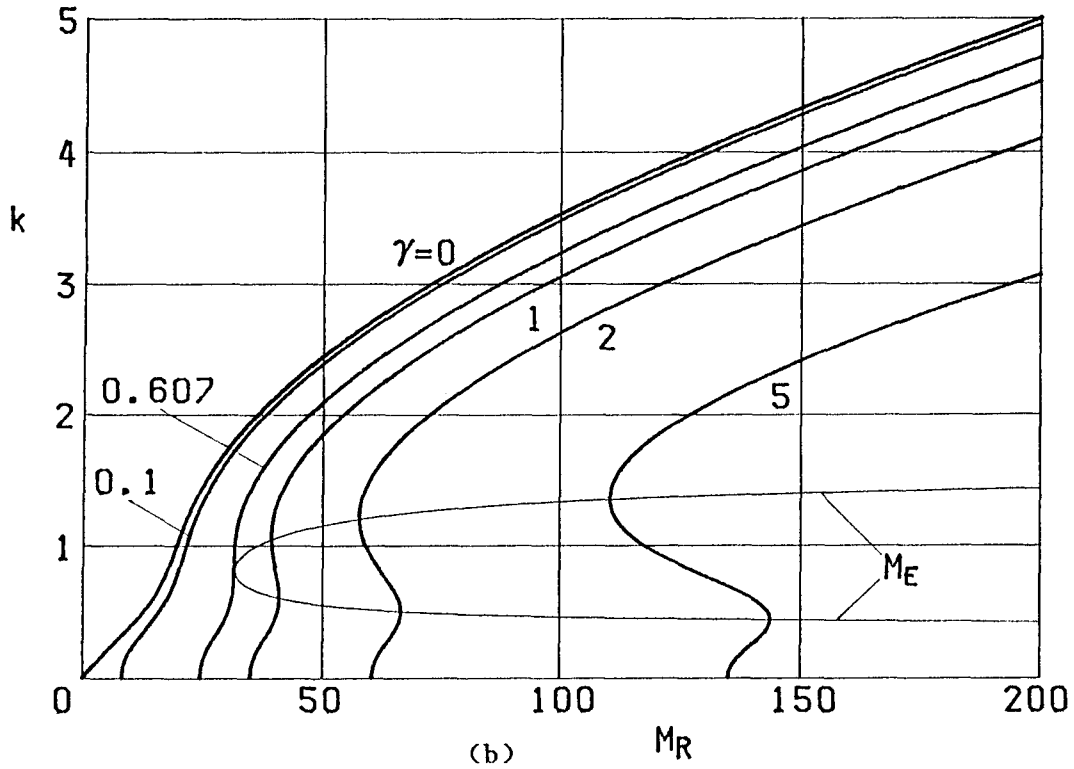

Fig. 2. Neutral curves for Case(ii): (a) N_C=0.0001 and (b) N_C=0.005. M_R and M_E are drawn as in Fig. 1.

(B) (see the curves for $\gamma \leqq 0.01$), while for large γ by minima of Type(A) (see the curves for $\gamma \geqq 0.1$: note that the minima for $N_C>0$ are slightly smaller than those for $N_C=0$). As N_C becomes large, this tendency is found more clearly, as shown in Fig.2(b) for $N_C=0.005$. It is then found from Fig.2(b) that the curve of M_E is in contact with the neutral curve for $\gamma=0.607$ and M_E disappears for $\gamma<0.607$. To illustrate such variation of M_E with N_C, the solution $G(k,N_C)$ given by (3.7) is drawn in Fig.3 as

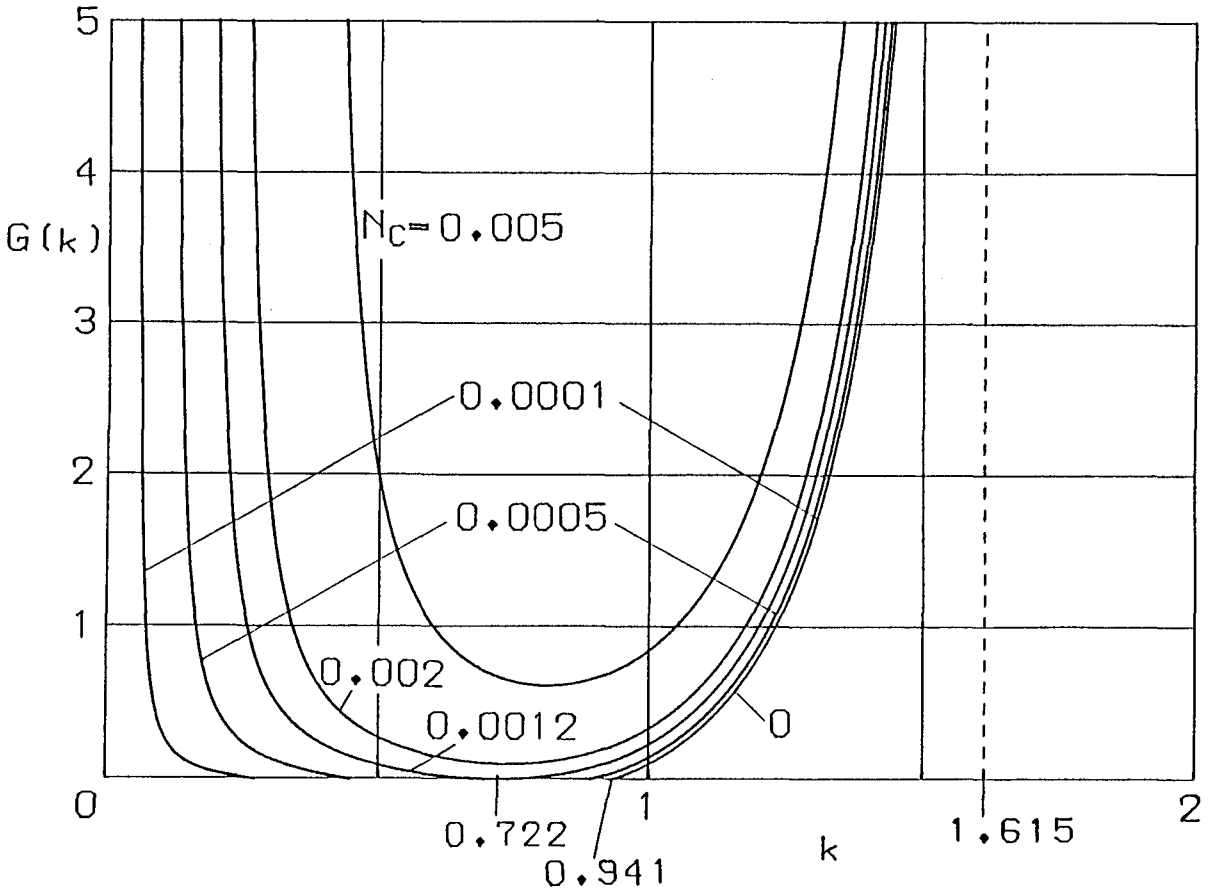

Fig.3. Solution $G(k,N_C)$ obtained from the extremum condition for M_R.

functions of k for various values of N_C, for which the equations $\partial G/\partial k=0$ and $G(k,N_C)=0$ (that is denoted as a quadratic equation for N_C) give $k=0.722$ and $N_C=0.0012$: thus this value of N_C satisfies the condition $N_C<<N_A$. When $N_C \leqq 0.0012$, the wavenumbers ranging between 0.722 and 1.615 give the minima of M_E (see also Fig.2(a)), while those smaller than 0.722 give the maxima: note that the curve of maxima gives a guide line below which, i.e., for the smaller wavenumbers, the effects of surface deformations are dominant. When $N_C>0.0012$, the solution $G(k,N_C)$ is always positive (Fig.3), so that Type(A) disappears and only Type(B) does exist for smaller γ ($<G(k,N_C)$) (see again Fig.2(b)). To compare the two types of instability for various values of N_C, the minima M_E and the values of M_R at $k=0$ given by (3.5) are displayed against γ in Fig.4. It follows from this that even for the values of N_C which allow both types of instability, Type(B) gives smaller values of M_R than Type(A) whenever γ is small. Hence, the critical Marangoni number for Case(ii) is given by Type(B) for small γ and it decreases with increasing N_C under the condition $N_C<<N_A$.

For a larger γ, the critical Marangoni number for both Types(A) and (B) becomes larger. This is interpreted as follows: if γ becomes infinity, the boundary conditions (2.29) and (2.33) reduce to

$$g + s_I = 0 \quad \text{at } y=1, \text{ and} \quad g + s_{II} = 0 \quad \text{at } y=-1, \qquad (3.9a,b)$$

so that the surface tension gradients in (2.27) and (2.31) do vanish.

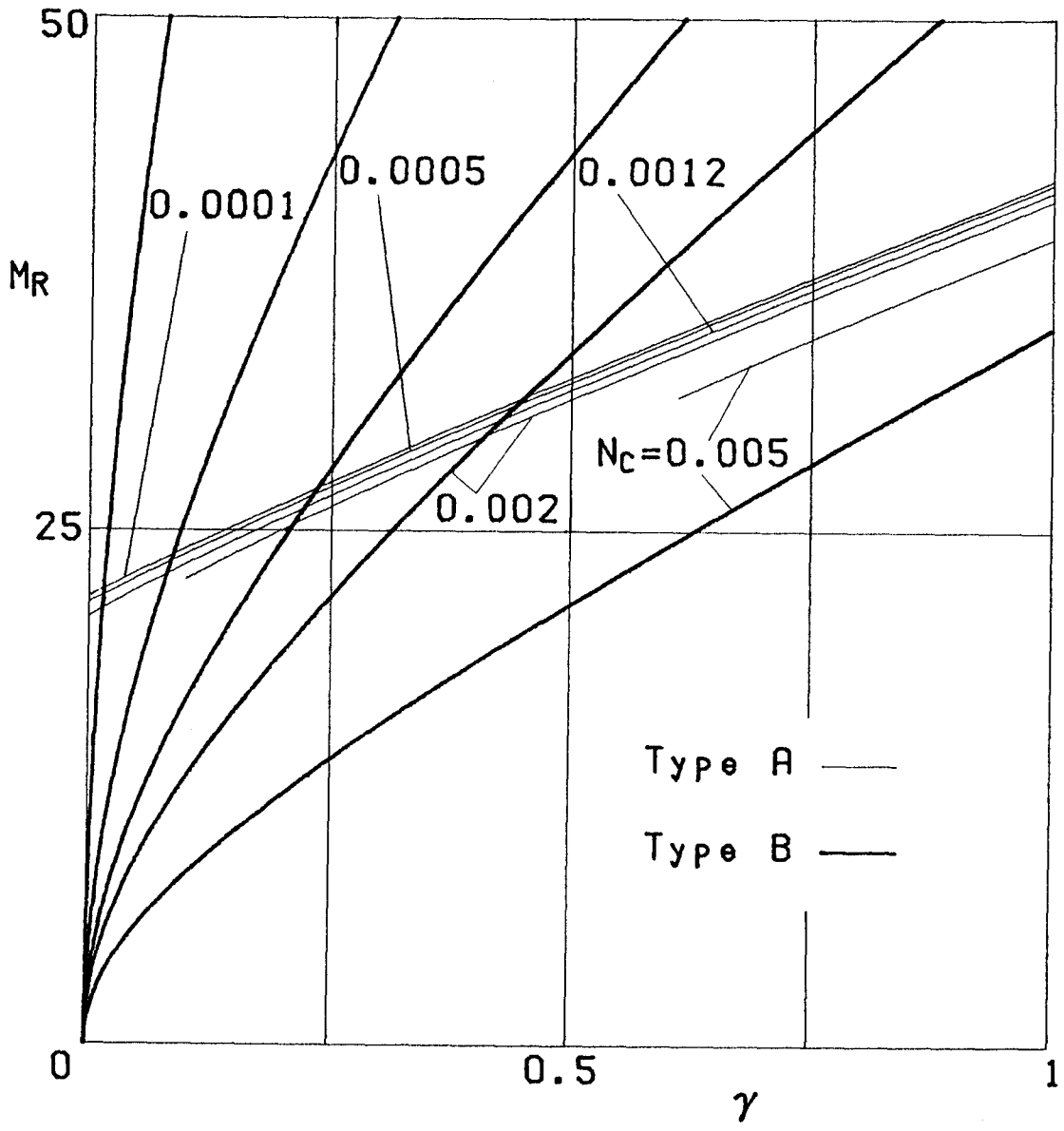

Fig. 4. Comparison of Types(A) and (B) for Case(ii).

§ 4. Effects of Deviation of the Surface Tension Coefficient

Let us now consider the general case where the deviation of the surface tension coefficient (which is given in (2.7) and (2.8)) is taken into account. To this end, the boundary conditions (2.28) and (2.32) have to be replaced, for Case(iii) of the steady mode ($\lambda=0$), by

$$(\mathfrak{L} - 2k^2)\frac{df}{dy} = \frac{k^4}{N_C}(1 + N_C M_R)s_I \qquad \text{at } y=1, \tag{4.1}$$

$$(\mathfrak{L} - 2k^2)\frac{df}{dy} = -\frac{k^4}{N_C}(1 - N_C M_R)s_{II} \qquad \text{at } y=-1. \tag{4.2}$$

Using the solutions (2.35) and (2.36) and the equations (2.37a,b), the boundary conditions (4.1) and (4.2) yield the following equations for the surface deformations:

$$s_I = -\frac{2N_C}{k}\frac{A_1 Z - A_2}{1 + N_C M_R}\frac{1}{\sinh(k)}, \tag{4.3}$$

$$s_{II} = \frac{2N_C}{k}\frac{A_1 Z + A_2}{1 - N_C M_R}\frac{1}{\sinh(k)}. \tag{4.4}$$

After tedious but straightforward calculation as was made in § 2, we find that the eigenvalue relation for this Case(iii) can be expressed by a cubic equation for M_R^2, which is then factorized as a product of $M_R^2 - N_C^{-2}$ and a quadratic for M_R^2: the latter reduces, in the limit of $N_C \to 0$, to a linear equation giving (3.1) for Case(ii). Thus we can obtain the eigenvalues explicitly for Case(iii) as

$$M_R = \pm\sqrt{C_1 - \sqrt{C_1^2 - C_2}}, \tag{4.5}$$

$$M_R = \pm \frac{1}{N_C}, \tag{4.6}$$

$$M_R = \pm \sqrt{C_1 + \sqrt{C_1^2 - C_2}}, \tag{4.7}$$

where

$$C_1 = \frac{1}{2}\frac{1}{N_C^2} - \frac{4}{N_C}\left(\frac{F_2}{F_3} + \frac{F_2^*}{F_3^*}\right) + \frac{32}{F_3 F_3^*}(F_1 + F_2)(F_1^* + F_2^*), \tag{4.8}$$

$$C_2 = \frac{64}{N_C^2}\frac{F_1 F_1^*}{F_3 F_3^*},$$

$F_1 \sim F_3$ and $F_1^* \sim F_3^*$ being given in (2.42); the double sign $\pm$ in (4.5)-(4.7) can be interpreted as in § 3. It turns out that for sufficiently small values of N_C and k, the magnitude of M_R given by (4.5), (4.6) and (4.7) is, respectively, smaller than, equal to and larger than N_C^{-1}. Thus (4.5) can be approximated by (3.1) when N_C is sufficiently small, which suggests a critical Marangoni number at k=0 (Type(B)) as in Case(ii).

To examine the eigenvalue for Case(iii) in comparison with that for Case(ii), we introduce here a condition $N_C | M_R | \leqq 1$ and focus our attention only to (4.5). The asymptotic form of (4.5) for $k \ll 1$ is obtained as

$$M_R = \pm \sqrt{\frac{1}{N_C}\frac{3\gamma(\gamma+1)}{1 + 3N_C(\gamma-1)(\gamma+2)}}, \tag{4.9}$$

which leads to $M_R=0$ for $\gamma=0$. (Note that (4.5) takes the form of $M_R \propto \pm k$ when $\gamma=0$ and $k \ll 1$, while it approaches (4.6) as k becomes large.) Using (4.9), the condition $N_C | M_R | \leqq 1$ is found to be expressed as $N_C \leqq 1/6$. It is also found that (4.9) has two

distinct features according as γ is smaller than unity or not. When $\gamma \geqq 1$, M_R given by (4.9) with the positive sign decreases monotonically with increasing N_C. When $\gamma<1$, N_C in (4.9) has the upper limit, say N_B ($\equiv 1/[3(1-\gamma)(\gamma+2)]$, which takes the lowest value 1/6 in the limit of $\gamma \to 0$). Thus we find that M_R decreases with increasing N_C in the range $N_C \leqq N_B/2$, while increases with N_C in $N_B/2<N_C<N_B$ (note that the condition $N_B/2 \leqq 1/6$ always holds for $0 \leqq \gamma \leqq (\sqrt{5}-1)/2$). Therefore N_C in the latter range has a stabilizing effect on the disturbances, whose typical example is shown in Fig. 5: at a certain value of γ (for example, at $\gamma=1/4$, for which $N_B=0.1975$), M_R increases with increasing N_C over $N_B/2$. This seems very interesting in contrast to the destabilizing effect of the surface deformation obtained in ref. 6. If N_C approaches N_B, however, M_R at k=0 becomes very large, and the condition $N_C \leqq 1/6$ cannot be satisfied for larger values of γ (<1).

The neutral curves for Case(iii), which is given by (4.5) with the positive sign, are shown in Fig. 6(a,b) for $N_C=0.005$ and $N_C=0.01$. To compare the values of M_R for Cases(iii) and (ii), we set (4.9) equal with (3.5), then we get $\gamma=(\sqrt{5}-1)/2 \equiv \gamma_1$, say. According as $\gamma<\gamma_1$ or $\gamma_1<\gamma$, the positive value of M_R given by (4.9) becomes larger or smaller than that given by (3.5). For the small values of γ and for N_C sufficiently small, the critical Marangoni number given at k=0 (Fig. 6(a)), i.e., Type(B), may be approximated by that for Case(ii) (Figs. 2(b) and 4). For γ of order unity, maxima and minima of M_R given by (4.5) can be found in Fig. 6(a), where the latter, Type(A), gives the critical

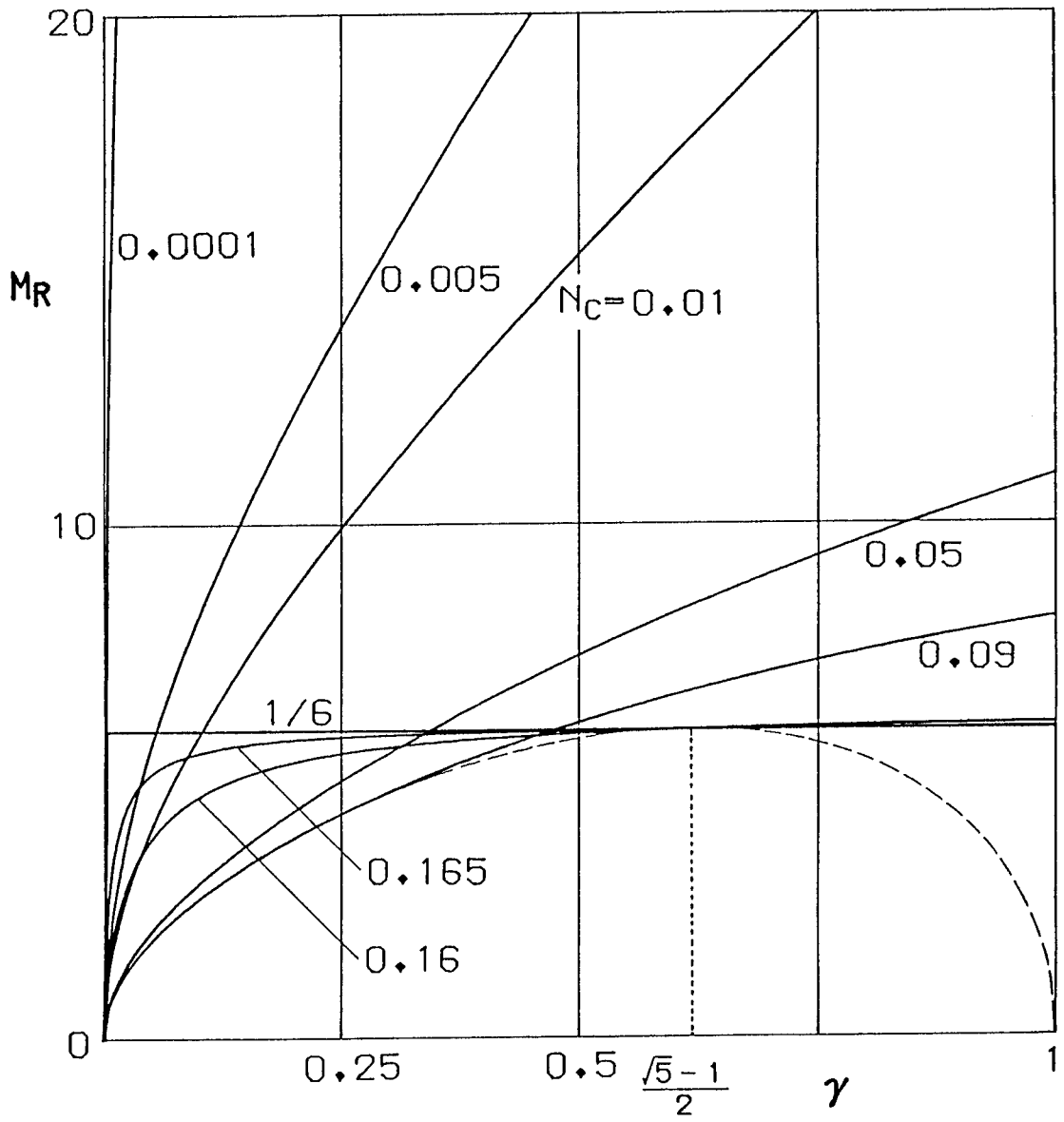

Fig. 5. Neutral curves in the limit of small wavenumbers given by (4.9) for various values of N_C: the 'stabilizing effect' arises when N_C changes within the range $N_B/2<N_C<N_B$, for which the value of $N_B=0.1975$ is obtained at $\gamma=1/4$. (The broken line denotes $M_R=F(0, \gamma, N_B/2)=\pm 6\sqrt{\gamma(\gamma+1)(\gamma+2)(1-\gamma)}$ derived from (4.9), which implies the envelope for M_R with respect to N_C.)

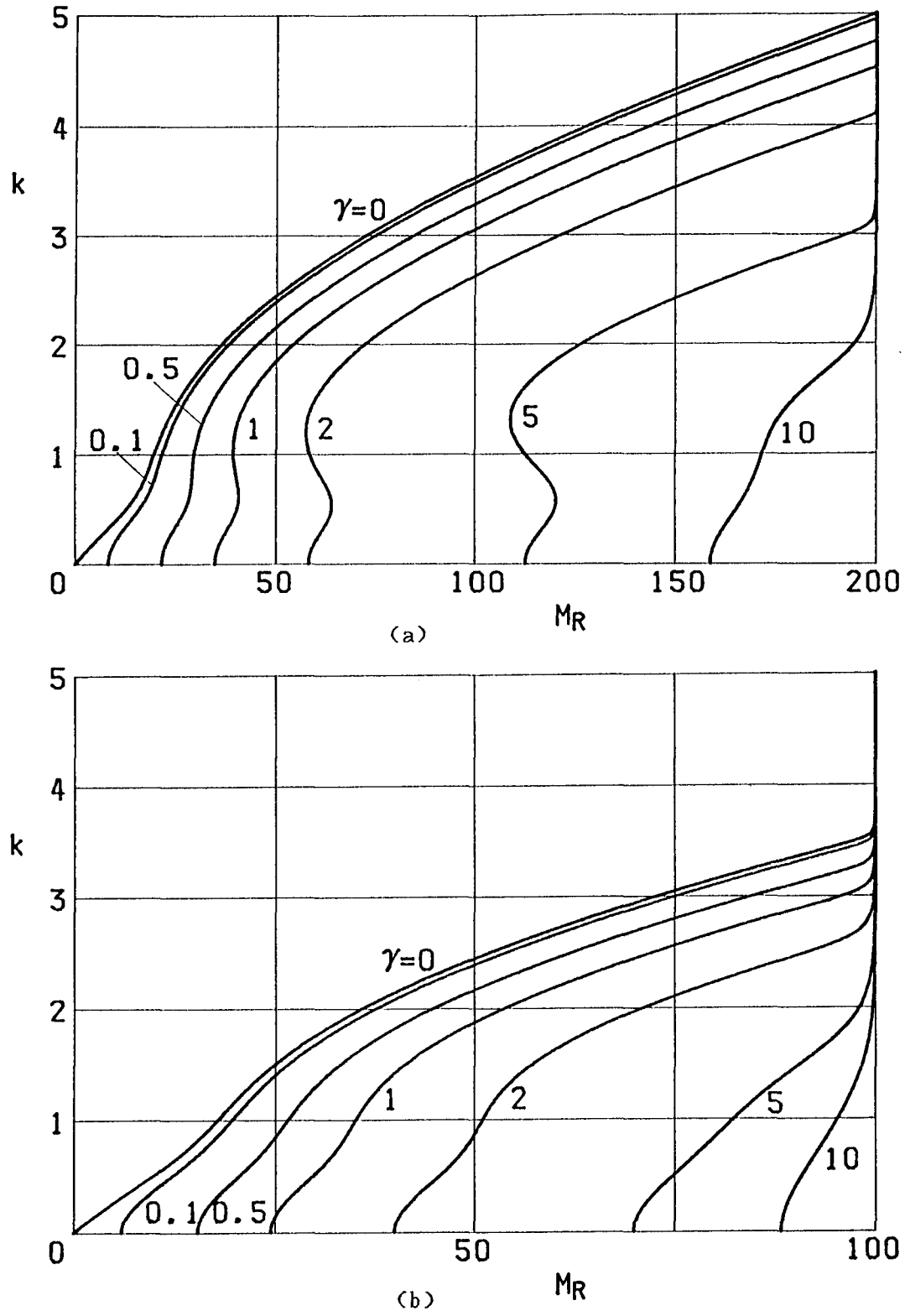

Fig. 6. Neutral curves for Case(iii) given by (4.5): (a) N_C=0.005, (b) N_C=0.01.

value (see the curve for $\gamma=5$). For $\gamma=10$, again Type(B) dominates. These show that the maxima and the minima are on a closed curve that is given in the range $0 \leqq M_R < N_C^{-1}$ by a set of equations $\partial M_R / \partial k = 0$ and (4.5), for which Type(A) disappears for both small and large values of γ. As N_C becomes large, the curve is then contracted, so that only Type(B) gives the critical value, as seen in Fig.6(b). This is the most typical result for Case(iii): the critical Marangoni number is given at k=0 by (4.9) for larger values of N_C so far as the condition $N_C \mid M_R \mid \leqq 1$ is satisfied.

§ 5. Surface Pattern at Small Wavenumbers

The surface pattern relative to the induced flow gives a very important criterion for what mechanical effect causes an instability for the steady mode.[6] Then it may be interested to ask what sort of surface pattern arises at the upper and the lower surfaces of the liquid sheet. Since the effects of surface deformations for Cases(ii) and (iii) are remarkable for the disturbances of small wavenumbers, we examine here the surface pattern and the flow direction in the limit of small wavenumbers.

For $k \to 0$, the equation (2.41a) for Case(ii) can be written as

$$\frac{A_2}{A_1} = \xi k, \tag{5.1}$$

with

$$\xi = \frac{N_C M_R}{\gamma + 1}. \tag{5.2}$$

Using (5.1), (2.35) and (2.37)-(2.39), we have the following equations:

$$\frac{s_{II}}{s_I} = \frac{\xi + 1}{\xi - 1}, \tag{5.3}$$

$$\frac{s_I}{\left(\frac{df}{dy}\right)_{y=1}} = \frac{N_C}{k^2}\left(\frac{1}{\xi} - 1\right), \tag{5.4}$$

$$\frac{s_{II}}{\left(\frac{df}{dy}\right)_{y=-1}} = \frac{N_C}{k^2}\left(\frac{1}{\xi} + 1\right). \tag{5.5}$$

On the other hand, the relation between A_1 and A_2 for Case(iii) can be written, for $k \to 0$, as

$$\frac{A_2}{A_1} = \frac{k}{\eta}, \tag{5.6}$$

with

$$\eta = \frac{(2 + \gamma)(1 - N_C{}^2 M_R{}^2) - 1}{N_C M_R}. \tag{5.7}$$

We thus get the following equations from (2.35), (2.37), (4.3) and (4.4):

$$\frac{s_{II}}{s_I} = \frac{\zeta + 1}{\zeta - 1}, \tag{5.8}$$

$$\frac{s_I}{\left(\frac{df}{dy}\right)_{y=1}} = \frac{N_C}{k^2}\frac{\eta - 1}{1 + N_C M_R}, \tag{5.9}$$

$$\frac{s_{II}}{\left(\frac{df}{dy}\right)_{y=-1}} = \frac{N_C}{k^2}\,\frac{\eta + 1}{1 - N_C M_R}, \tag{5.10}$$

where

$$\zeta = \frac{\gamma + 2}{\gamma + 1}\, N_C M_R. \tag{5.11}$$

It should be remarked here that M_R in (5.1)-(5.5) is given by (3.5) and that in (5.6)-(5.11) by (4.9).

Making use of the above relations, we consider the surface deformations at a certain station, say x=0, in a fixed plane z=0. For simplicity, we assume that s_I and s_{II} are real functions of k, by which the levels of the free surfaces at x=0 are set as $y=1+s_I$ and $y=-1+s_{II}$. In the limit of $\gamma \to 0$, in which $M_R=0$ for both Cases(ii) and (iii), the right-hand-side of (5.3) and that of (5.8) reduce to -1 (i.e., $s_{II}=-s_I$). This means that if s_I is a surface depression (i.e., $s_I<0$), then s_{II} is a surface elevation. The corresponding surface deformations at another station $x=\pi/k$ (or $x=-\pi/k$) should be an elevation $-s_I$ and a depression $-s_{II}$ respectively. Therefore the surface pattern for $\gamma \to 0$ is a symmetric type with respect to the center plane of the sheet (y=0). When $\gamma>0$, on the other hand, the condition for Case(ii) and (5.2) yield $|\xi| \leqq N_C |M_R| \ll 1$, so that the sign of (5.3) does not change. It turns out from this that the amplitude s_I is always smaller than s_{II} for (3.5) with the positive sign, while vice versa with the negative sign: for the double sign in (3.5), the surface pattern for Case(ii) is somewhat similar to the sym-

metric type. For Case(iii), three kinds of surface pattern may be found subject to ζ in (5.8). Setting $|\zeta|=1$, we have from (4.9) the following relation between N_C and γ:

$$N_C = \frac{1}{3}\frac{\gamma+1}{(2\gamma+1)(\gamma+2)} \quad (\equiv N_G, \text{ say}). \tag{5.12}$$

When $N_C<N_G$, i.e., $|\zeta|<1$, the surface pattern for Case(iii) is qualitatively similar to that for Case(ii). When $N_C=N_G$, the upper surface becomes flat for $\zeta=1$, while the lower surface becomes flat for $\zeta=-1$. When $N_C>N_G$, both of the surface deformations become in-phase, so that only the elevations or the depressions do appear at x=0.

Let us now consider the induced flow relative to the surface deformations, with assuming that f is a real function of k and y. When an upflow (a downflow) occurs near y=1, $(df/dy)_{y=1}$ must be negative (positive), because the kinematic condition (2.26) (for $\lambda=0$) gives f(1)=0. To the contrary, an upflow near y=-1 makes $(df/dy)_{y=-1}$ positive, because (2.30) gives f(-1)=0. In accordance with these and under the condition for Case(ii) ($N_C|M_R| \ll 1$), the equations (5.4) and (5.5) with $0<\xi \ll 1$ show that when a surface depression s_I and an elevation s_{II} exist at x=0, an upflow arises near y=1 and y=-1; then, at the station $x=\pi/k$, the elevation $-s_I$ and the depression $-s_{II}$ arise together with a downflow near y=1 and y=-1. A typical example of such cellular flows is given in Fig. 7, where the steady convection and the surface deformations for Case(ii) are displayed in the cross plane of the sheet (which is denoted by $-\pi/k \leqq x \leqq \pi/k$ and $-1 \leqq y \leqq 1$ at z=0).

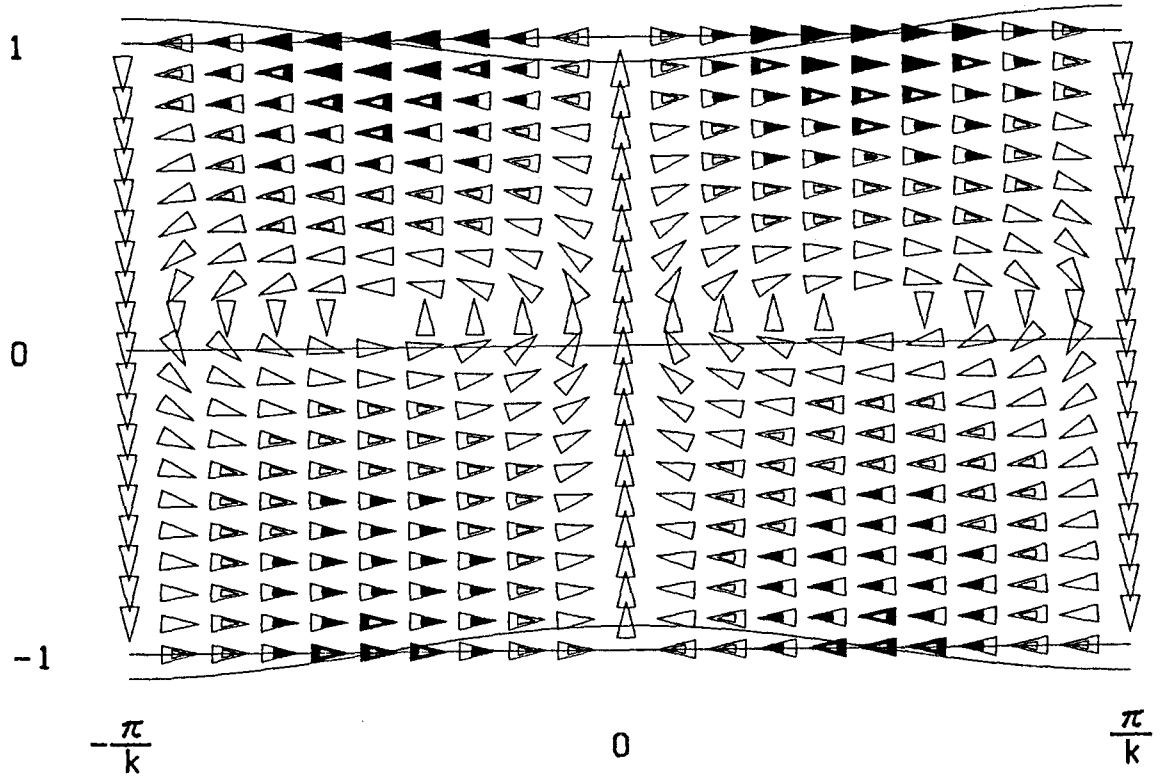

Fig. 7. A typical flow pattern for Case(ii). By setting k=0.125, γ=1, N_C=0.0001 and A_1=1, the eigenvalue relation (3.1) leads to M_R=243, $s_I=-1.57\times10^{-3}$, $s_{II}=1.61\times10^{-3}$, the maximum velocity of the steady convection Max(|v' |)=0.036 (which is drawn by the black triangles), and Min(|v' |)=0 (i.e., stagnation points, which are indicated by the blank); the center of each triangle denotes the coordinate (x,y) in the cross plane of the sheet ($-\pi/k\leqq x\leqq \pi/k$, $-1\leqq y\leqq 1$ at z=0), intermediate intensities of the velocity are painted in four ranks (single triangles, double ones, top-painted ones, and heavy-lined ones) and the top of the triangles denotes the direction of the cellular flow; the amplitude s_I and s_{II} are intensified.

For Case(iii), the relations between the induced flow and the surface deformations are given by (5.9) and (5.10). The condition $|\eta|=1$ gives $N_C=N_G$ and $N_C=1/6$, while the condition $\eta=0$ leads to

$$N_C = \frac{1}{3}\frac{1}{\gamma+2} \quad (\equiv N_E, \text{ say}). \tag{5.13}$$

This gives the relation $0<N_G \leqq N_E \leqq 1/6$, where the equality holds only for $\gamma=0$. Using (4.9) with the positive sign, it is found that $\eta=1$ corresponds to $N_C=N_G$ and $\eta=-1$ to $N_C=1/6$. From these relations and the condition $N_C \leqq 1/6$, η can be classified into two ranges: $\infty > \eta \geqq 0$ for $0<N_C<N_E$ and $0 \geqq \eta > -1$ for $N_E<N_C<1/6$. Although the sign of (5.9) changes across the critical state $N_C=N_G$ ($\eta=\zeta=1$), the sign of s_I also changes at the same time: the direction of the induced flow near y=1 at x=0 does not change irrespective of the sign of s_I. Contrary to this, (5.10) does not change the sign, so that the induced flow near y=-1 (at x=0) has the same direction as that near y=1 even when N_C increases within the range $0<N_C<1/6$. Therefore, we can conclude for Case(iii) that an upflow occurs when s_{II} is an elevation, while a downflow occurs when s_{II} is a depression, irrespective of the situation of the upper surface deformation.

Finally, let us evaluate typical values of the parameters for aqueous solution. The data of pure water at 25℃ provides the following values: $\mu=0.89\times10^{-3}$ [N·sec·m^{-2}], $D_T=1.42\times10^{-7}$ [m^2/sec], $D_C=2.14\times10^{-9}$ [m^2/sec], $\sigma(b)=7.2\times10^{-2}$ [N/m] and $\beta=-1.6\times10^{-4}$ [N/m·deg] at air-water surface for heat transfer.[8]

These lead to $N_C=1.76\times10^{-9}/d$ and $M_R=-1.27\times10^{6}ad^2$ for $D=D_T$, and $N_C=2.65\times10^{-11}/d$ for $D=D_C$, where d (the half-thickness of the sheet in the undisturbed state) is measured in meter and ad (the temperature difference) is in degree (Celsius). When d is less than 10^{-4}[m], Type(A) of instability may arise for large γ, while Type(B) for small γ: both the types may drive the Marangoni convection in the sheet. Although the order of magnitude of the diffusivity changes little for almost all substances solved in water, some substances such as glycerin and sucrose change the viscosity of aqueous solution as a hundred times as large compared with pure water. Furthermore, some substances such as acetone and surface active agencies make $N_C\,|\,M_R\,|$ close to unity. These properties changing N_C or N_CM_R suggest that the liquid sheet can easily become unstable when the surface deformations do exist. This conjecture seems to be reasonable, because a soap bubble cannot be made up when the temperature difference between the inside and the outside temperatures is large.

The results for the relation between the surface pattern and the induced flow may also give a criterion to distinguish the Marangoni convection from other convections which do not include the Marangoni effect, and may be applicable to study the break-up of the sheet.

Appendix: Temporal Evolution of Disturbances in the Vicinity of the Steady Disturbed State

Let us now consider a temporal evolution of disturbances in the vicinity of the steady disturbed state for Cases(i) and (ii). Assuming that the evolution occurs very slowly, we take the following perturbation expansion:

$$f = f_0 + \varepsilon f_1 + O(\varepsilon^2), \tag{A.1}$$

$$g = g_0 + \varepsilon g_1 + O(\varepsilon^2), \tag{A.2}$$

$$M_R = M_{R0} + \varepsilon M_{R1} + O(\varepsilon^2), \tag{A.3}$$

$$\lambda = \varepsilon \lambda_1 + O(\varepsilon^2), \tag{A.4}$$

where ε ($<<1$) denotes the magnitude of the complex growth rate λ, where λ_1 is scaled as of O(1). Substituting (A.1)-(A.4) into (2.24)-(2.33), and arranging them by like powers of ε, we get the governing system of equations for O(1) and $O(\varepsilon)$. For O(1), we readily find that f_0, g_0 and M_{R0} take the same forms as (2.35), (2.36) and (3.1), respectively.

To seek solutions of $O(\varepsilon)$, we have to solve an adjoint problem for the disturbed state for O(1): it is given by the equations for f^+ and g^+:

$$\mathcal{L}^2 f^+ - g^+ = 0, \tag{A.5}$$

$$\mathcal{L} g^+ = 0, \tag{A.6}$$

together with the boundary conditions:

$$\frac{d^2 f^+}{dy^2} + k^2 f^+ = 0 \qquad \text{at } y = \pm 1, \tag{A.7a,b}$$

$$\frac{k^4}{N_C} f^+ = M_{R0} k^2 \frac{df^+}{dy} + \gamma g^+ \qquad \text{at } y = \pm 1, \tag{A.8a,b}$$

$$\frac{dg^+}{dy} = -\gamma g^+ - M_{R0}k^2 \frac{df^+}{dy} \qquad \text{at } y=1, \qquad \text{(A. 9a)}$$

$$\frac{dg^+}{dy} = \gamma g^+ + M_{R0}k^2 \frac{df^+}{dy} \qquad \text{at } y=-1, \qquad \text{(A. 9b)}$$

for which the following relation is always satisfied:

$$\langle f^+ \pounds^2 f_0 \rangle + \langle g^+ (\pounds g_0 - f_0) \rangle = \langle f_0 (\pounds^2 f^+ - g^+) \rangle + \langle g_0 \pounds g^+ \rangle, \qquad \text{(A. 10)}$$

where the angular brackets stand for the integration in the range $-1 \leqq y \leqq 1$. By setting $N_C=0$, (A. 8a, b) reduce to the conditions such that $f^+=0$ at $y=\pm 1$, which correspond to the conditions of Case(i). The solutions to (A. 5) and (A. 6) are obtained as

$$g^+ = (B_1 Y + B_2)\cosh(ky), \qquad \text{(A. 11)}$$

$$f^+ = [B_3 Y + B_4 + y(B_5 + B_6 Y) + \frac{B_1 y}{8k^2}(yY - \frac{1}{k}) + \frac{B_2 y}{8k^2}(y - \frac{Y}{k})]\cosh(ky), \qquad \text{(A. 12)}$$

where integration constants $B_1 \sim B_6$ can be expressed, by using (A. 7)-(A. 9), as

$$B_1 = \frac{-M_{R0}B_2}{8(\gamma + kZ^*)}\{[Z^* + k(8N_C-2)](1-Z^2) - \frac{1}{k}\}, \qquad \text{(A. 13a)}$$

$$B_2 = \frac{-M_{R0}B_1}{8(\gamma + kZ)}\{[Z + k(8N_C-2)](1-Z^{*2}) - \frac{1}{k}\}, \qquad \text{(A. 13b)}$$

$$B_3 = -\frac{B_1}{8k^2}[(8N_C-2)Z^{*2} + 1 + \frac{8N_C-1}{k}Z^*], \qquad \text{(A. 14a)}$$

$$B_4 = -\frac{B_2}{8k^2}[(8N_C-2)Z^2 + 1 + \frac{8N_C-1}{k}Z], \qquad \text{(A. 14b)}$$

$$B_5 = \frac{B_1}{8k^2}(8N_C-2)Z^*, \qquad B_6 = \frac{B_2}{8k^2}(8N_C-2)Z. \qquad \text{(A. 15a, b)}$$

The simultaneous equations (A.13a,b) lead to the same eigenvalue relation as (3.1).

From (A.1)-(A.15), one obtains the solvability condition for f_1 and g_1:

$$\frac{\lambda_1}{M_{R1}} = \frac{-k^2 Q}{\langle f_0 \pounds f^+ \rangle / P_r + \langle g_0 g^+ \rangle + R} \quad (\equiv H, \text{ say}), \tag{A.16}$$

where

$$Q = \left[\frac{df^+}{dy}(g_0 + s_I)\right]_{y=1} + \left[\frac{df^+}{dy}(g_0 + s_{II})\right]_{y=-1}, \tag{A.17a}$$

$$R = s_I\left[(\pounds - 2k^2)\frac{df^+}{dy}\right]_{y=1} - s_{II}\left[(\pounds - 2k^2)\frac{df^+}{dy}\right]_{y=-1}. \tag{A.17b}$$

Using (A.16), the equation (A.3) is then expressed as

$$M_{R0} + \varepsilon M_{R1} = M_{R0} + \varepsilon \frac{\lambda_1}{H}. \tag{A.18}$$

The function H (=H(k, γ, N_C, P_r)) is found to be positive, so that λ_1 ($\equiv \lambda_{1r} + i\lambda_{1i}$) has to be real ($\lambda_{1i}=0$): the oscillatory mode does not exist in the vicinity of the steady disturbed state. This also means that λ_{1r} becomes positive for the supercritical state ($M_{R1}>0$), but negative for the subcritical state. The typical examples given by (A.18) with a fixed value $\varepsilon\lambda_{1r}=0.1$ are illustrated in Fig.A1 for Case(i) ($N_C=0$) and in Fig.A2 for Case (ii) ($N_C=0.005$), where the parameters are set as $\gamma=0$, 1, 5 and $P_r=0.1$, 1, 10. Figure A1 shows that M_R ($=M_{R0}+\varepsilon M_{R1}$) takes larger values at larger wavenumbers especially when P_r is small, which should be compared with the curves of M_{R0} (drawn by the broken lines): when $P_r=0.1$, the minimum of M_R for $\gamma=0$ is given by

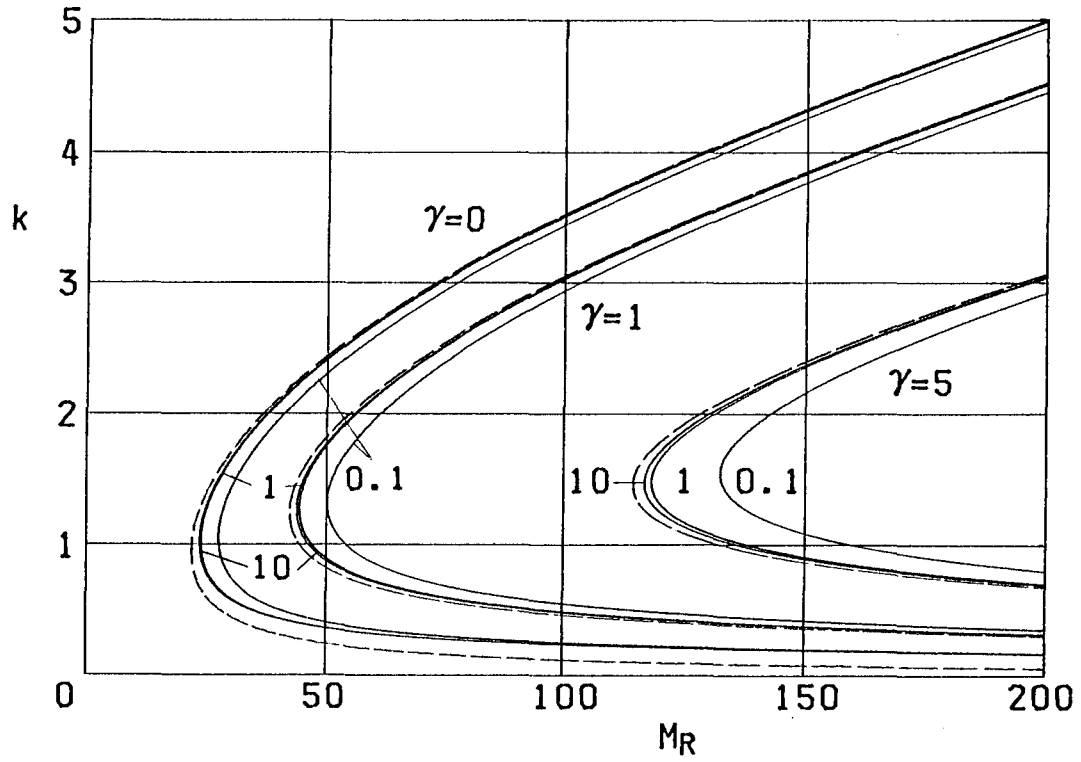

Fig. A1. Examples of the temporal evolution of disturbances in the vicinity of the steady disturbed state for Case(i) (N_C=0), with setting γ=0, 1, 5 and P_r=0.1, 1, 10. The equi-growth rate curves M_R ($=M_{R0}+\varepsilon M_{R1}$) with $\varepsilon \lambda_{r1}$=0.1 are drawn by the solid lines, and M_{R0} by the broken lines.

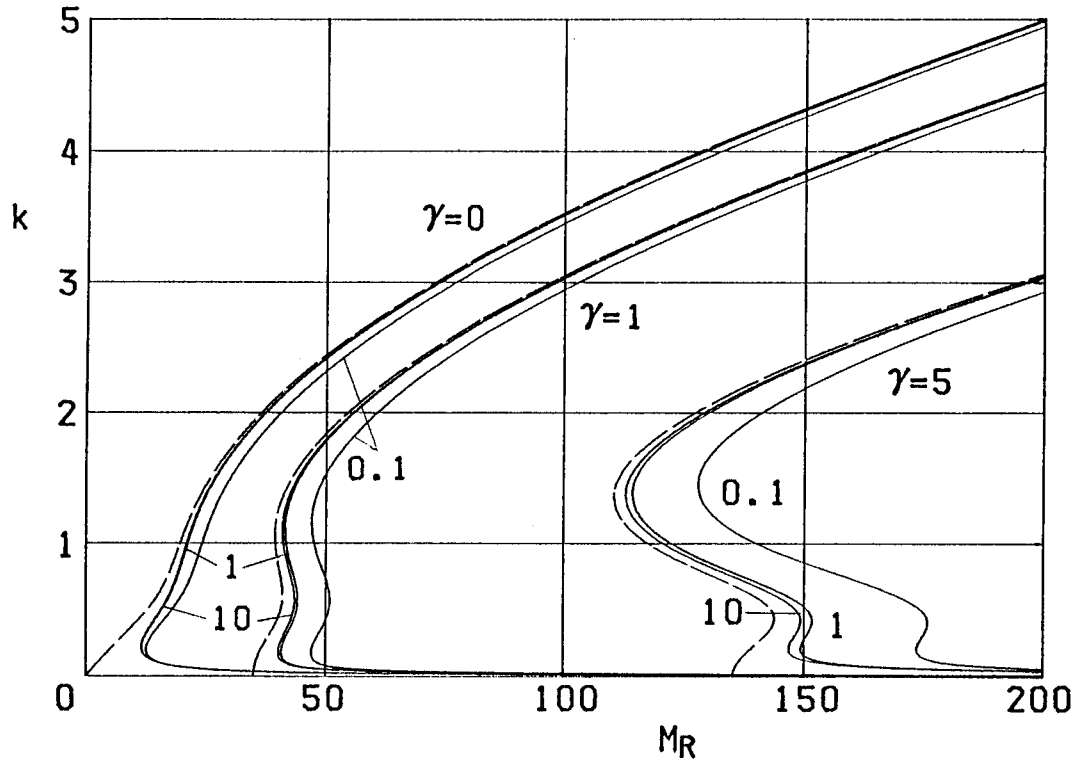

Fig. A2. Examples of the temporal evolution of disturbances in the vicinity of the steady disturbed state for Case(ii) (N_C=0.005): the parameters are taken as in Fig. A1.

27.385 at k=1.042 (recall that the critical Marangoni number was given by 21.864 at k=0.941). This tendency becomes remarkable as γ increases. It is then shown that when $\varepsilon \lambda_{1r}=0.2$ and $P_r=0.1$, M_R for $\gamma=0$ takes the minimum of 32.616 at k=1.109: both the minimum and the corresponding wavenumber increase with the growth rate. Similar results can be obtained for Case(ii) in Fig.A2. For Type(B) of instability, it is found that M_R takes minima at finite wavenumbers: for $P_r=0.1$ and $\gamma=0$, they are given by 12.536 at k=0.199 when $\varepsilon \lambda_{1r}=0.1$, and by 19.386 at k=0.259 when $\varepsilon \lambda_{1r}=0.2$ (note in Fig.A2 that if $\lambda_{1r} \neq 0$, M_R becomes infinity at k=0). This suggests that when the sheet becomes unstable, the convection cells of finite size may grow up.

List of Principal Symbols

a, gradient of equilibrium distribution of X (temperature or concentration);

b, mean value of equilibrium distribution of X;

C, concentration in liquid;

D, thermometric diffusivity ($D=D_T$) or diffusivity ($D=D_C$);

d, half-thickness of the sheet;

F, eigenvalue relation;

f, function of y, denoting disturbance of velocity v;

f^+, function in adjoint problem, corresponding to f;

G, solution of Biot number obtained from extremum condition for eigenvalue;

g, function of y, denoting disturbance of X;

g^+, function in adjoint problem, corresponding to g;

h'_I, h'_{II}, surface deformations, respectively, at the upper and the lower surfaces;

$k=(k_x, 0, k_z)$, wavenumber vector of magnitude k;

M_R, Marangoni number;

M_E, extremum of eigenvalue M_R with respect to wavenumber;

N_C, Crispation number;

P_r, Prandtl number;

p, pressure;

p', pressure disturbance;

s_I, s_{II}, amplitude of surface deformation, respectively, at the upper and the lower surfaces;

T, temperature;

t, time variable;

v=(u,v,w), velocity vector;

v'=(u',v',w'), velocity disturbance;

X, temperature (X=T) or concentration (X=C);

X_I, X_{II}, value of X, respectively, in gas phase I and II;

X', disturbance of X;

x,y,z, variables in Cartesian coordinates;

Y, function, $Y \equiv \tanh(ky)$;

Z, function, $Z \equiv \tanh(k)$;

Z^*, function, $Z^* \equiv 1/Z = \coth(k)$;

β, derivative of the surface tension coefficient with respect to X (temperature or concentration);

Γ, transfer coefficient across boundaries of the sheet;

Γ_I, Γ_{II}, transfer coefficient, respectively, across the upper and the lower surfaces;

γ, Biot number, transfer coefficient across the free surface;

λ, complex growth rate;

μ, viscosity of liquid;

ν, kinematic viscosity of liquid;

ρ, density of liquid;

σ_I, σ_{II}, surface tension coefficient, respectively, at the upper and lower surfaces;

$\sigma(b)$, mean value of the surface tension coefficient at two free surfaces;

References

1) J. R. A. Pearson: J. Fluid Mech. 4 (1958) 489.

2) C. V. Sternling and L. E. Scriven: AIChE J. 5 (1959) 514.

3) J. C. Berg, A. Acrivos and M. Boudart: Adv. Chem. Engrg. 6 (1966) 61.

4) V. G. Levich and V. S. Krylov: Ann. Rev. Fluid Mech. 1 (1969) 293.

5) B. N. Antor, F. G. Collins and G. H. Fichtl: Int. J. Heat Mass Transfer 23 (1980) 191.

6) L. E. Scriven and C. V. Sternling: J. Fluid Mech. 19 (1964) 321.

7) L. E. Scriven: Chem. Engrg. Sci. 12 (1960) 98.

8) The Chemical Society of Japan, ed.: Kagaku Binran, Kiso-hen (Handbook of Chemistry, Fundamentals) (Maruzen, 1975) Chap. 6 [in Japanese].

9) N. Imaishi and K. Fujinawa: Kagaku Kogaku Ronbunsyu (Collected Papers on Chemical Engineering) 4 (1978) 490 [in Japanese].

Chapter 3. Nonlinear Surface Waves Driven by the Marangoni Instability in a Heat Transfer System

§ 1. Introduction

When heat and mass transfers occur across or near phase boundaries of fluids, the surface tension gradient due to variations of temperature and of mass concentration often drives convections called the interfacial turbulence or the Marangoni convection.[1] Since the pioneering work of Pearson[2] and of Sternling and Scriven,[3] many studies on the Marangoni convection have been made by means of a linear stability theory. A further interesting problem may arise if one includes the effect of surface deformation. The effect of surface deformation on the Marangoni convection has been studied first by Scriven and Sternling.[4] They have shown that there is no critical Marangoni number for the onset of steady convection and that the limiting case of zero wavenumber is always unstable: this gives one of the most typical examples of the effect of surface deformation. Smith[5] has shown, for the Marangoni instability of two immiscible liquid layers, that the effect of interface deformation appears remarkably at small wavenumbers. He has also discussed how the gravity affects the neutral stability condition for the steady mode. Zeren and Reynolds[6] have shown, for the Rayleigh-Marangoni instability of two immiscible liquid layers, that the effect of interface deformation arises at small wavenumbers when-

ever the Marangoni instability surpasses the Rayleigh instability. Furthermore, when the surface deformation is taken into account, similar results have been obtained for various Marangoni convection systems (see Takashima,[7,8] Chapters 2 and 4 of this thesis): note that even for the oscillatory mode, the effect of surface deformation arises at small wavenumbers.[8] Therefore, it is almost certain that the effects of surface and interface deformations on the Marangoni convection are always remarkable for the disturbances of small wavenumbers rather than those of large wavenumbers. This motivates the present study (Chapter 3) to consider a nonlinear effect of the surface deformation on the Marangoni convection.

Quite recently, Kai et al.[9] have found experimentally that the interface deformation between two immiscible liquid layers grows as macroscopic angular waves in double concentric or single cylindrical containers. They have suggested that one but strong candidate of this mechanism is the Marangoni effect due to chemical reactions. For such surface waves driven by the Marangoni effect, it has been shown that the surface deformation is governed by a nonlinear evolution equation of diffusion type and that an explosive solution can exist for a special case of the equation.[10] The special case has also been studied numerically by Pimputkar and Ostrach.[11] Then, Kopbosynov and Pukhnachev have derived an extended version of the evolution equation (for their investigation, refer to the textbook[12]). On the other hand, Kuramoto[13] has derived a similar type of equation for

phase dynamics in reaction-diffusion systems. Kawahara and Toh[14] have also derived a similar equation for the nonlinear cross-field instability in weakly ionized plasma, and they have found an explosive type of solution numerically. Yamada[15] has derived, in nonlinear phase dynamics, a more extended equation as a typical example with spatial periodicity. A main purpose of this chapter is to discuss typical solutions to the nonlinear diffusion equation and to extend the previous theory.[10]

On the other hand, much attention has been paid to the Kuramoto-Sivashinsky equation[16,17] because of the importance to describe finite amplitude waves in various dissipative systems. The extended equation (including a dispersion term) has been studied numerically and analytically by Kawahara and Toh.[18,19] These give one of recent topics for the nonlinear waves giving rise to chaos. It is quite interesting to ask whether the surface waves due to the Marangoni instability are governed by this kind of equation.

We now consider nonlinear surface waves of long wavelength driven by the Marangoni instability, which occur in a thin layer of viscous liquid between a free surface and a plane wall. We assume that a temperature of the liquid causes variations of the surface tension coefficient, while all the other material properties are kept constant. Thus the heat transfer affects a flow field only through the boundary conditions at the free surface, and the gravity force is taken into account with a constant density of the liquid. Along this line, formulation of the problem

is made in § 2, in which each parameter is put to a typical magnitude and then two examples are proposed. The first one, say Example (i), is examined in § 3 as compared with the results from the linear stability analysis.[4,7] An evolution equation governing the surface waves is derived there, and its steady solution is shown to be expressed by the cnoidal function. Initial value problems of the evolution equation are numerically solved in § 4, where damping, steady and explosive solutions are obtained for prescribed values of parameters. Then a condition to classify the three types of solutions is derived by applying the method developed by Kawahara and Toh.[18,19] The second one, say Example (ii), is discussed in § 5, in which an inhomogeneous temperature distribution along the plane wall is taken into account and then two types of shock wave solutions progressing with a constant velocity are shown.

§ 2. Formulation of the Problem

Let us suppose that a heat transfer occurs through a thin layer of viscous liquid between a plane wall and a still gas phase, and that a temperature T of the liquid causes a variation of the surface tension coefficient $\sigma(T)$ in the following manner:

$$\sigma(T) = \sigma(T_a) + \left(\frac{\partial \sigma}{\partial T}\right)(T - T_a), \tag{2.1}$$

where T_a denotes an equilibrium value of the temperature at the free surface. Thus the Marangoni convection and a surface deformation may arise due to the surface tension gradient, the surface

tension itself and the gravity. Using a system of Cartesian coordinates, we put the horizontal plane wall at y=0 in the (x, z) plane and a mean level of the free surface at $y=h_a$. To simplify the analysis, we consider two-dimensional configuration in the sense that the flow velocity, the pressure of the liquid and the temperature depend upon x, y and time t, and the surface deformation depends upon x and t. All the characteristic quantities for this liquid layer are thus listed as follows: density ρ, viscosity μ, the mean thickness h_a, the wavelength ι, the equilibrium temperature T_a, thermometric diffusivity D, heat transfer coefficients K_g and K_w for the free surface and the plane wall respectively, specific heat c of the liquid, the acceleration due to gravity (0, -g, 0) (or (0, g, 0) when the gravity acts upwards with respect to the liquid layer), and the surface tension coefficient given by (2.1). From these quantities, representative values can be taken as follows: h_a for the y scale, ι for the x scale, $\iota h_a/D$ for the time, D for the stream function, $\mu D/h_a^2$ for the pressure and T_a for the temperature. In this connection, various nondimensional parameters are defined as

$$\varepsilon = \frac{h_a}{\iota} \qquad \text{Shallow water parameter,}$$

$$P_r = \frac{\mu}{\rho D} \qquad \text{Prandtl number,}$$

$$M_R = \frac{\partial \sigma}{\partial T} \frac{T_a h_a}{\mu D} \qquad \text{Marangoni number,} \qquad (2.2)$$

$$N_C = \frac{\mu D}{\sigma(T_a) h_a} \qquad \text{Crispation number,}$$

$$B_o = \frac{\rho g h_a^2}{\sigma(T_a)} \qquad \text{Bond number,}$$

$$B_g = \frac{K_g h_a}{\rho c D} \qquad \text{Biot number for the free surface,}$$

$$B_w = \frac{K_w h_a}{\rho c D} \qquad \text{Biot number for the plane wall.}$$

Since we consider the surface waves of long wavelength, the shallow water parameter ε is taken to be sufficiently small and it is adopted as a measure for the small order of magnitude. It should be noted here that the Marangoni number takes negative values, since $\partial\sigma/\partial T$ is negative for most liquids.[20] The Bond number is set to be positive when the gravity acts downwards, while negative when it acts upwards.

Basic equations for this Marangoni convection system are given, in nondimensional form, as

$$\frac{\varepsilon}{P_r}\frac{D}{Dt}\frac{\partial\psi}{\partial y} = -\varepsilon\frac{\partial p}{\partial x} + L^+\frac{\partial\psi}{\partial y}, \tag{2.3}$$

$$\frac{\varepsilon^2}{P_r}\frac{D}{Dt}\frac{\partial\psi}{\partial x} = \frac{\partial p}{\partial y} + W + \varepsilon L^+\frac{\partial\psi}{\partial x}, \tag{2.4}$$

$$\varepsilon\frac{DZ}{Dt} = L^+Z, \tag{2.5}$$

where ψ is the stream function, p is the pressure, $W \equiv B_o/N_C$, and $Z \equiv (T-T_a)/T_a$ denotes the deviation of temperature; the operators D/Dt and L^+ are defined as

$$\frac{D}{Dt} = \frac{\partial}{\partial t} + \frac{\partial \psi}{\partial y}\frac{\partial}{\partial x} - \frac{\partial \psi}{\partial x}\frac{\partial}{\partial y}, \tag{2.6a}$$

$$L^+ = \frac{\partial^2}{\partial y^2} + \varepsilon^2 \frac{\partial^2}{\partial x^2}. \tag{2.6b}$$

The boundary conditions at the free surface $y=h(x,t)$ are given by the tangential stress balance, the normal stress balance, the kinematic condition and the Newton's cooling law:

$$\cos 2\theta\,(L^- \psi) - 2\varepsilon \sin 2\theta \frac{\partial^2 \psi}{\partial x\,\partial y} = M_R\left(\varepsilon \cos\theta \frac{\partial Z}{\partial x} + \sin\theta \frac{\partial Z}{\partial y}\right), \tag{2.7}$$

$$p - p_g + 2\varepsilon \cos 2\theta \frac{\partial^2 \psi}{\partial x\,\partial y} + \sin 2\theta\,(L^- \psi) = -\varepsilon^2\left(\frac{1}{N_C} + M_R Z\right)\cos^3\theta \frac{\partial^2 h}{\partial x^2}, \tag{2.8}$$

$$\frac{\partial h}{\partial t} + \frac{\partial \psi}{\partial y}\frac{\partial h}{\partial x} = -\frac{\partial \psi}{\partial x}, \tag{2.9}$$

$$\left(\frac{\partial Z}{\partial y} - \varepsilon^2 \frac{\partial h}{\partial x}\frac{\partial Z}{\partial x}\right)\cos\theta = -B_g(Z - Z_g), \tag{2.10}$$

where $\sigma(T)$ given by (2.1) causes the surface tension gradient in (2.7) and the surface tension in (2.8), and p_g and Z_g denote,

respectively, the constant pressure and the constant temperature in the still gas phase; θ and L^- are defined as

$$\tan\theta = \varepsilon \frac{\partial h}{\partial x}, \qquad L^- = \frac{\partial^2}{\partial y^2} - \varepsilon^2 \frac{\partial^2}{\partial x^2}. \tag{2.11a,b}$$

The boundary conditions at the plane wall y=0 are given by

$$\frac{\partial \psi}{\partial x} = \frac{\partial \psi}{\partial y} = 0, \tag{2.12a,b}$$

$$\frac{\partial Z}{\partial y} = B_w(Z - Z_w), \tag{2.13}$$

where Z_w denotes the temperature of the plane wall and it may depend upon x and t.

From typical material values cited in ref. 20, it is seen that, for most liquids, the typical order of magnitude of P_r is about 10. When we take the liquid layer of mean thickness about $10^{-5}\sim10^{-4}$[m], the order of magnitude of each parameter can be estimated as

$$M_R=10^2\sim10^3,\ N_C=10^{-4}\sim10^{-5},\ W=10^{-1}\sim10^2, \tag{2.14}$$

which are evaluated for pure water at about 20 [℃]. It should be noted, however, that M_R and N_C become large as the temperature of the liquid increases, or if some substance making the free surface active is solved in the liquid. On the other hand, when the wall is metal, it is well-known that the ratio B_g/B_w is sufficiently small in usual circumstances.[20] Taking these facts into account, we consider two examples, say Examples (i) and (ii) respectively, given by the following scalings:

(i) $\varepsilon = 0.001$, $Z_w = 0$, $B \equiv B_g/\varepsilon = O(1)$, $B_w \to \infty$,

$M \equiv M_R \varepsilon = O(1)$, $N_1 \equiv \varepsilon / N_C = O(1)$, $W = O(1)$; (2.15)

(ii) $\varepsilon = 0.01$, $Z_w = Ax$, $B_g = 0$, $B_w \to \infty$,

$M \equiv M_R \varepsilon = O(1)$, $N_2 \equiv \varepsilon^2 / N_C = O(1)$, $W = O(1)$, (2.16)

where the values of Z_w in (2.15) and of Z_w at $x=0$ in (2.16) have been set zero, since, by virtue of the ordering for B_g, the temperature distribution for the lowest order of ε becomes constant in the direction of thickness of the liquid layer. The temperature gradient A in (2.16) along the plane wall is taken as a constant of O(1). Example (i) is proposed to examine a nonlinear behavior of the surface deformation in the vicinity of zero wavenumber, which is compared with the existing results based on the linear stability analysis.[4,7] (To check a temporal variation of disturbances, a linear analysis for the unsteady mode is made in Appendix A.) Example (ii) may be of practical importance, because such an inhomogeneous temperature distribution along the wall often arises in actual phenomena. Quite recently, Sen[21] has investigated steady cavity flows due to the Marangoni effect with the constant temperature gradient along the bottom wall but without effects of the gravity. Example (ii) may also relate to such cavity flows due to the Marangoni effect.

§ 3. Nonlinear Analysis of Surface Waves (Example(i))

Making use of the small parameter ε and the ordering (2.15), we can carry out the iteration procedure for the equa-

tions (2.3)-(2.5) and the boundary conditions (2.7), (2.8), (2.10), (2.12) and (2.13). We thus obtain the following solutions for ψ, p and Z:

$$\psi = \varepsilon \frac{M_A}{2} \frac{\partial h}{\partial x} y^2 + \varepsilon \left(W \frac{\partial h}{\partial x} - \varepsilon N_1 \frac{\partial^3 h}{\partial x^3}\right)\left(\frac{1}{6} y^3 - \frac{1}{2} h y^2\right) - \varepsilon^2 M_A B h \frac{\partial h}{\partial x} y^2 + O\left(\frac{\varepsilon^2}{P_r}, \varepsilon^3\right), \tag{3.1}$$

$$p = p_g + W(h - y) - \varepsilon N_1 \frac{\partial^2 h}{\partial x^2} + O(\varepsilon^2), \tag{3.2}$$

$$Z = \varepsilon B Z_g (1 - \varepsilon B h) y + O(\varepsilon^3), \tag{3.3}$$

where $M_A = M \cdot B \cdot Z_g$ (whose meaning is given in Appendix A). In (3.1), we have neglected $O(\varepsilon^2/P_r)$ as well as $O(\varepsilon^3)$, because the effects of finite Prandtl number are little different from those of $P_r \to \infty$ as far as $P_r > 5$. Using (3.1), the kinematic condition (2.9) is now written as

$$\frac{\partial h}{\partial t_1} + \frac{M_A}{2} \frac{\partial}{\partial x}\left(h^2 \frac{\partial h}{\partial x}\right) - \left(\frac{W}{3} + \varepsilon M_A B\right) \frac{\partial}{\partial x}\left(h^3 \frac{\partial h}{\partial x}\right) + \frac{\varepsilon}{3} N_1 \frac{\partial}{\partial x}\left(h^3 \frac{\partial^3 h}{\partial x^3}\right) = O\left(\frac{\varepsilon}{P_r}, \varepsilon^2\right). \tag{3.4}$$

Here we have introduced a slow time variable $t_1 \equiv \varepsilon t$, since a temporal variation of h must occur very slowly with respect to the original time variable t: although such a stretching of the time scale can be justified systematically by invoking the method of multiple scales,[22] the details of derivation are very cumbersome and omitted here. Because of this time scaling, the equa-

tion (3.4) describes a temporal evolution of $h(x, t_1)$ on discarding the terms of $O(\varepsilon/P_r, \varepsilon^2)$. It should be noted here that, since M is negative, M_A must take opposite sign to Z_g: if $M_A<0$ (i.e., $Z_g>0$), the Marangoni effect plays a role of nonlinear diffusion, but if $M_A>0$, it acts as an inverse diffusion. In the third term, the effect of gravity plays a similar role according as $W>0$ or $W<0$. In contrast to these, the fourth term acts always as a diffusion. When we set as $M_A>0$ and $W=0$ and discard the terms of $O(\varepsilon)$, (3.4) is reduced to a simple nonlinear equation with the inverse diffusion, which causes explosion of its solution at a certain time.[10] A special case of (3.4) with $M_A=N_1=0$ and $W>0$ has been studied for nonlinear thermal conduction,[23] spreading viscous liquid drop[24] and weakly nonlinear waves on highly viscous liquid layer.[25]

Following the results of the linear stability analysis,[4,7] the critical Marangoni number M_{AC} (i.e., the eigenvalue in the limit of zero wavenumber for the steady mode) can be given, in our notation, as

$$M_{AC} = \frac{2}{3} W(1 + \varepsilon B)^2. \tag{3.5}$$

Therefore, if M_A is taken, with a constant shift M_a (>0), as

$$M_A = \frac{2}{3} W(1 + 2\varepsilon B) + \varepsilon M_a > M_{AC}, \tag{3.6}$$

values of M_A correspond to an unstable state predicted by the linear stability theory (refer to Fig.A1 in Appendix A). Substituting (3.6) into (3.4), and setting $h=1+\varepsilon\tilde{h}$, we get the ap-

proximate form of (3.4):

$$\frac{\partial \tilde{h}}{\partial t_2} + \alpha \frac{\partial}{\partial x}\left(\tilde{h} \frac{\partial \tilde{h}}{\partial x}\right) + \beta \frac{\partial^2 \tilde{h}}{\partial x^2} + \gamma \frac{\partial^4 \tilde{h}}{\partial x^4} = 0, \tag{3.7}$$

where

$$\alpha = -\frac{W}{3}, \quad \beta = \frac{M_a}{2}, \quad \text{and} \quad \gamma = \frac{N_1}{3}. \tag{3.8}$$

The slower time variable $t_2 \equiv \varepsilon t_1 \equiv \varepsilon^2 t$ is employed here, which is again guaranteed by the method of multiple scales. If the amplitude of $\tilde{h}$ is taken to be infinitesimal, (3.7) admits the solution of the form $\tilde{h} \propto \exp(ikx + \lambda t_2)$ with the wavenumber k and the complex growth rate λ, for which the characteristic equation for λ is given by

$$\lambda = k^2(\beta - \gamma k^2). \tag{3.9}$$

It follows from this that $\tilde{h}$ decreases in time if $0 < \beta < \gamma k^2$, i.e., the disturbances of non-zero wavenumbers still decay for β in this range, though values of M_A given by (3.6) are over the critical Marangoni number in the limit of zero wavenumber. It should be noted, however, that surface deformations of small but finite amplitude may become steady or even unstable for $0 < \beta < \gamma k^2$, as will be shown in § 4. If $\beta > \gamma k^2$, the surface deformations are always unstable even for an infinitesimal amplitude of $\tilde{h}$, as predicted by the linear stability analysis.[4,7]

Let us consider the equation (3.7) under the spatially periodic condition with a period L:

$$\tilde{h}(x, t_2) = \tilde{h}(x+L, t_2). \tag{3.10}$$

Integrating (3.7) in the range $0 \leqq x \leqq L$, and using (3.10), we find

that the first moment of $\tilde{h}(x, t_2)$ is always conserved:

$$\frac{d}{dt_2}\int_0^L \tilde{h}\, dx = 0. \tag{3.11}$$

Then, we find that the higher moments of $\tilde{h}(x, t_2)$ may not be conserved. On the other hand, we can obtain the steady periodic solution of (3.7):

$$\tilde{h}(x) = \frac{48\gamma}{\alpha L^2} u(x), \tag{3.12a}$$

where $u(x)$ is expressed by the cnoidal function:

$$u(x) = u_0 + u_1\, cn^2(ax, m), \tag{3.12b}$$

with

$$u_0 = -K(m)[E(m) + (m^2-1)K(m)], \tag{3.13a}$$

$$u_1 = m^2 K(m)^2, \tag{3.13b}$$

$$a = 2\sqrt{u_1}/mL, \tag{3.13c}$$

$$m = \frac{1}{K(m)}\sqrt{\frac{\beta L^2}{16\gamma} - 3K(m)E(m) + 2K(m)^2}, \tag{3.13d}$$

where $K(m)$ and $E(m)$ denote, respectively, the complete elliptic integrals of the first and the second kinds. The modulus m in (3.13d) can be determined by the iteration procedure for given values of β, γ and L. Using (3.12) and (3.13), the second moment of $\tilde{h}(x)$ can be expressed, in terms of $u(x)$, as

$$\frac{1}{L}\int_0^L u^2\, dx = \frac{1}{3}K(m)^2[(m^2-1)K(m)^2 - (2m^2-4)K(m)E(m) - 3E(m)^2]. \tag{3.14}$$

These expressions for the steady solution ((3.12)-(3.14)) give an important condition to classify various solutions of (3.7), which will be shown in §4.

§4. Numerical Analysis for Equation (3.7)

Let us solve (3.7) numerically using the method of finite difference. The calculation procedure is given in Appendix B, where the difference equation (B.2) approximating (3.7) is derived. We now take an initial value as

$$\tilde{h}(x,0) = -\cos \pi x, \tag{4.1}$$

for which the period is set as $L=2\pi/k=2$, the first moment of $\tilde{h}(x,0)$ as zero, and the second moment as unity. The actual calculations have been carried out for $\alpha=1$ and for various values of β and γ, whose representative values are shown in Table I together with a rough type-classification of the solutions thus obtained. The asymptotic behavior of the surface deformation at large times may be classified into three types: damping type (labeled as 'D'), steady type, and explosive type ('E'). It should be noted here that the classification for $\gamma=1$ and 0.1 (for the first and the second columns in Table I) may be predicted by (3.9), but that for $\gamma=0.01$ shows always explosive type even when $\beta<\gamma k^2$. To illustrate temporal variations of the numerical solutions, the value of $\tilde{h}(x,t_2)$ at the center plane ($x=L/2=1$), which is denoted by h_{max}, is plotted against t_2 in Fig. 1 for each typical set of β and γ: note that the final sampling time has been set as $t_2=t_s\times 64=0.08192$ for the sampling

Table I. Classification of numerical solutions (α=1):

D --- Damping type and E --- Explosive type.

β \ γ	1.0	0.1	0.01	0.001
2.0	D	E1	E3	E5
1.75	D	E1	E3	E5
1.5	D	E1	E3	E5
1.25	D	E1	E3	E5
1.0	D	E1	E3	E4
0.75	D	D	E3	E4
0.5	D	D	E3	E4
0.25	D	D	E3	E4
0.1	D	D	E2	E4
0.075	D	D	E2	E4
0.05	D	D	E2	E4
0.025	D	D	E2	E4
0.01	D	D	E2	E4

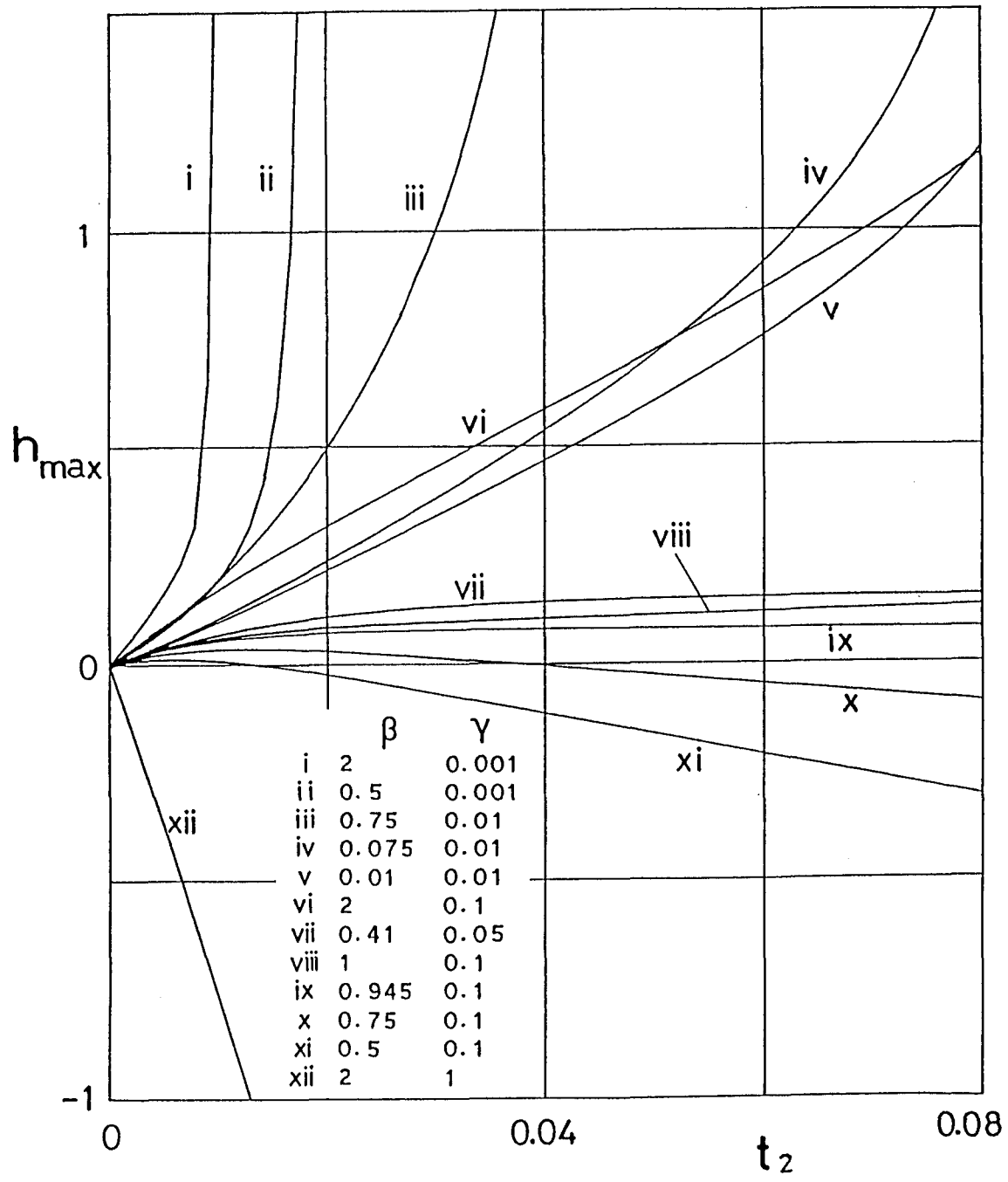

Fig. 1. Temporal variation of h_{max} (the value of $\tilde{h}$ at x=L/2) (natural-logarithmic scale) versus t_2 for various values of β and γ.

interval t_s (for the definition of t_s, see Appendix B). In view of Fig. 1 and Table I, we now discuss the wave profile for each typical case.

One typical example of the damping solution is shown in Fig. 2, where the solid line denotes the wave profile at t_2=0.0256 and the broken line denotes the initial profile (4.1). This solution decreases subject to (3.9), so that h_{max} vanishes before the final sampling time (see the result for β=2 and γ=1 in Fig. 1). The other example is the damping solution such that h_{max} grows for small t_2 but decays at large t_2 (see the results for β=0.5 and β=0.75 with γ=0.1 in Fig. 1): note that (3.9) may also be applied to predict the decaying manner.

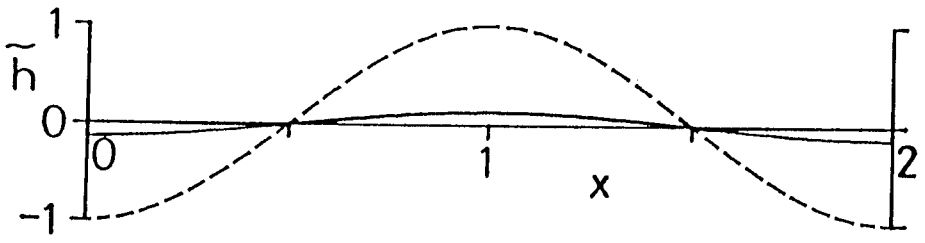

Fig. 2. Damping solution at t_2=0 (broken line) and t_2=0.0256 (solid line) for β=2 and γ=1.

Owing to the inverse diffusion term in (3.7), the explosive solution, which is characterized by a continuously growing h_{max}, can be found more easily rather than the steady solution. According to the classification in Table I, five typical patterns of explosion are displayed in Figs. 3-7. The first example shown in Fig. 3 represents the solutions labeled as 'E1' (which include an unstable harmonic component giving $\beta > \gamma k^2$). Comparing this with the initial profile, we find that the convex portion of $\tilde{h}(x, t_2)$ becomes more convex, while the concave portion becomes more concave, as indicated by the arrows in Fig. 3. It is then found that higher harmonics affect the growth of h_{max} at large t_2 (see the results for $\beta=2$ and $\beta=1$ with $\gamma=0.1$ in Fig. 1). The second example 'E2' (Fig. 4), which is found for $\beta < \gamma k^2$, shows that the concave portion becomes flat, though the convex portion shows a similar behavior to that in Fig. 3. It seems that the growth of h_{max} is due to the nonlinear inverse diffusion and such tendency becomes remarkable for smaller β and γ. (see the results for $\beta=0.01$ and $\beta=0.075$ with $\gamma=0.01$ in Fig. 1). The third example 'E3' (Fig. 5 for $\beta=0.75$ and $\gamma=0.01$) exhibits more remarkable tendency to explosion (see also Fig. 1), because h_{max} becomes larger than the critical value (that has been set twenty in the numerical calculation) before the final sampling time. Note that this example includes two unstable harmonics (i.e., $k=\pi$ and 2π). Furthermore, for the fourth example 'E4' shown in Fig. 6, it is seen that h_{max} grows more rapidly than those in Figs. 3-5, since this includes seven unstable harmonics (refer

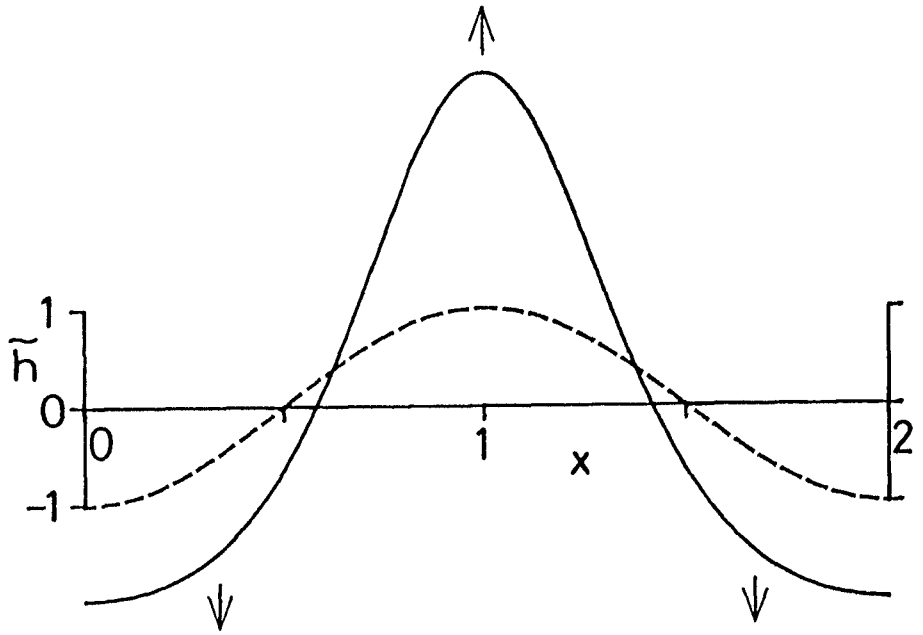

Fig. 3. Explosive solution of type E1 at $t_2=0$ (broken line) and $t_2=0.08192$ (solid line) for $\beta=2$ and $\gamma=0.1$.

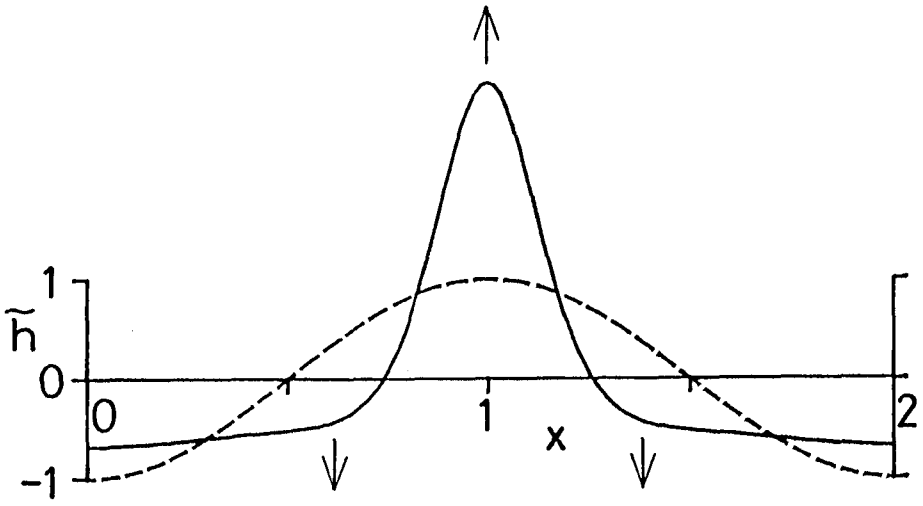

Fig. 4. Explosive solution of type E2 at $t_2=0$ (broken line) and $t_2=0.0768$ (solid line) for $\beta=0.01$ and $\gamma=0.01$.

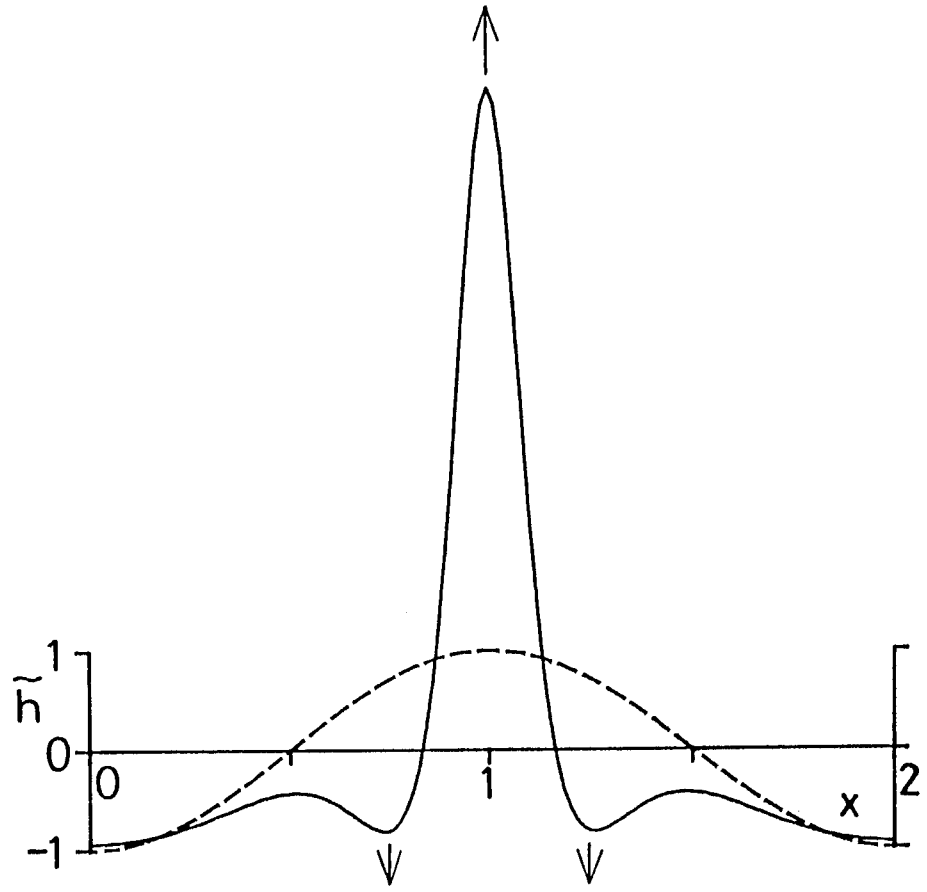

Fig. 5. Explosive solution of type E3 at $t_2=0$ (broken line) and $t_2=0.0384$ (solid line) for $\beta=0.75$ and $\gamma=0.01$.

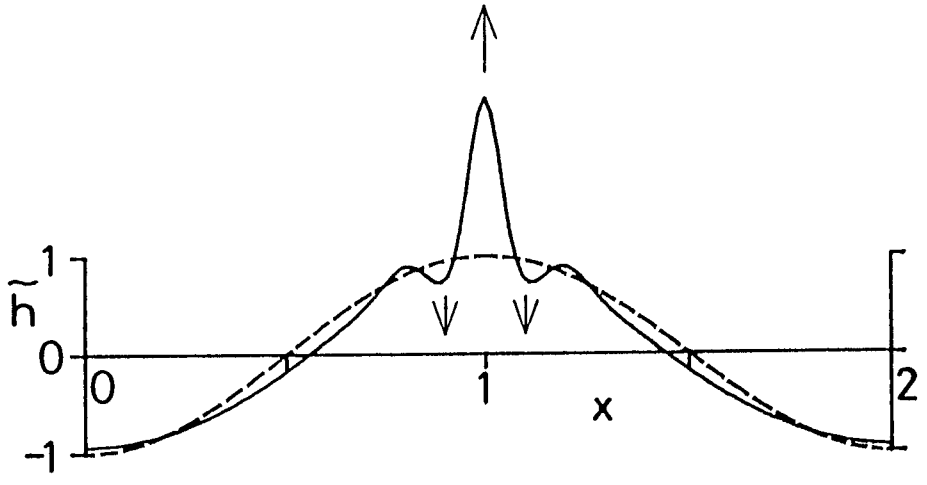

Fig. 6. Explosive solution of type E4 at $t_2=0$ (broken line) and $t_2=0.0166$ (solid line) for $\beta=0.5$ and $\gamma=0.001$.

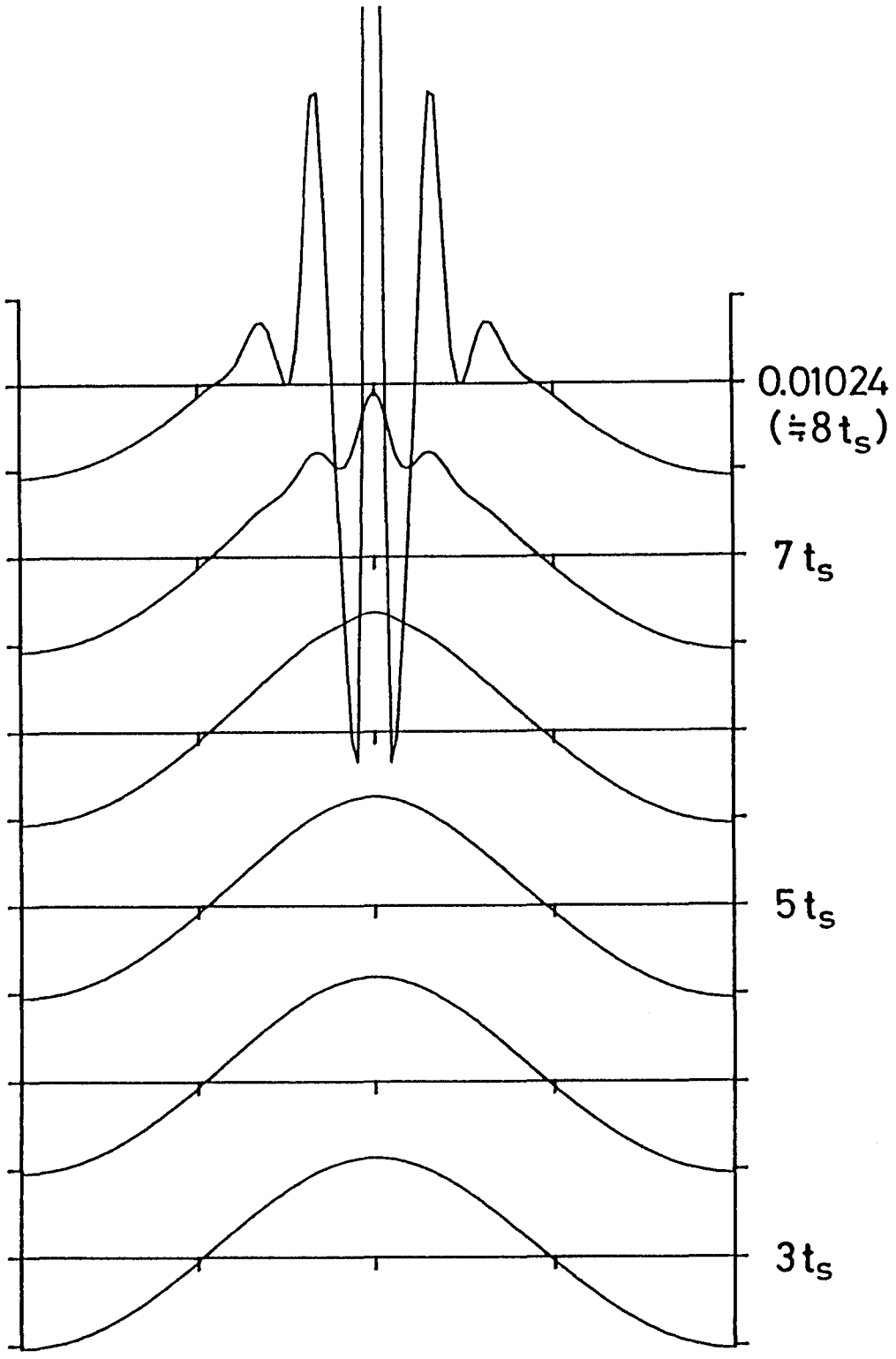

Fig. 7. Evolutional process of explosive solution of type E5 for $\beta=2$ and $\gamma=0.001$ from $t_2=3\times t_s$ to 0.01024 ($\fallingdotseq 8\times t_s$).

also to the result for $\beta=0.5$ and $\gamma=0.001$ in Fig. 1). Comparing Fig. 6 with Fig. 3, we find that the explosion of solution arises locally around the center (x=1). The evolution process of type 'E5' is illustrated in Fig. 7 for several time steps: the convex portion at the center grows, two additional convex portions appear around the center, and h_{max} then grows explosively (note that this example includes fourteen unstable harmonics). This is because the effect of the nonlinear inverse diffusion becomes so dominant that the growth of h_{max} is much accelerated (see the result for $\beta=2$ and $\gamma=0.001$ in Fig. 1). It is interesting to note here that the explosion process (Fig. 7) is very similar to that in Fig. 1 of ref. 14 (where the parameters were taken as $\alpha=1$, $\beta=0.01$ and $\gamma=5.066\times10^{-6}$ in our notation).

From the classification in Table I, it may be expected that the steady solution is possible for β and γ between their values giving Types 'D' and 'E'. Figure 1 also shows that h_{max} for $\gamma=0.1$ grows slowly for $\beta=1$, while it decays slowly for $\beta=0.75$: thus the range $0.75<\beta<1$ is suggested. The steady solution is found, in fact, for $\beta=0.945$ and $\gamma=0.1$ (see Fig. 1), and it is displayed in Fig. 8 in comparison with the analytical solution (3.12): both wave profiles show an excellent agreement. In this case, the second moment of $\tilde{h}(x, t_2)$ is found to change little from the initial instant up to the final sampling time (note that the second moment grows if we set initially $\beta=0.946$ but decays if we set $\beta=0.944$). The steady solutions are also found so far for four other cases: $\beta=0.006$ and $\gamma=0.02$, $\beta=0.1$ and $\gamma=$

0.02585, β=0.41 and γ=0.05 (given in Fig. 1), and β=0.088 and γ=0.025.

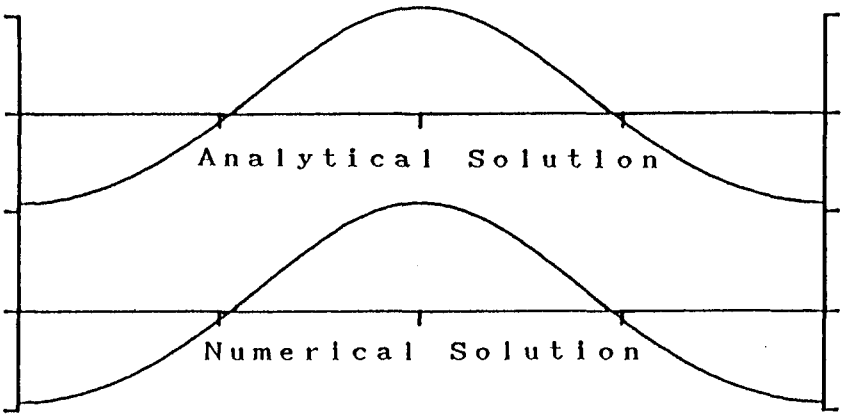

Fig. 8. Comparison of numerical steady solution with analytical one expressed by the cnoidal function for β=0.945 and γ=0.1.

For the solutions shown above, the second moment of the initial value (4.1) is transformed, to adapt it for the expression (3.14), into $(\alpha L^2/48\gamma)^2/L$, whose values are plotted against β/γ $(\equiv \beta L^2/4\gamma)$ in Fig.9 by the black circles. The data for cnoidal waves*) are also displayed by the white circles. The second moment given by (3.14) (for the left ordinate) and the modulus m given by (3.13d) (for the right ordinate) are drawn by the solid lines. The circles on the curve of (3.14) represent the steady solutions obtained numerically, while the circles below or above the curve denote, respectively, the damping solutions or the explosive ones: note that the data of $(\alpha L^2/48\gamma)^2/L$ for each column in Table I are given as 3.472×10^{-3} for $\gamma=1$, 0.3472 for $\gamma=0.1$, and 34.72 for $\gamma=0.01$. Therefore it is found that if and only if the initial second moment for prescribed values of β and γ takes the same value as (3.14), the wave form is deformed in time without changing both values of the first and the second moments, and it arrives asymptotically at the steady

---

*) The numerical analysis has also been carried out by taking the cnoidal wave as initial value. Using (3.12)-(3.14), the initial wave forms with numerical accuracy of 8 figures have been employed. For these initial values, the tendency to converge to the steady solutions (3.12) has been confirmed. However, when perturbations of small magnitude about 10^{-5} are added to the cnoidal waves, the convergence to the steady solutions becomes unstable.

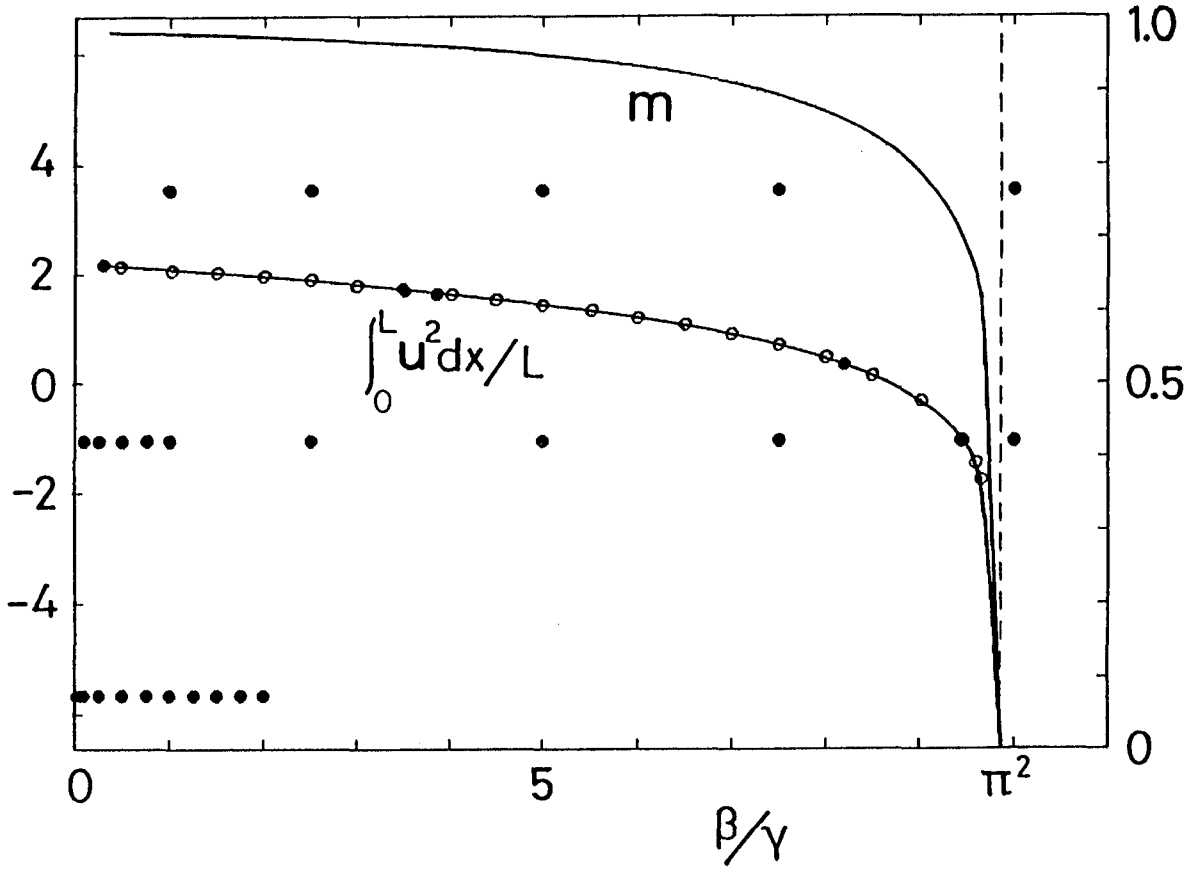

Fig. 9. The second moment $\int_0^L u^2\,dx/L$ (taken in natural-logarithmic scale for the left ordinate) and the modulus m of the complete elliptic integral (taken in linear scale for the right ordinate) versus β/γ with fixed values $\alpha=1$ and L=2: the black circles denote the data of the second moment for harmonic waves, while the white ones for cnoidal waves.

solution (3.12), though the time necessary to attain the steady solution depends strongly upon the deviation of the initial wave form from the steady solution. It is also interesting to note that solitary waves may arise for small values of β/γ, i.e., for Marangoni numbers slightly above the critical Marangoni number M_{AC}, while harmonic waves can arise on the neutral curve of linear stability. These may remind us of the critical amplitude of disturbances for subcritical state in the theory of nonlinear stability.[26] On the other hand, for the explosive type of solutions with $\beta > \gamma k^2$, it seems that the evolution equation (3.7) becomes invalid after some finite time (refer also to the discussions in ref. 14).

For the initial values given by the cnoidal wave, we can derive another condition to arrive at the steady solutions. If we take the steady solution $\tilde{h}$ given by (3.12) as an initial condition to the following equation:

$$\frac{\partial \tilde{h}}{\partial t_2} + \alpha \frac{\partial}{\partial x}\left(\tilde{h} \frac{\partial \tilde{h}}{\partial x}\right) + (\beta + \beta^+)\frac{\partial^2 \tilde{h}}{\partial x^2} + \gamma \frac{\partial^4 \tilde{h}}{\partial x^4} = 0, \qquad (4.2)$$

$\tilde{h}$ governed by (4.2) must evolve in time due to the parameter perturbation β^+. For a short interval from the initial instant, we can consider that the evolution of $\tilde{h}$ subject to (4.2) satisfies the periodic condition (3.10) and the conservation relation (3.11), then the second moment of $\tilde{h}$ should satisfy the following equation:

$$\frac{d}{dt_2}\int_0^L \tilde{h}^2 \, dx = 2\beta^+ \int_0^L \left(\frac{\partial \tilde{h}}{\partial x}\right)^2 dx. \qquad (4.3)^*$$

---

* The initial condition $\tilde{h}$ taken above satisfies the following equation: $\alpha \frac{\partial}{\partial x}(\tilde{h} \frac{\partial \tilde{h}}{\partial x}) + \beta \frac{\partial^2 \tilde{h}}{\partial x^2} + \gamma \frac{\partial^4 \tilde{h}}{\partial x^4} = 0$ together with the conditions (3.10) and (3.11). Taking the difference between this equation and (4.2), one obtains $\frac{\partial \tilde{h}}{\partial t_2} + \beta^+ \frac{\partial^2 \tilde{h}}{\partial x^2} = 0$. Multiplying it by $\tilde{h}$ and integrating the resultant with respect to x, we have (4.3).

Thus we find that the second moment of $\tilde{h}$ increases in time if $\beta^+ > 0$, but decreases if $\beta^+ < 0$. This implies the mismatch of the second moment between the value given by the prescribed parameters and that required to make up the steady solution to the equation (4.2). Therefore, it follows from this that the steady surface deformations arise only when $\beta^+ = 0$. This approach can be applied similarly to a parameter perturbation for γ.

§ 5. Effect of Inhomogeneous Temperature Distribution (Example (ii))

Carrying out a similar iteration procedure to that in § 3, subject to the ordering (2.16), we obtain

$$\psi = \frac{M_b}{2} y^2 + \varepsilon \left(W \frac{\partial h}{\partial x} - N_2 \frac{\partial^3 h}{\partial x^3} \right) \left(\frac{1}{6} y^3 - \frac{1}{2} h y^2 \right) - \frac{\varepsilon M_b^2}{2} h^2 \frac{\partial h}{\partial x} y^2 + O(\varepsilon^2), \tag{5.1}$$

$$p = p_g + W(h-y) - (N_2 + \varepsilon M_b x)\frac{\partial^2 h}{\partial x^2} - 2\varepsilon M_b \frac{\partial h}{\partial x} + O(\varepsilon^2), \quad (5.2)$$

$$Z = Ax + \varepsilon M_b A\left(\frac{1}{6} y^3 - \frac{1}{2} h^2 y\right) + O(\varepsilon^2), \quad (5.3)$$

where $M_b = M \cdot A$. Using (5.1) and (2.9), we can obtain the evolution equation for Example (ii). Then, its approximate form can be derived as follows: setting $h = 1 + \varepsilon \tilde{h}(x, t)$ and retaining the terms up to $O(\varepsilon)$, one obtains

$$\frac{\partial \tilde{h}}{\partial t_1} + M_b \tilde{h} \frac{\partial \tilde{h}}{\partial \xi} - W_1 \frac{\partial^2 \tilde{h}}{\partial \xi^2} + \frac{N_2}{3} \frac{\partial^4 \tilde{h}}{\partial \xi^4} = 0, \quad (5.4)$$

where $\xi \equiv x - M_b t$, $t_1 \equiv \varepsilon t$ and $W_1 \equiv W/3 + M_b{}^2/2$. This describes the evolution of $\tilde{h}$ with respect to the slow time variable t_1 in a frame of reference moving with the constant velocity M_b. When $W_1 < 0$ (i.e., for the liquid layer bounded above by the wall and below by the gas phase), (5.4) corresponds to the Kuramoto-Sivashinsky equation.[16,17] As was shown by Kuramoto and Tsuzuki,[16] the equation (5.4) with $W_1 < 0$ has a 'steady' shock-like solution which is expressed, in our notation, as

$$\tilde{h}(\xi) = \frac{2N_2}{3M_b} v(\xi), \quad (5.5a)$$

where

$$v(\xi) = 60\left(\left(-\kappa^3 - \frac{3W_1}{38N_2}\kappa\right)\tanh \kappa \xi + \kappa^3 \tanh^3 \kappa \xi\right), \quad (5.5b)$$

with

$$\kappa = \sqrt{-\frac{33W_1}{76N_2}} . \qquad (5.6)$$

On the other hand, when W_1 is positive, (5.5) does also hold if one takes κ as

$$\kappa = \sqrt{\frac{3W_1}{76N_2}} . \qquad (5.7)$$

The typical wave form given by (5.5) and (5.6) (say Type(A)) and that given by (5.5) and (5.7) (say Type(B)) are illustrated in Fig. 10. For both wave forms of Types(A) and (B), the sign of M_b determines the progressive direction of the waves.

Quite recently, Alekseenko et al.[27] have made experiments for nonlinear waves on a falling liquid film, and they have found several types of traveling wave solutions governed by the Kuramoto-Sivashinsky equation. (Refer also to Chang.[28]) Such solutions may also arise in the Marangoni convection systems subject to (5.4).

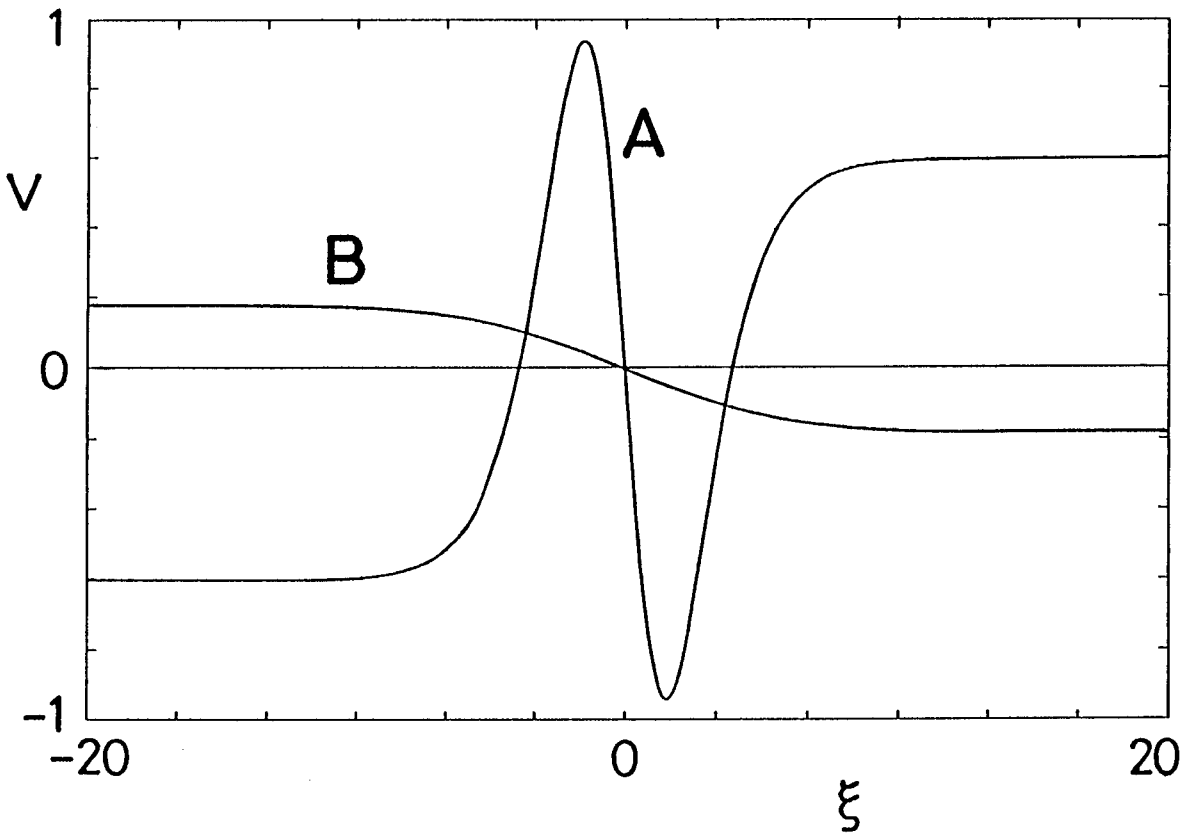

Fig. 10. Two types of shock wave solutions $v(\xi)$ for $M_b>0$, propagating in the positive direction of ξ (for simplicity, the absolute value of W_1/N_2 is set as 1/3).

Appendix A: Linear Theory for the Unsteady Mode

In order to examine an unsteady problem against small disturbances, we begin by showing the basic, equilibrium rest state with a flat free surface. Its temperature $T=\bar{T}(y)$ is governed by the equation:

$$\frac{d^2\bar{T}}{dy^2} = 0, \tag{A. 1}$$

with the boundary conditions:

$$\frac{d\bar{T}}{dy} = -B_g(\bar{T} - T_g) \qquad \text{at the flat surface } y=1, \tag{A. 2a}$$

$$\frac{d\bar{T}}{dy} = B_w(\bar{T} - T_w) \qquad \text{at the plane wall } y=0, \tag{A. 2b}$$

where T_g and T_w denote, respectively, the temperature of the gas phase and that of the wall, the Biot numbers B_g and B_w being given in (2. 2); to specify again the scaling of temperature, T_g, T_w and $\bar{T}(y)$ are taken in dimensional form. From (A. 1) and (A. 2), we have $\bar{T}(y)$:

$$\bar{T}(y) = ay + b, \tag{A. 3}$$

where

$$a = \frac{B_gB_w(T_g - T_w)}{B_gB_w + B_w + B_g}, \qquad b = \frac{B_gT_g + B_w(1 + B_g)T_w}{B_gB_w + B_w + B_g}, \tag{A. 4a, b}$$

for which the equilibrium temperature T_a at the free surface is expressed as

$$T_a \equiv \bar{T}(1) = a + b. \tag{A. 4c}$$

Using (A. 4), we re-define the Marangoni number as $M_B \equiv aM_R/T_a$ in terms of the temperature difference $a=\bar{T}(1)-\bar{T}(0)$ and M_R given in

(2.2). When $B_g \to 0$, we get $T(0)=b=T_w$ and $T(1)=a+b=T_w$, so that a uniform distribution $\bar{T}(y)=T_w$, for which $Z \equiv (\bar{T}-T_a)/T_a=0$, holds in the liquid layer. When $B_w \to \infty$, we get $a=T_a B_g (Z_g-Z_w)/(1+B_g)$. Therefore, for this limiting case, we may set $M_B=M_A/(1+\varepsilon B)$ where $M_A \equiv M_R B_g Z_g = MBZ_g$ and $B_g=\varepsilon B$.

For a perturbed state, small disturbances which are denoted with prime are superimposed upon the equilibrium state. They are decomposed in the normal mode as

$$[-\frac{\partial \psi'}{\partial x}, \frac{T'}{a}, h'] = [f(y), g(y), s] \exp(ikx + \lambda t), \qquad (A.5)$$

where k is the wavenumber, λ is the complex growth rate, and εx is replaced here by x. Linearizing the equations (2.3)-(2.13) with respect to the disturbances, and using (A.5), we obtain the governing system of equations for f, g and s:

$$(\mathcal{L} - \frac{\lambda}{P_r})\mathcal{L} f = 0, \qquad (A.6)$$

$$(\mathcal{L} - \lambda) g = f, \qquad (A.7)$$

$$f = \lambda s \qquad \text{at } y=1, \qquad (A.8)$$

$$(\mathcal{L} + 2k^2) f = M_B k^2 (g + s) \qquad \text{at } y=1, \qquad (A.9)$$

$$(\mathcal{L} - 2k^2 - \frac{\lambda}{P_r})\frac{df}{dy} = k^2(k^2 + B_o)\frac{s}{N_C} \qquad \text{at } y=1, \qquad (A.10)$$

$$\frac{dg}{dy} = - B_g (g + s) \qquad \text{at } y=1, \qquad (A.11)$$

$$f = \frac{df}{dy} = \frac{dg}{dy} - B_w g = 0 \qquad \text{at } y=0, \qquad (A.12)$$

where $\mathcal{L}=d^2/dy^2-k^2$. Solving (A.6)-(A.12), we obtain an eigen-

value relation:

$$M_B = F(k, B_g, B_w, N_C, B_o, \lambda, P_r). \tag{A.13}$$

From this, we then get the asymptotic form of M_B in the limit of $k \to 0$:

$$M_B \sim \frac{\lambda}{k^2 P_r} G(B_g, B_w, N_C, B_o, \lambda, P_r). \tag{A.14}$$

The explicit form of G is omitted here. It should be noted that (A.14) has very different dependence on the wavenumber k as compared with the asymptotic form of M_B (M_{BC}, say) for the steady mode:

$$M_{BC} = \frac{2B_o}{3N_C} \frac{B_w(1 + B_g) + B_g}{B_w} + O(k^2), \tag{A.15}$$

which is derived from (A.13) by setting $k \ll 1$ and $\lambda = 0$: this reduces for $B_w \to \infty$ to the critical Marangoni number in the limit of zero wavenumber which corresponds to (3.5). For $B_w \to \infty$ and for λ sufficiently small (i.e., slow time variation), (A.14) and (A.15) lead to the following relation of λ:

$$\lambda \propto \frac{2B_o}{3N_C}(1 + B_g)k^2 + (M_B - M_{BC})k^2 + O(k^4), \tag{A.16}$$

which assures the derivation of (3.7).

Examples of the eigenvalue relation (A.13) are displayed in Fig.A1 for various values of the equi-growth rate λ (=real constant), in which we set as $P_r = 10$, $B_w = 10^5$, $B_g = 10^{-5}$, and $N_C = B_o = 0.0005$ (that gives W=1) on account of the scaling (2.15). The steady neutral curve of M_B (which is given at k=0 by (A.15)) may

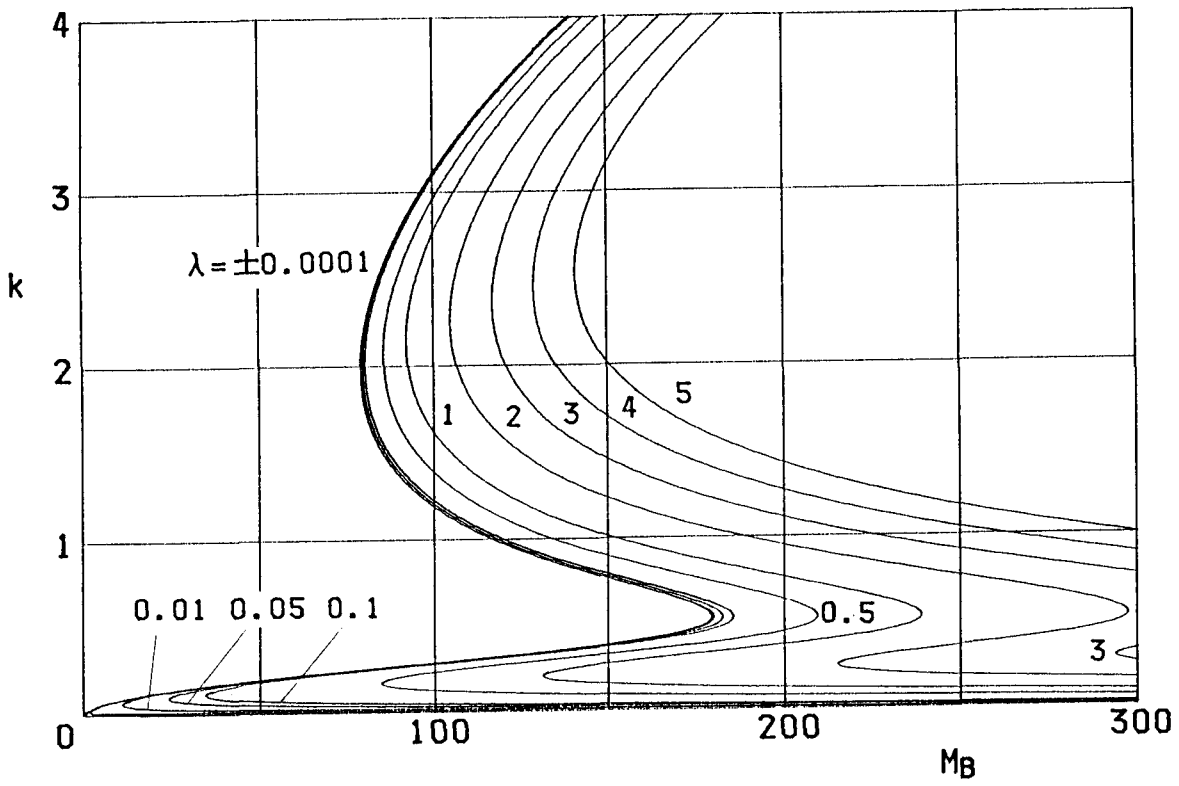

Fig. A1. Curves of equi-growth rate for various values of λ with setting $P_r=10$, $B_w=10^5$, $B_g=10^{-5}$, and $N_C=B_o=0.0005$ (which gives W=1).

arise in between the curves for $\lambda=-0.0001$ and $\lambda=0.0001$. Maximal values of M_B with respect to k give a guide line below which, i.e., for the smaller wavenumbers, the effect of surface deformation dominates over the convective term in (A.7). In Fig.A1, we find that the curves for $|\lambda|<0.1$ exist near the steady neutral curve, which supports the validity of the slow time scale introduced in § 3. For $\lambda \lesssim 0$, the disturbances of non-zero wavenumbers will decay if their amplitude is infinitesimal, but they may become steady or even unstable if it is finite: this is the case that was discussed in § 3 and § 4. It is also found that the lowest value of M_B for $0<\lambda<<1$ appears at small but finite values of k, which is often called 'extrinsic' instability: the effect of surface deformation may give rise to large but finite size of convection cells when M_B increases over M_{BC}.

We now examine typical examples which may be found in other heat transfer systems. The case of small Prandtl number ($P_r=0.1$) and the insulating case ($B_g=B_w=0$) are shown, respectively, in Figs.A2 and A3. It follows from Fig.A2 that the deviation of M_B (for $\lambda \neq 0$) from the steady neutral curve (which is again found in between the curves for $\lambda=\pm 0.0001$) appears remarkably in contrast to that in Fig.A1: the growth rate seems to be estimated by λ/P_r rather than λ itself. In Fig.A3, the curves for $|\lambda|<0.1$ are found around the steady neutral curve (that gives the critical Marangoni number as $M_{BC}=48$ at $k=0$[2]).

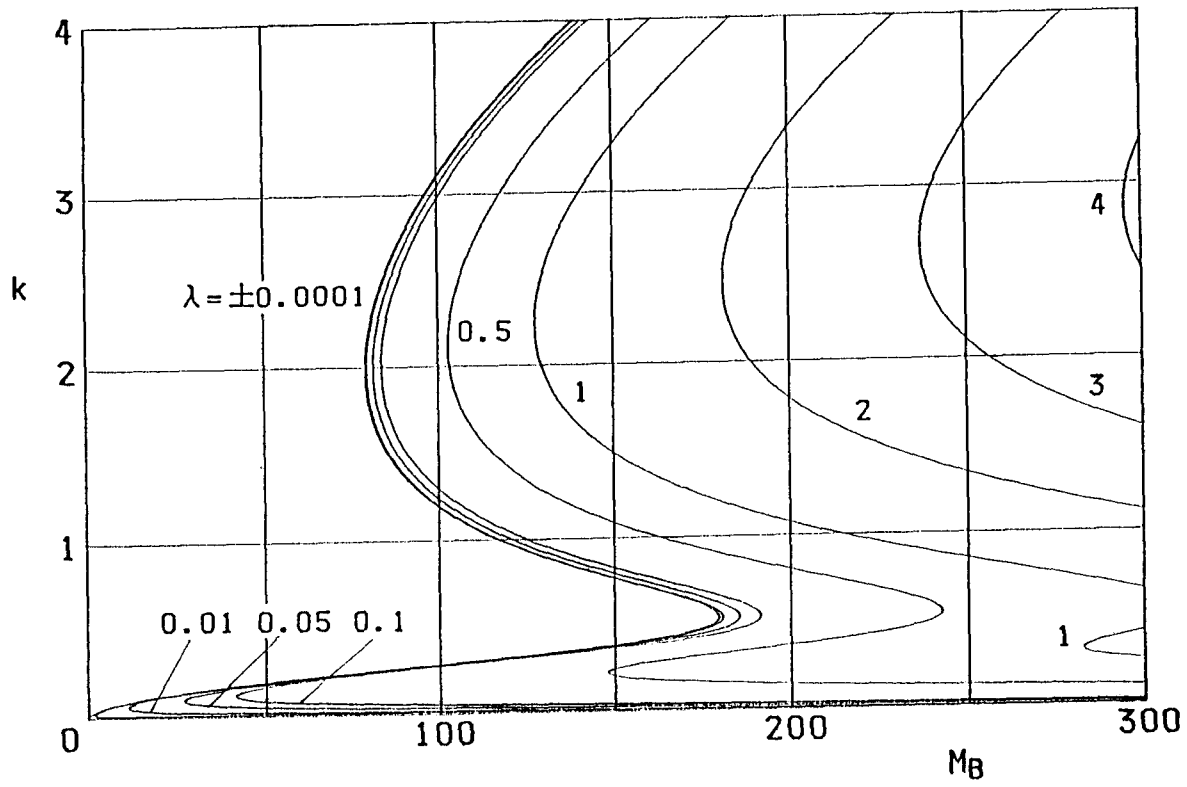

Fig. A2. Curves of equi-growth rate for various values of λ with setting $P_r=0.1$, $B_w=10^5$, $B_g=10^{-5}$, and $N_C=B_o=0.0005$ (which gives W=1).

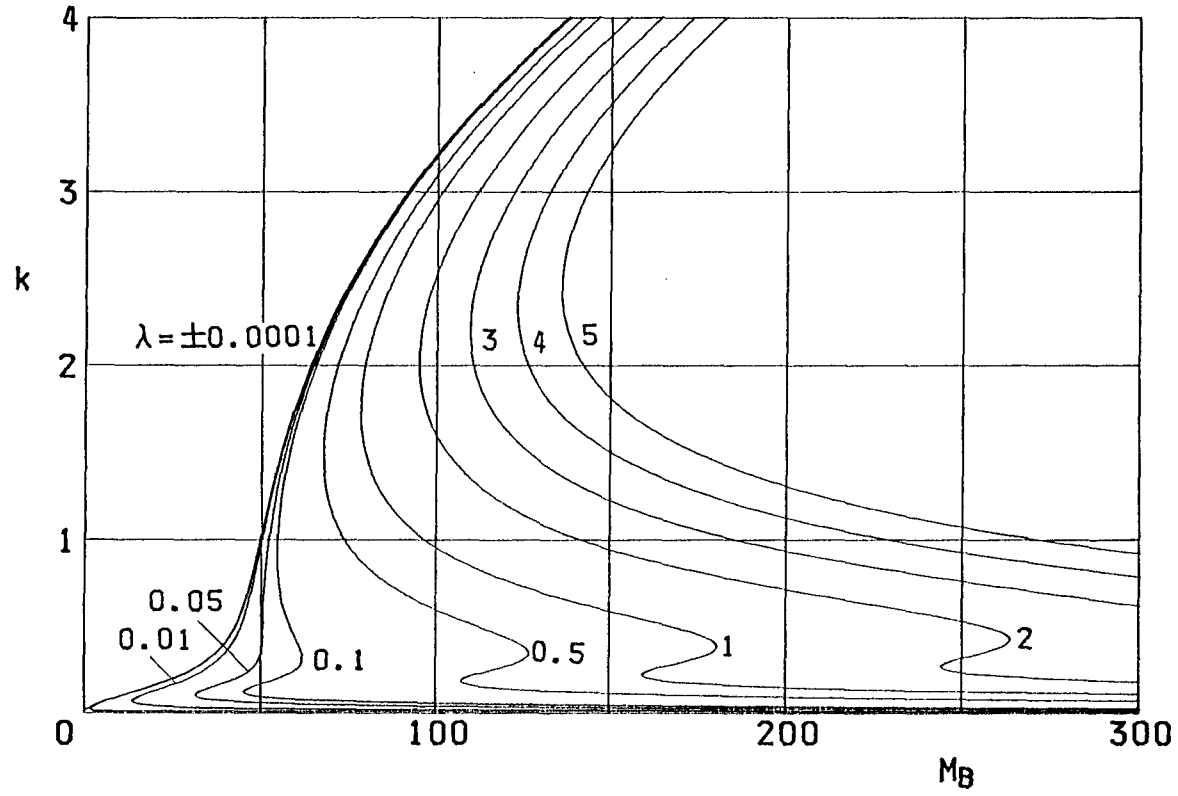

Fig. A3. Curves of equi-growth rate for various values of λ with setting $P_r=10$, $B_w=B_g=0$, and $N_C=B_o=0.0005$ (which gives W=1).

Appendix B: Procedure of the Numerical Analysis

We specify the procedure to solve the equation (3.7) numerically. By following the method of finite difference, the surface deformation $\tilde{h}(x, t_2)$ is now written as

$$\tilde{h}(x, t_2) = \tilde{h}(i\,\delta,\ j\,\tau) \equiv h_{i,j}, \tag{B.1}$$

where δ and τ stand for the finite differences for space and time respectively, thus $h_{i,j}$ denotes the value of $\tilde{h}(x, t_2)$ at a mesh point (i, j) in the (x, t_2) plane. Using (B.1), we can obtain the following difference equation approximating (3.7):

$$\begin{aligned} h_{i,j+1} = h_{i,j} &- \frac{\alpha\,\tau}{4\,\delta^2}[h_{i+1,j}(h_{i+2,j} - h_{i,j}) - h_{i-1,j}(h_{i,j} - h_{i-2,j})] \\ &- \frac{\beta\,\tau}{\delta^2}(h_{i+1,j} - 2h_{i,j} + h_{i-1,j}) \\ &- \frac{\gamma\,\tau}{\delta^4}(h_{i+2,j} - 4h_{i+1,j} + 6h_{i,j} - 4h_{i-1,j} + h_{i-2,j}) \\ &+ E_{i,j}, \end{aligned} \tag{B.2}$$

with the total error $E_{i,j}$ given by

$$E_{i,j} = \tau\,(E^{(1)}{}_{i,j} + \alpha E^{(2)}{}_{i,j} + \beta E^{(3)}{}_{i,j} + \gamma E^{(4)}{}_{i,j}). \tag{B.3}$$

Here $E^{(n)}{}_{i,j}$ for $n=1,2,3,4$ (for the respective terms in (3.7)) denote the deviations arising from the finite difference scheme. Using the Taylor-expansion, they may be estimated as

$$E^{(1)}{}_{i,j} = \frac{\tau}{2}\left(\frac{\partial^2 \tilde{h}}{\partial t_2{}^2}\right)_{i,j} + O(\tau^2), \tag{B.4a}$$

$$E^{(2)}_{i,j} = \frac{\delta^2}{2}\left[\frac{\partial^2}{\partial x^2}\left(\tilde{h}\frac{\partial^2 \tilde{h}}{\partial x^2}\right) - \frac{1}{3}\frac{\partial}{\partial x}\left(\tilde{h}\frac{\partial^3 \tilde{h}}{\partial x^3}\right)\right]_{i,j} + O(\delta^4), \tag{B.4b}$$

$$E^{(3)}_{i,j} = \frac{\delta^2}{12}\left(\frac{\partial^4 \tilde{h}}{\partial x^4}\right)_{i,j} + O(\delta^4), \tag{B.4c}$$

$$E^{(4)}_{i,j} = \frac{\delta^2}{6}\left(\frac{\partial^6 \tilde{h}}{\partial x^6}\right)_{i,j} + O(\delta^4). \tag{B.4d}$$

The period L (which is set as L=2 for the initial value (4.1)) and the finite difference δ lead to the equation $N=L/\delta$ for the number N of the mesh points along x, so that $h_{i,j}$ is taken for i=0 to N (note that the equation $h_{0,j}=h_{N,j}$ holds at every step of j, which corresponds to the periodic condition (3.10)). Although a lot of the mesh points may need to get high accuracy, due to the restricted performance of the computer, we set here as N=128 for which $\delta=1/64$. On the other hand, it is seen from (B.2) that the time difference τ should be taken so as to make the numerical calculation stable. To do so, strictly speaking, all the deviations $E^{(n)}_{i,j}$ given by (B.4a-d) should be taken into account. However, we content ourselves by adopting a loose condition as $\tau=\delta^4$ ($\fallingdotseq 5.953125\times10^{-8}=\tau_1$, say) for $\gamma<1$ and $\tau=0.1\times\delta^4$ ($\fallingdotseq 5.953125\times10^{-9}=\tau_2$, say) for $1\leqq\gamma<10$. Therefore, if the parameters α, β and γ and the magnitude of $h_{i,j}$ are of order unity, this setting for δ and τ implies that the total deviation $E_{i,j}$ is of order δ^6 and will be neglected in the actual calculations.

Following the algorithm mentioned above, $h_{i,j}$ can be ob-

tained at each step of j. But the number of results over many time-steps becomes enormous. To deal with this under the restriction of the memory capacity of the computer, we sample a series of data at every time interval t_s (where $t_s=21501\times\tau_1=1.28\times10^{-3}$ for $\gamma<1$ and $t_s=215013\times\tau_2=1.28\times10^{-3}$ for $1\leqq\gamma<10$), and we set the total number of sampling times as 64, for which the final sampling time is given by $t_s\times64=0.08192$. On the other hand, when (B.2) has an explosive solution (which was shown in § 4), the numerical calculation breaks down at a certain time step before the final sampling time, which is due to a numerical over-flow in the computer. To avoid the trouble, the actual calculation is terminated at the time step when the maximum value of $h_{i,j}$ becomes larger than twenty.

To check the numerical accuracy of $h_{i,j}$, we calculate the first moment of $h_{i,j}$ at every time step, and compare the result with the first moment of the initial value (4.1). The main results obtained from the numerical check are as follows: in accordance with trapezoidal rule, the integration of $h_{i,j}$ (the first moment) is of order of 10^{-15} for (4.1); $O(10^{-13})$ for the damping solution (Fig.2) at every time step; $O(10^{-11})$ for the explosive solutions (Figs.3-7) at the terminated time step; $O(10^{-12})$ for the steady solution (Fig.8) at the final sampling time. These data assure that all the computations hold with very high accuracy.

The numerical calculation has been carried out on the electronic computer MS-175 of Wakayama College of Technology.

List of Principal Symbols

A, temperature gradient along plane wall;

B_g, Biot number for free surface;

B_o, Bond number;

B_w, Biot number for plane wall;

c, specific heat of liquid;

D, thermometric diffusivity;

g, acceleration due to gravity;

h, level of free surface;

h, surface deformation;

h_a mean level of free surface, mean thickness of liquid layer;

h_{max}, value of surface deformation at center plane (x=1);

$h_{i,j}$, value of surface deformation at mesh point (i,j) (in Appendix B);

K_g, heat transfer coefficient across free surface;

K_w, heat transfer coefficient across plane wall;

k, wavenumber;

L, spatial period;

M_A, Marangoni number of the steady mode in Example (i);

M_{AC}, critical Marangoni number of the steady mode;

M_B, Marangoni number re-defined in Appendix A;

M_b, Marangoni number in Example (ii);

M_R, Marangoni number;

N_C, Crispation number;

P_r, Prandtl number;

p, pressure;

p_g, constant pressure in gas phase;

T, temperature;

T_a, equilibrium temperature at free surface;

T_g, gas temperature (in Appendix A);

T_w, wall temperature (in Appendix A);

t, time variable;

t_1, t_2, slow time-variable;

t_s, sampling interval in numerical calculation;

u, steady solution of Example (i);

v, steady solution of Example (ii);

W, $W \equiv B_o/N_C$;

x, y, z, variables in Cartesian coordinates;

Z, temperature in nondimensional form;

Z_g, gas temperature in nondimensional form;

Z_w, wall temperature in nondimensional form;

α, β, γ, coefficients in equation (3.7);

δ, finite difference of coordinate x (in Appendix B);

ε, shallow water parameter;

ι, wavelength;

λ, complex growth rate (in Appendix A);

μ, viscosity of liquid;

ν, kinematic viscosity of liquid;

ρ, density of liquid;

σ(T), surface tension coefficient as function of temperature T;

τ, finite difference of time (in Appendix B);

ψ, stream function;

References

1) T. K. Sherwood, R. L. Pigford and C. R. Wilke: Mass Transfer (McGraw-Hill, 1975) Chap. 5.

2) J. R. A. Pearson: J. Fluid Mech. 4 (1958) 489.

3) C. V. Sternling and L. E. Scriven: AIChE J. 5 (1959) 514.

4) L. E. Scriven and C. V. Sternling: J. Fluid Mech. 19 (1964) 321.

5) K. A. Smith: J. Fluid Mech. 24 (1966) 401.

6) R. W. Zeren and W. C. Reynolds: J. Fluid Mech. 53 (1972) 305.

7) M. Takashima: J. Phys. Soc. Jpn. 50 (1981) 2745.

8) M. Takashima: J. Phys. Soc. Jpn. 50 (1981) 2751.

9) S. Kai, E. Ooishi and M. Imasaki: J. Phys. Soc. Jpn. 54 (1985) 1274; S. Kai: Nagare (J. Japan Soc. Fluid Mech.) 3 (1984) 215 [in Japanese]; S. Kai: Suuri-Kagaku (Mathematical science) No. 267 (1985) 55 [in Japanese].

10) T. Funada: Memoirs of the Wakayama College of Technology (1983) Vol. 18, p. 19 [in Japanese]; T. Funada: Note of Res. Inst. Math. Sci., Kyoto Univ., No. 510 (1984) p. 33 [in Japanese].

11) S. M. Pimputkar and S. Ostrach: Phys. Fluids 23 (1980) 1281.

12) A. D. Myshkis, V. G. Babskii, N. D. Kopachevskii, L. A. Slobozhanin and A. D. Tyuptsov: Low-Gravity Fluid Mechanics (Springer-Verlag, 1987); in this textbook, the following paper has been reviewed. B. K. Kopbosynov and V. V. Pukhnachev: Ural. Nauch. Tsentr Akad. Nauk SSSR, Sverdlovsk (1983), p. 116 [in Russian].

13) Y. Kuramoto: Prog. Theor. Phys. 71 (1984) 1182.

14) T. Kawahara and S. Toh: Phys. Lett. 113A (1985) 21.

15) M. Yamada: J. Phys. Soc. Jpn. 55 (1986) 3059.

16) Y. Kuramoto and T. Tsuzuki: Prog. Theor. Phys. 55 (1976) 356.

17) Y. Kuramoto: Chemical Oscillations, Waves, and Turbulence (Springer-Verlag, 1984).

18) T. Kawahara and S. Toh: Phys. Fluids 28 (1985) 1636.

19) S. Toh and T. Kawahara: J. Phys. Soc. Jpn. 54 (1985) 1257.

20) The Chemical Society of Japan, ed.: Kagaku Binran, Kiso-hen (Handbook of Chemistry, Fundamentals) (Maruzen, 1975) [in Japanese].

21) A. K. Sen: Phys. Fluids 29 (1986) 3881.

22) T. Kakutani and T. Kawahara: Butsuri (Physics) 31 (1976) 287 [in Japanese].

23) L. D. Landau and E. M. Lifshitz: Fluid Mechanics (Pergamon Press, London, 1966) Chap. 5.

24) C. Nakaya: J. Phys. Soc. Jpn. 37 (1974) 539.

25) T. Kakutani and K. Matsuuchi: J. Phys. Soc. Jpn. 39 (1975) 237.

26) T. Tatsumi and K. Gotoh: Nagare no Anteisei Riron (Theory of Stability of Fluid Flows) (Sangyo-Tosho, 1976) [in Japanese].

27) S. V. Alekseenko, V. Ye. Nakoryakov and B. G. Pokusaev: AIChE J. 31 (1985) 1446.

28) H.-C. Chang: Phys. Fluids 29 (1986) 3142.

Chapter 4. Marangoni Instability Due to Chemical Absorption with an Irreversible Reaction

§ 1. Introduction

For the mass transfer across phase boundaries of fluids, it has been found experimentally that the rate of mass transfer often increases over the values estimated by penetration theories.[1] It has also been found from visual observations that the Marangoni convection occurs and activates the mass transfer. From engineering point of view, especially in chemical engineering, it is of great significance to study what causes the Marangoni convection and whether we can control it.

On the basis of the experimental results so far obtained for various chemical absorption systems, Imaishi and Fujinawa[2] have discussed roles of temperature, solute and product causing the Marangoni convection, and they have found that the most important factor in the chemical absorption is an inactive product. Then they have studied the linear stability of a chemical absorption system where a gas absorbed into a liquid makes a product through the first order irreversible reaction, and they have shown that the Marangoni instability arises, indeed, from the inactive product. (Refer also to Imaishi[3] for the details.) It seems, however, that a more extensive investigation is required for stability problems of such chemical absorption systems, by taking account of detailed reaction processes, Marangoni effects due to

multiple components and various types of boundary conditions. The purpose of this chapter is to examine this sort of problems.

We consider the Marangoni instability due to a chemical absorption, which occurs in a viscous liquid layer between a plane wall and a gas phase. The gas component is absorbed into the liquid and reacts on the solute, so that a product is made up according to an irreversible reaction. Thus, the gas, the solute and the product may cause surface tension gradients (Marangoni effects) at the free surface. A typical example of such chemical absorption so far found experimentally is the absorption of carbon dioxide into aqueous monoethanolamine in a short wetted-wall column, where the reaction proceeds as an irreversible process.[2,3] For this sort of systems, Imaishi and Fujinawa[2] proposed a simplified model in a liquid layer at rest, that is, they assumed that the Marangoni convections may occur from a rest state of the liquid layer. This model seems to be very reasonable in the following situation. In fact, as shown in a textbook by Landau and Lifshitz,[4] the basic equations of a 'single' component fluid may also be applied to two component fluid if each small portion moves without changing its components, which is possible for fluids with a dilute component. Extending this model to the multi-component system, we assume that the solute is very rich in the liquid and that the heat transfer concerning the reaction is negligible. This reaction is thus approximated by a first order irreversible process in an isothermal state. The mass transfer of the three components occurs in the liquid from

the reaction, diffusion and convection, and it is assumed to be prescribed by boundary conditions of the type of Newton's cooling law, in which the gas-liquid resistance (the so-called contact-resistance) that may occur at the free surface is taken into account as a simple model. It is also assumed that material properties of the liquid (except for the surface tension coefficient) are constant and that the effect of gravity is negligible. Under these assumptions, equilibrium solutions for a steady static state are obtained in § 2, and then a stability problem against small disturbances of the steady mode is proposed with including effects of a surface deformation. To clarify roles of the components causing the Marangoni instability, the problem is divided into three elementary ones each of which is given as an eigenvalue problem. Since the Marangoni effect can occur even when the free surface is flat, results for the flat free surface are given in § 3. First, the Marangoni instability due to an inactive product (Case (i)) is examined in detail with noting the mass transfer of the gas across the boundaries of the liquid layer. The critical Marangoni number for the product and the corresponding critical wavenumber are discussed there for various values of parameters involved. In particular, it is shown that the Marangoni instability due to the product may occur most easily when the reaction proceeds at a slow rate and when the mass transfer of the gas is prescribed as a constant concentration at the plane wall and zero flux at the free surface. Next, it is shown, for a special case (which is given by $\chi=0$ in § 3.2,

see (2.24) for the definition of χ), that the eigenvalue relation for an active solute (Case (ii)) is equivalent to that for an inactive product. The eigenvalue relation for the solute is examined further with changing values of the parameters. Results obtained for the solute seem to be interesting, because the Marangoni instability due to the active solute has been found experimentally (see also refs. 2 and 3). Furthermore, the Marangoni instability due to the gas (Case (iii)) is examined in § 3.3. By taking account of the Marangoni effects due to both the product and the solute, a general eigenvalue relation (a coupled Marangoni instability) for this chemical absorption system is discussed in § 3.4. In the final section 4, effects of the surface deformation are discussed in comparison with the results obtained for the flat free surface.

§ 2. Formulation of the Problem

Let us consider a chemical absorption for a liquid layer between a plane wall and a gas phase of a component A. The gas A is absorbed into the liquid across a free surface and reacts on a solute B, so that a product P is made up according to an irreversible reaction $A+mB \xrightarrow{k} nP$, where m and n are stoichiometric factors and the rate constant k depends upon the liquid temperature T. The rate equation for this reaction is given by

$$-r_A = -\frac{r_B}{m} = \frac{r_P}{n} = r, \tag{2.1a}$$

$$r = kC_AC_B^m, \tag{2.1b}$$

where r_A, r_B and r_P denote, respectively, the rate of production of the components A, B and P, r being a representative rate of production, and C_A and C_B are the concentrations of A and B. In order to simplify (2.1b), we assume here that B is very rich in the liquid throughout the reaction, so that we may divide C_B into two parts:

$$C_B = C_{B0} + C_{B1}, \tag{2.2}$$

where C_{B1} denotes a small deviation from the constant concentration C_{B0}, and it takes a negative value, because the solute decreases owing to the reaction. In addition, the heat transfer concerning the reaction is assumed to be negligible, so that the rate constant k may be expressed as

$$k = k(T) \cong k(T_0), \tag{2.3}$$

where T_0 is a mean temperature of the liquid. In view of (2.2)

and (2.3), r given by (2.1b) can now be approximated as

$$r = KC_A, \tag{2.4}$$

with the constant defined as $K \equiv k(T_0)C_{B0}{}^m$. The reaction process given by (2.1a) and (2.4) is thus regarded as the first order irreversible reaction in the isothermal state ($T=T_0$).

Through this reaction process, the components A, B and P may change the surface tension coefficient σ in the following manner:

$$\begin{aligned}\sigma &= \sigma(C_A, C_B, C_P) \\ &= \sigma_0 + \left(\frac{\partial \sigma}{\partial C_A}\right)\delta C_A + \left(\frac{\partial \sigma}{\partial C_B}\right)\delta C_B + \left(\frac{\partial \sigma}{\partial C_P}\right)\delta C_P,\end{aligned} \tag{2.5}$$

where σ_0 is a constant corresponding to a steady static state, and δC_A, δC_B and δC_P denote the deviations of the concentrations. We take the coefficients such that $(\partial\sigma/\partial C_B)<0$, $(\partial\sigma/\partial C_A)>0$ and $(\partial\sigma/\partial C_P)>0$: the negative one is referred to as active agency, while the positive ones as inactive agency. This setting of the coefficients provides a necessary condition to make σ larger than σ_0, by which a strong surface tension gradient to drive convections is to be realized. To simplify the analysis, the other material properties of the liquid, such as viscosity μ, density ρ, diffusivity D_A for the component A, D_B for B and D_P for P, are taken to be constant throughout the reaction.

Using a Cartesian coordinate system $x=(x_1, x_2, x_3)$, we take the x_2-axis in the direction of thickness of the liquid layer and the x_1- and x_3-axes on the plane wall ($x_2=0$). Then we put the

free surface at $x_2=d+\zeta'$ with a mean level d and a surface deformation ζ'. Under the assumptions made above, basic equations for this liquid layer are given by

$$\nabla \cdot v = 0, \tag{2.6}$$

$$\frac{Dv}{Dt} = -\frac{1}{\rho}\nabla p + \nu \nabla^2 v, \tag{2.7}$$

$$\frac{DC_A}{Dt} = D_A \nabla^2 C_A - KC_A, \tag{2.8a}$$

$$\frac{DC_{B1}}{Dt} = D_B \nabla^2 C_{B1} - mKC_A, \tag{2.8b}$$

$$\frac{DC_P}{Dt} = D_P \nabla^2 C_P + nKC_A, \tag{2.8c}$$

where $v=(v_1, v_2, v_3)$ is the velocity, p is the pressure, $\nu=\mu/\rho$ is the kinematic viscosity, and $D/Dt=\partial/\partial t+(v\cdot\nabla)$ with the time variable t. The reaction given by (2.1a) and (2.4) is taken into account in (2.8a-c).

The mass transfer of A across the free surface is assumed to be prescribed by a condition of the type of Newton's cooling law:

$$n\cdot\nabla C_A = -\frac{k_{AG}}{D_A}(C_A - C_{AG}), \tag{2.9}$$

where n is the unit normal vector taken outward from the liquid layer, k_{AG} denotes the mass transfer coefficient, and C_{AG} is the constant concentration of A defined in the gas phase. The value

of C_A at the free surface approaches C_{AG} as k_{AG} becomes large, and the state of $C_A=C_{AG}$ given by $k_{AG}\to\infty$ is referred to as the saturated state. In contrast to the gas, the solute B is assumed to be little in the gas phase, so that the transfer coefficient k_{BG} for B is taken to be sufficiently small. Using this and (2.2), the boundary condition for C_B at the free surface is approximated as

$$n\cdot\nabla C_{B1} \cong -\frac{k_{BG}}{D_B} C_{B0}. \tag{2.10}$$

The product P is assumed to be nonvolatile, so that C_P satisfies

$$n\cdot\nabla C_P = 0, \tag{2.11}$$

at the free surface. The kinematic condition and the balance of the momentum flux[4] at the free surface are expressed as

$$\frac{D\zeta'}{Dt} = v_2, \tag{2.12}$$

$$(p_G-p)n_i + \tau_{ij}n_j = \tilde{\nabla}_i\sigma + \sigma S n_i \quad \text{for } i=1,2,3, \tag{2.13a,b,c}$$

where the tensor notation is used in (2.13a,b,c) with taking the summation convention for the repeated index j; p_G denotes the constant pressure of the gas phase, the viscous stress tensor τ_{ij} is expressed as

$$\tau_{ij} = \mu\left(\frac{\partial v_i}{\partial x_j} + \frac{\partial v_j}{\partial x_i}\right), \tag{2.14}$$

and $\tilde{\nabla}_i$ stands for the i-th component of the gradient operator taken along the free surface. Since we will consider disturbances of small magnitude, the mean curvature S of the free sur-

face and the unit normal vector n are approximated as

$$S = \frac{\partial^2 \zeta'}{\partial x_1^2} + \frac{\partial^2 \zeta'}{\partial x_3^2}, \qquad n = (0,\ 1,\ 0). \tag{2.15a,b}$$

On the other hand, the boundary conditions at the plane wall (x_2=0) are given by

$$v = C_{B1} = C_P = 0, \tag{2.16}$$

$$\frac{\partial C_A}{\partial x_2} = \frac{k_{AW}}{D_A} C_A, \tag{2.17}$$

where k_{AW} is the transfer coefficient of A across the wall.

For a steady static state of the liquid layer with a flat free surface given by x_2=d, it is easy to find that (2.6)-(2.17) admit equilibrium solutions given by $v \equiv \bar{v}=0$, $p \equiv \bar{p}=p_G$ and

$$C_A \equiv \bar{C}_A = \bar{C}_{As}(B_{AW}\sinh \gamma y + \gamma \cosh \gamma y)/a, \tag{2.18}$$

$$C_{B1} \equiv \bar{C}_{B1} = \bar{C}_{B1s}\{-\chi y - \beta_B[\gamma(1 + a^* y)/a - \bar{C}_A/\bar{C}_{As}]\}, \tag{2.19}$$

$$C_P \equiv \bar{C}_P = \bar{C}_{Ps}\beta_P[\gamma(1 + a^* y)/a - \bar{C}_A/\bar{C}_{As}], \tag{2.20}$$

with

$$\bar{C}_{As} = \frac{C_{AG}B_{AG}}{\gamma a^*/a + B_{AG}}, \tag{2.21}$$

$$\beta_P \equiv \frac{nD_A\bar{C}_{As}}{D_P\bar{C}_{Ps}} = \frac{a}{\gamma(1 + a^*) - a}, \tag{2.22a}$$

$$\beta_B \equiv \frac{mD_A\bar{C}_{As}}{D_B\bar{C}_{B1s}} = -\frac{(1 + \chi)a}{\gamma(1 + a^*) - a}, \tag{2.22b}$$

$$a = B_{AW}\sinh\gamma + \gamma\cosh\gamma, \quad a^{*} = B_{AW}\cosh\gamma + \gamma\sinh\gamma, \quad (2.23a,b)$$

where the overbar attached denotes the steady static state, the suffix s stands for the values taken at the flat free surface, $y=x_2/d$, and the parameters are defined as

$$\gamma = d\sqrt{\frac{K}{D_A}} \qquad \text{Reaction parameter,}$$

$$B_{AG} = \frac{dk_{AG}}{D_A} \qquad \text{Gas Biot number for the free surface,}$$

$$B_{AW} = \frac{dk_{AW}}{D_A} \qquad \text{Gas Biot number for the plane wall,}$$

$$\varkappa = \frac{dk_{BG}C_{B0}}{D_B\bar{C}_{B1s}} \qquad \text{Solute flux parameter.} \qquad (2.24)$$

For the solutions (2.18)-(2.20), the distributions of $\bar{C}_A$, $\bar{C}_{B1}$ and $\bar{C}_P$ for $B_{AW}\to\infty$ differ from those for $B_{AW}=0$ when $\gamma \lesssim 3$ (i.e., for slow rates of the reaction), whereas the differences between the distributions for the two limiting cases disappear when $\gamma>3$. The latter is convincing from the fact that the solution (2.18) can be approximated, for $\gamma>>1$, as $\bar{C}_A \cong \bar{C}_{As}\exp[\gamma(y-1)]$ (i.e., $\bar{C}_A$, $\bar{C}_{B1}$ and $\bar{C}_P$ become independent of B_{AW}, because the reaction occurs only in a thin surface layer of thickness d/γ). From (2.21), the saturated state is found to be given by $B_{AG}\to\infty$. In contrast, when $B_{AG}=0$, $\bar{C}_{As}$ is taken as a perturbation from the value of $\bar{C}_{As}=0$ in order to take account of the absorption of gas. In (2.22a), β_P is found to be positive for all the values of γ and

B_{AW}. This implies that C_P is affected by the reaction even when $\gamma=0$. When $\chi=0$, we find that (2.22b) reduces to $\beta_B=-\beta_P$, so that we get $\bar{C}_{B1}/\bar{C}_{B1s}=\bar{C}_P/\bar{C}_{Ps}$ from (2.19) and (2.20). Equation (2.22b) also indicates that $\bar{C}_{B1s}$ becomes negative when $-1<\chi\leqq 0$. Thus this range of χ may be allowable to consider the distribution of $\bar{C}_{B1}$, though the approximation made in (2.10) holds well under the condition $|\chi|\ll 1$. At the same time, the case of $\chi=-1$ should be added to the range, because it describes the desorption of the active solute without the reaction. The cases examined above provide some typical examples which will be seen later. To adapt the normalization used before,[2,3,5] we introduce the following nondimensional expression for (2.18)-(2.20):

$$\left[\frac{\bar{C}_A}{\bar{C}_{As}}, \frac{\bar{C}_{B1}}{\bar{C}_{B1s}}, \frac{\bar{C}_P}{\bar{C}_{Ps}}\right], \tag{2.25}$$

and we will use henceforth the same symbols for the nondimensional forms of $\bar{C}_A$, $\bar{C}_{B1}$ and $\bar{C}_P$.

In a perturbed state, small disturbances which are denoted with prime are superimposed upon the steady static state. Following the usual linear stability theory, we can obtain a governing system of equations for the disturbances from (2.6)-(2.17). Let us represent the disturbances by $[v_2', C_A', C_{B1}', C_P', \zeta']$ after eliminating v_1', v_3' and p', and take the normal mode decomposition:

$$\left[\frac{v_2'}{D_P/d}, \frac{C_A'}{\bar{C}_{As}}, \frac{C_{B1}'}{\bar{C}_{B1s}}, \frac{C_P'}{\bar{C}_{Ps}}, \frac{\zeta'}{d}\right]$$

$$= [f(y), g(y), G(y), h(y), s] \exp[(i\alpha_1 x_1 + i\alpha_3 x_3)/d], \tag{2.26}$$

with the wavenumber vector $(\alpha_1, 0, \alpha_3)$ of magnitude α; here we restrict ourselves only to the disturbances of the steady mode, because the stability problem previously solved for the disturbances v_2', C_A' and C_P' has shown that the critical Marangoni number is given by positive values for the steady mode,[2,3,5] while by negative values of large magnitude for the oscillatory mode.[6] The governing system of equations for the steady mode are written as follows:

$$\mathcal{L}^2 f = 0, \tag{2.27}$$

$$(\mathcal{L} - \gamma^2) g = \frac{1}{L_A} f\left(\frac{d\bar{C}_A}{dy}\right), \tag{2.28}$$

$$\mathcal{L} G = \frac{1}{L_B} f\left(\frac{d\bar{C}_{B1}}{dy}\right) + \beta_B \gamma^2 g, \tag{2.29}$$

$$\mathcal{L} h = f\left(\frac{d\bar{C}_P}{dy}\right) - \beta_P \gamma^2 g, \tag{2.30}$$

together with the boundary conditions at y=1:

$$\frac{dg}{dy} + \gamma^2 s + B_{AG}\left(g + s \frac{d\bar{C}_A}{dy}\right) = 0, \tag{2.31}$$

$$\frac{dG}{dy} + \beta_B \gamma^2 s = 0, \tag{2.32}$$

$$\frac{dh}{dy} - \beta_P \gamma^2 s = 0, \tag{2.33}$$

$$f = 0, \tag{2.34}$$

$$\frac{d^2f}{dy^2} = \alpha^2[M_{Ph} + L_B M_B(G + s\frac{d\bar{C}_{B1}}{dy}) + L_A M_A(g + s\frac{d\bar{C}_A}{dy})], \quad (2.35)$$

$$(\pounds - 2\alpha^2)\frac{df}{dy} = \frac{\alpha^4}{N_C} s, \quad (2.36)$$

and the boundary conditions at y=0:

$$f = \frac{df}{dy} = G = h = 0, \quad (2.37)$$

$$\frac{dg}{dy} - B_{AW}g = 0, \quad (2.38)$$

where $\pounds = d^2/dy^2 - \alpha^2$, and the parameters are defined as

$$M_P = (\frac{\partial \sigma}{\partial C_P})\frac{\bar{C}_{Ps}d}{\mu D_P} \quad \text{Product Marangoni number,}$$

$$M_B = (\frac{\partial \sigma}{\partial C_B})\frac{\bar{C}_{B1s}d}{\mu D_B} \quad \text{Solute Marangoni number,}$$

$$M_A = (\frac{\partial \sigma}{\partial C_A})\frac{\bar{C}_{As}d}{\mu D_A} \quad \text{Gas Marangoni number,} \quad (2.39)$$

$$L_A = \frac{D_A}{D_P} \quad \text{Diffusivity ratio to gas,}$$

$$L_B = \frac{D_B}{D_P} \quad \text{Diffusivity ratio to solute,}$$

$$N_C = \frac{\mu D_P}{\sigma_0 d} \quad \text{Crispation number.}$$

Here σ_0 in (2.5) is taken as $\sigma_0=\sigma(\bar{C}_{As}, C_{B0}+\bar{C}_{B1s}, \bar{C}_{Ps})$, and the deviations δC_A, δC_B and δC_P are taken, respectively, as the disturbance of concentration plus a variation of the equilibrium concentration caused by the surface deformation (see the right-hand-side of (2.35) implying the surface tension gradient).

From (2.27), (2.34) and (2.37), we readily obtain

$$f(y) = b_0[\sinh\alpha y - \alpha y\cosh\alpha y + (\alpha\coth\alpha - 1)y\sinh\alpha y], \tag{2.40}$$

where b_0 is an integration constant which may be set as unity. Equations (2.36) and (2.40) yield

$$s = -\frac{2N_C}{\sinh\alpha}. \tag{2.41}$$

It follows from this that N_C should be zero whenever the free surface is flat (i.e., s=0), while N_C should be non-zero when the surface deformation does exist. It is also found that the magnitude of s becomes large for $\alpha<<1$ but small for $\alpha>>1$. This suggests that effects of the surface deformation manifest remarkably at small wavenumbers. Using (2.40) and the equilibrium solutions $\bar{C}_A$, $\bar{C}_{B1}$ and $\bar{C}_P$, we obtain the following solutions to (2.28)-(2.30):

$$g(y) = b_1\sinh\eta y + b_2\cosh\eta y + \frac{1}{L_A}U(y), \tag{2.42}$$

$$G(y) = b_3\sinh\alpha y + b_4\cosh\alpha y - \frac{1}{L_B}\left(\chi + \frac{a^*}{a}\gamma\beta_B\right)V(y) + \beta_B\left[g(y) + \left(\frac{1}{L_B} - \frac{1}{L_A}\right)W(y)\right], \tag{2.43}$$

$$h(y) = b_5 \sinh \alpha y + b_6 \cosh \alpha y$$
$$+ \beta_P \left[\frac{a^*}{a} \gamma V(y) - g(y) - \left(1 - \frac{1}{L_A}\right) W(y)\right], \qquad (2.44)$$

where $\eta = \sqrt{\alpha^2 + \gamma^2}$, and $b_1 \sim b_6$ are integration constants; the explicit forms of the functions U(y), V(y) and W(y) are given in Appendix.

Substituting (2.41)-(2.44) into (2.31)-(2.33), (2.37) and (2.38), we can determine the constants $b_1 \sim b_6$. Thus, from (2.35), we obtain an eigenvalue relation:

$$F(M_P, M_B, M_A, \alpha, \gamma, L_A, L_B, B_{AW}, B_{AG}, \chi, N_C) = 0, \qquad (2.45)$$

which describes a neutrally stable state for the disturbances of the steady mode. To clarify roles of the three components causing the Marangoni instability, we divide this into three elementary problems (Cases (i), (ii) and (iii) respectively):

$$\text{(i)} \quad M_P = F_P(\alpha, \gamma, L_A, B_{AW}, B_{AG}, N_C), \qquad M_A = M_B = 0, \qquad (2.46a)$$

$$\text{(ii)} \quad M_B = F_B(\alpha, \gamma, L_A/L_B, B_{AW}, B_{AG}, \chi, N_C), \quad M_A = M_P = 0, \qquad (2.46b)$$

$$\text{(iii)} \quad M_A = F_A(\alpha, \gamma, B_{AW}, B_{AG}, N_C), \qquad M_P = M_B = 0. \qquad (2.46c)$$

Since the diffusivity of the product can be eliminated for Cases (ii) and (iii), (2.46b) contains $L_A/L_B (=D_A/D_B)$ only, and (2.46c) does not contain such diffusivity ratios. This simply implies a normalization of the velocity in terms of the diffusivity of each component (i.e., D_B or D_A): note that in accordance with this, N_C in (2.46b,c) is redefined as well. It should be noted here that,

as the Marangoni effect can occur even when the free surface is flat, eigenvalue problems for the flat free surface (s=0) are most elementary. Hence, setting $N_C=0$, let us discuss the three elementary problems given by (2.46a-c) and then proceed to the general problem given by (2.45). Effects of the surface deformation will be discussed in § 4.

§ 3. Results for the Flat Free Surface

3.1 Eigenvalue M_P (Case (i)) for $N_C=0$

The eigenvalue relation $M_P=F_P(\alpha, \gamma, L_A, B_{AW}, B_{AG}, 0)$ includes one typical case studied in ref. 2, which is given by $B_{AW}\to\infty$ and $B_{AG}\to\infty$. We now examine in more detail the effects of mass transfer of the gas across the boundaries of the liquid layer. In addition to the above case, we take $B_{AW}=1$ and $B_{AW}=0$ as two representative values in $0\leqq B_{AW}<\infty$ and $B_{AG}=0$ as the opposite limiting case (in which the mass transfer of the gas across the free surface may be suppressed in contrast to the saturated state given by $B_{AG}\to\infty$): other values of B_{AW} and B_{AG} will be examined after these typical cases. Then, we choose L_A as 0.1, 1 and 10 in view of the data of various liquids.[7] Since L_A^{-1} denotes the magnitude of the convective transfer against the diffusion (see the equation (2.28) for the disturbance of gas concentration), this choice gives the typical examples such that the convective transfer is dominant ($L_A=0.1$), the diffusion is dominant ($L_A=10$), and both balance ($L_A=1$).

Let us begin with the case of $B_{AW}=1$ and $B_{AG}\to\infty$. Figure 1

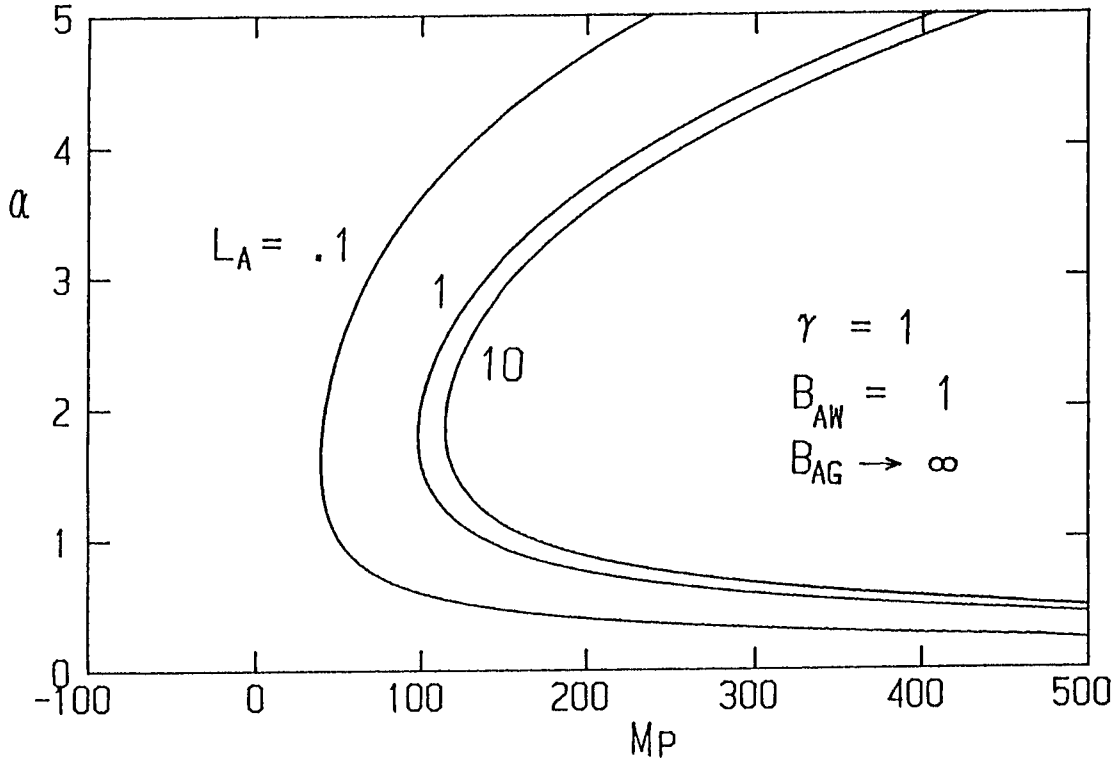

Fig. 1. Neutral stability curves for B_{AW}=1 and $B_{AG} \to \infty$ displayed in the (α, M_P) plane with taking the three typical values of L_A and γ=1.

shows some examples of the neutral stability curves displayed in the (α, M_P) plane with taking the three typical values of L_A and $\gamma=1$. Positive values of M_P on the curves of Fig. 1 support that the inactive product can cause the Marangoni instability. For each set of values of γ, L_A, B_{AW} and B_{AG} as in Fig. 1, the eigenvalue M_P has the lowest value M_{PC} at a critical wavenumber α_C, which is given just by the minimum of M_P with respect to α. Using this eigenvalue relation, the critical value M_{PC} and the corresponding critical wavenumber α_C versus γ for $B_{AG}\to\infty$ are shown in Fig. 2 for the typical values of L_A, where the curves of M_{PC} and α_C for $B_{AW}=1$ are drawn by the solid lines and those for $B_{AW}=0$ by the chain lines. For the sake of comparison, the previous results[2] for $B_{AW}\to\infty$ (drawn by the broken lines) are also cited in Fig. 2(a). When $\gamma\lesssim 5$, for each L_A, the critical value M_{PC} for $B_{AW}=0$ becomes larger than that for $B_{AW}\to\infty$ and concentrates upon $M_{PC}=130.91$ given at $\gamma=0$, because the convection term in (2.28) vanishes, i.e., $\bar{C}_A$ becomes uniform when $\gamma=B_{AW}=0$. Then, M_{PC} for $B_{AW}=1$ ranges in between the curve of M_{PC} for $B_{AW}\to\infty$ and that for $B_{AW}=0$. When $\gamma>5$, all the curves in Fig. 2(a) are independent of B_{AW} since the reaction occurs only within a thin surface layer, as noted in § 2. Figure 2(a) also shows that when the convective transfer of the gas is dominant (i.e., $L_A=0.1$), M_{PC} takes smaller values, except for $M_{PC}=130.91$ given at $\gamma=0$ for $B_{AW}=0$. For smaller values of L_A, the minimum of M_{PC} with respect to γ occurs at remarkably smaller values of γ. It is then found that M_{PC} decreases monotonically as B_{AW}

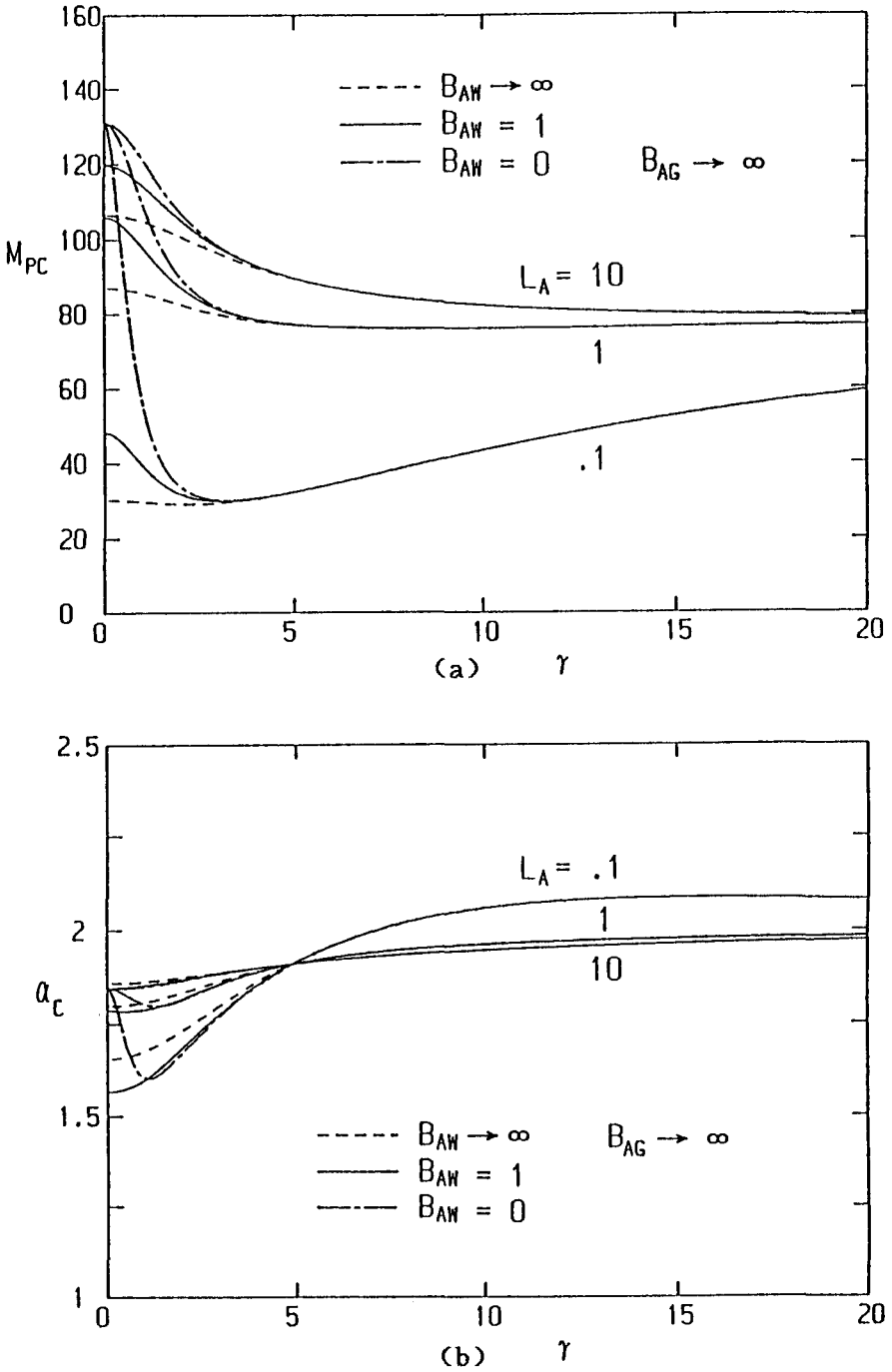

Fig. 2. Critical values M_{PC} and α_C for $B_{AG} \to \infty$ versus γ: (a) M_{PC} and (b) α_C. The curves of M_{PC} for $B_{AW}=1$ are drawn by the solid lines, while those for $B_{AW}=0$ by the chain lines and for $B_{AW} \to \infty$ by the broken lines. The curves of α_C are classified as well by the three values of B_{AW}.

increases from zero to infinity, and that it appears between the largest value M_{PC}=130.91 and the smallest value of M_{PC}=29.09 given at γ=2.27 for L_A=0.1 and $B_{AW}\rightarrow\infty$. Therefore the effects of B_{AW} on M_{PC} appear most typically at γ=0 (i.e., in the limit of slow rate of reaction). In Fig.2(b), if L_A changes from 10 to 0.1, the critical wavenumber α_C for each B_{AW} decreases when $\gamma \lesssim 5$, whereas α_C increases when γ>5: the variation of α_C versus γ is larger for smaller values of L_A. We also find for small values of L_A that α_C for B_{AW}=0 takes a minimum with respect to γ, and it concentrates upon α_C=1.844 giving M_{PC}=130.91 at γ=0. In this respect, detailed check for various values of B_{AW} shows that, as B_{AW} decreases from infinity to zero, the value of α_C at γ=0 decreases until it attains the minimum (that is obtained, for example, as α_C=1.567 at B_{AW}=0.92 for L_A=0.1, for which M_{PC}=49.61), and then it increases again, by which the minimum of α_C shifts to a positive value of γ (e.g., the minimum for L_A=0.1 and B_{AW}=0 is found to be α_C=1.603 at γ=1.1, which gives M_{PC}=51.16). Figure 2(b) also shows that α_C for L_A=0.1 has a maximum at $\gamma \fallingdotseq 16$. (The maximum of α_C for a larger L_A exists at a much larger γ, but is less than that for L_A=0.1.) Therefore α_C can be found within this maximum and the minimum of α_C given at γ=0 for L_A=0.1, with changing γ, L_A and B_{AW}. If γ increases further, all the values of α_C approach the fixed value 1.993 given in the limit of $\gamma\rightarrow\infty$. The typical values of M_{PC} and α_C at γ=0 for $B_{AG}\rightarrow\infty$ (Fig.2) are listed in the left side column of Table I. (Those for B_{AG}=0 listed in the

right side column will be discussed below.) Other typical values for $B_{AG}\to\infty$ are given by M_{PC}=109.41 at α_C=1.867 for γ=0, $L_A\to\infty$ and $B_{AW}\to\infty$ and by M_{PC}=79.61 at α_C=1.993 in the limit of $\gamma\to\infty$. It should be remarked here that the latter critical value corresponds to the results obtained for the Marangoni instability due to the heat transfer[8,9] or due to the physical absorption-desorption.[10]

Table I. Typical values of M_{PC} and α_C given at γ=0 for $B_{AG}\to\infty$ and those for B_{AG}=0 with taking various values of L_A and B_{AW}.

L_A	B_{AW}	$B_{AG}\to\infty$		B_{AG}=0	
		M_{PC}	α_C	M_{PC}	α_C
10	∞	106.70	1.858	101.79	1.815
	1	119.67	1.846	116.42	1.809
	0	130.91	1.844	130.91	1.844
1	∞	87.07	1.798	60.70	1.566
	1	106.04	1.785	81.78	1.489
	0	130.91	1.844	130.91	1.844
0.1	∞	30.27	1.655	11.41	1.359
	1	48.25	1.567	17.35	1.096
	0	130.91	1.844	130.91	1.844

For the case of B_{AG}=0, examples of M_{PC} and α_C versus γ are shown in Fig. 3 with setting the same values of L_A and B_{AW} as in Fig. 2. Comparing Fig. 3 with Fig. 2, we find that the dependences of M_{PC} and α_C on the parameters γ, L_A and B_{AW} are qualitatively

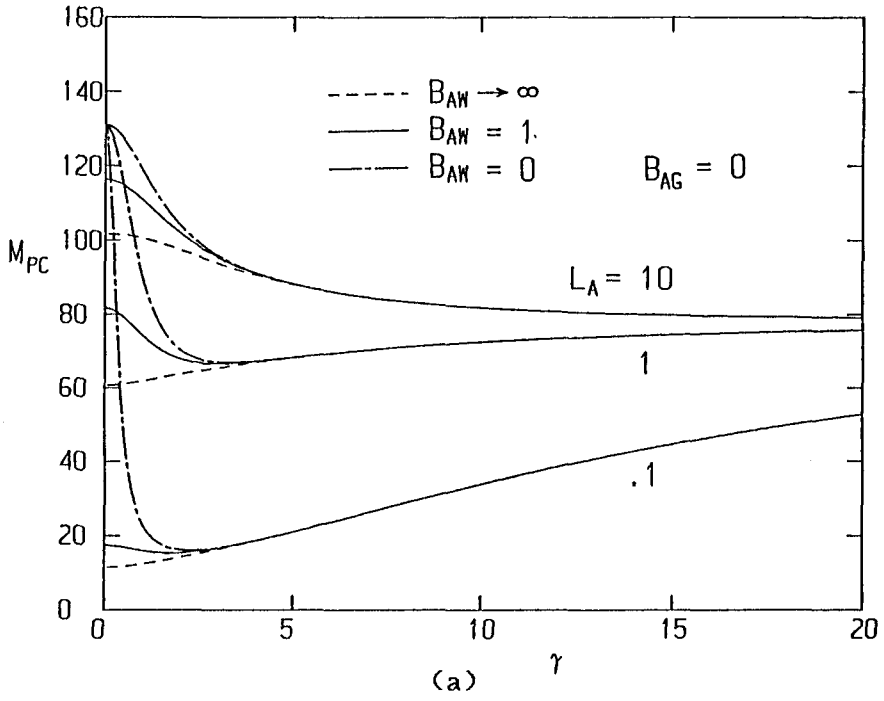

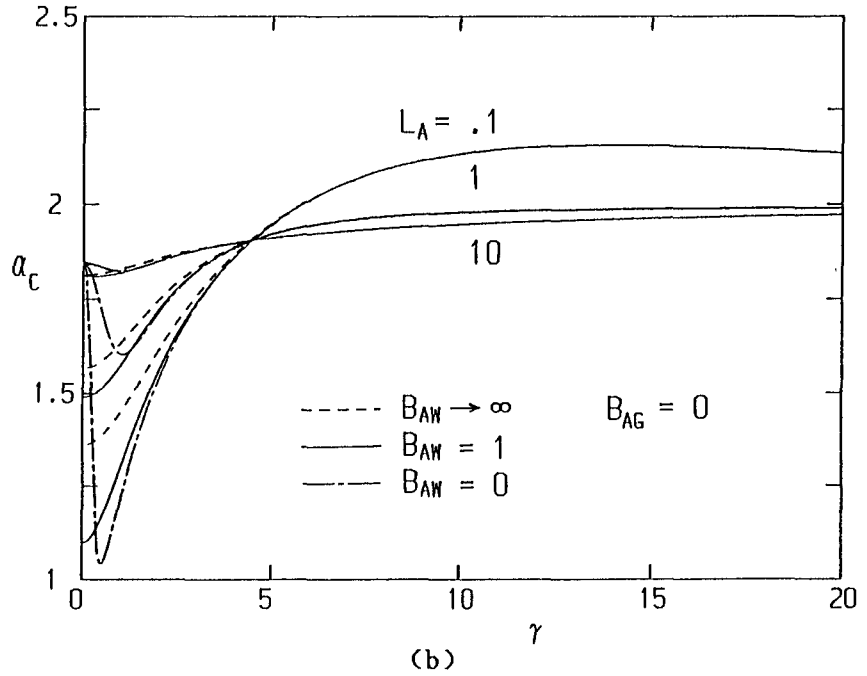

Fig. 3. Critical values M_{PC} and α_C for $B_{AG}=0$ versus γ: (a) M_{PC} and (b) α_C. The three sorts of lines have the same meaning as in Fig. 2.

similar to each other. It should be noted, however, that the values of M_{PC} for $B_{AG}=0$ (Fig. 3(a)) are smaller than those for $B_{AG}\rightarrow\infty$ (Fig. 2(a)) and such tendency can be seen more remarkably for smaller values of L_A (refer also to Table I). This result implies that, with decrease of B_{AG}, the disturbed value g(1) of the gas concentration at the flat free surface has a remarkable effect on the disturbed value h(1) of the product concentration (see the boundary condition (2.31) and the solution h(y) given by (2.44)). On the other hand, as B_{AG} increases, the value of g(1) approaches a constant (which is given, for $B_{AG}\rightarrow\infty$, as g(1)=0 from (2.31) with s=0), so that the value of h(1) becomes small as seen from (2.44). Thus, the larger value of g(1), arising from decrease of B_{AG} and especially for small values of L_A, leads to the larger value of h(1) (which gives rise to a stronger surface tension gradient due to the inactive product in (2.35)), for which M_{PC} becomes smaller. We also find from Fig. 3(a) that the curve of M_{PC} for $L_A=0.1$ and $B_{AW}\rightarrow\infty$ exhibits the smallest value at $\gamma=0$, and thus both the largest and the smallest values of M_{PC} exist at $\gamma=0$ (refer again to Table I). Figure 3(b) shows that the variations of α_C against γ are more remarkable than those in Fig. 2(b): e.g., α_C for $L_A=0.1$ and $B_{AW}=0$ changes about two times. In this connection, it is worth noting that, on the curves of α_C for $L_A=0.1$, the minimum at $\gamma=0$ is given by $\alpha_C=0.901$ when $B_{AW}=0.16$, for which $M_{PC}=43.84$, and the minimum for $B_{AW}=0$ is given by $\alpha_C=1.035$ at $\gamma=0.49$, for which $M_{PC}=47.66$. On the other hand, M_{PC} and α_C for $B_{AG}=0$ take the same values as

those for $B_{AG}\to\infty$ in the three limiting cases: they are given, respectively, at $\gamma=0$ when $B_{AW}\neq 0$ and $L_A\to\infty$ (where M_{PC} and α_C depend on B_{AW}), at $\gamma=0$ for $B_{AW}=0$, and in the limit of $\gamma\to\infty$.

When $0<B_{AG}<\infty$, it is found that both M_{PC} and α_C range between the values for $B_{AG}\to\infty$ (Fig. 2) and those for $B_{AG}=0$ (Fig. 3), for all values of γ, L_A and B_{AW} considered here. Therefore, the two limiting cases are representative of various values of B_{AG}.

3.2 Eigenvalue M_B (Case (ii)) for $N_C=0$

A simple but typical example of the eigenvalue relation $M_B=F_B(\alpha,\gamma,L_A/L_B,B_{AW},B_{AG},\chi,0)$ is the case for which $\chi=0$, since the results of this case can be obtained by Figs. 1–3 if one simply replaces L_A by L_A/L_B and M_P by M_B in the problem solved in § 3.1. This is not surprising, because decrease of the active solute at the free surface gives rise to increase of the surface tension coefficient subject to (2.5), as if the inactive product increases at the free surface. (Refer also to refs. 2 and 3.)

In addition to the case of $\chi=0$, we now examine the cases of $\chi=-0.25$, -0.5 and -1. The examples of M_{BC} (the critical value of M_B) and α_C versus γ are shown in Fig. 4, where we set as $L_A/L_B=0.1$ and $B_{AG}=0$ to display the effects of χ clearly. When $\chi=-1$, as already suggested in § 2, the eigenvalue M_B given by (2.46b) depends upon α only, so that one obtains the fixed values $M_{BC}=79.61$ and $\alpha_C=1.993$. This indicates that the desorption of the active solute leads to the Marangoni instability. (Note that the desorption of the solute without the reaction corresponds to the physical absorption of inactive substances.)

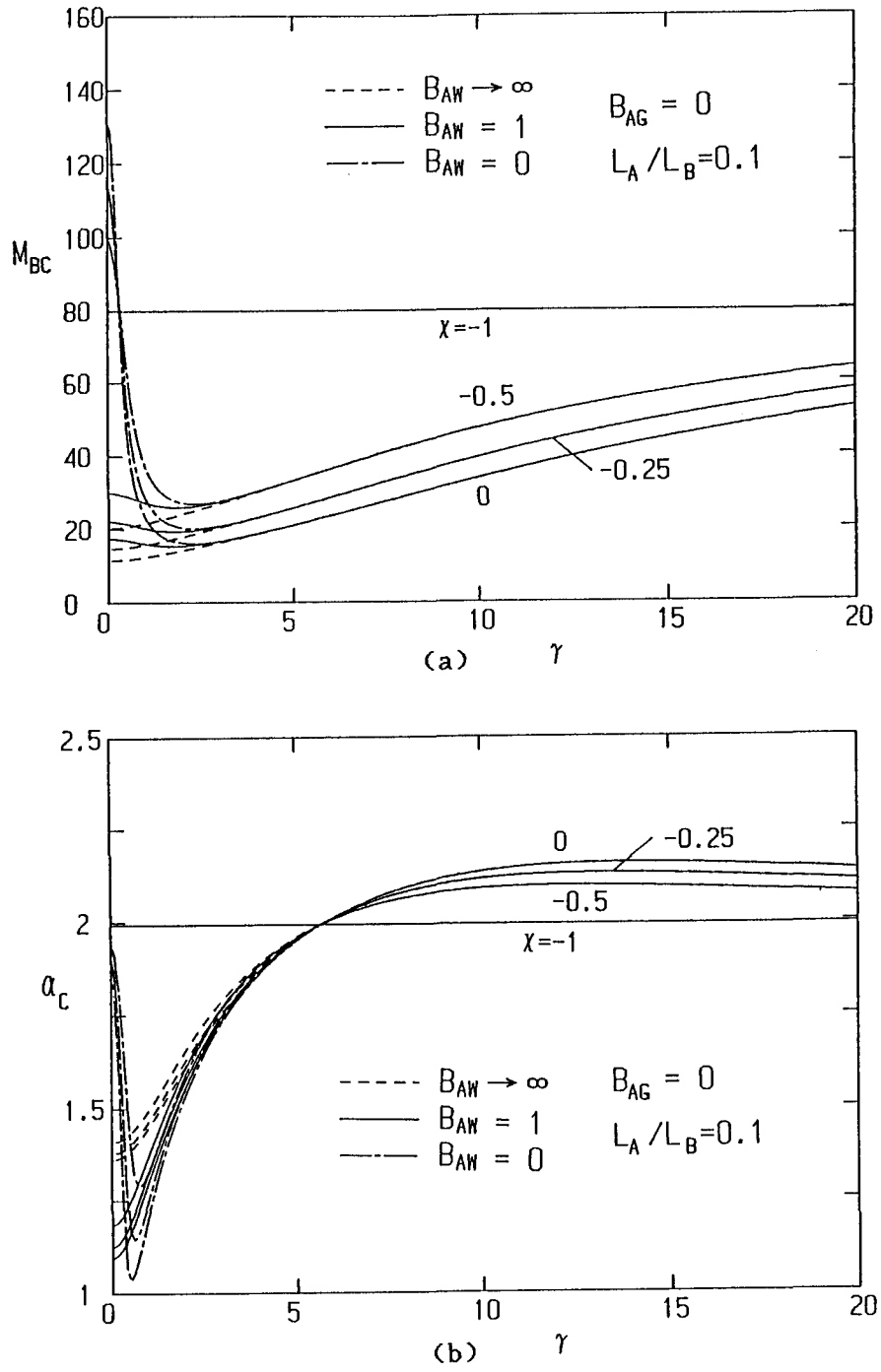

Fig. 4. Critical values of M_{BC} and α_C versus γ for various values of χ on setting $L_A/L_B=0.1$ and $B_{AG}=0$: (a) M_{BC} and (b) α_C.

Figure 4 also shows that, as χ decreases from 0 to −1, both curves of M_{BC} and α_C change gradually and attain, respectively, to the straight line corresponding to the fixed value: the variations of M_{BC} and α_C against γ become small. It turns out from this that when $\gamma \lesssim 3$, M_{BC} increases for $B_{AW} \to \infty$ (which means 'stabilizing') but decreases for $B_{AW}=0$ ('destabilizing'). It is thus found that a balance among γ, L_A/L_B, B_{AW}, B_{AG} and χ always yields $M_{BC}=79.61$ (see the curves of M_{BC} for $B_{AW}=0$ in Fig. 4(a)). Such tendency is observed as well for other values of L_A/L_B, B_{AW} and B_{AG}, so that M_{BC} and α_C can be found within the values for $\chi=0$ and for $\chi=-1$. The typical values of M_{BC} and α_C at $\gamma=0$ for $B_{AG}=0$ (Fig. 4) together with those for $B_{AG} \to \infty$ are listed in Table II.

Table II. Typical values of M_{BC} and α_C given at $\gamma=0$ for the two limiting cases of B_{AG} with taking various values of χ and B_{AW} and the fixed value $L_A/L_B=0.1$.

		$B_{AG} \to \infty$		$B_{AG}=0$	
χ	B_{AW}	M_{BC}	α_C	M_{BC}	α_C
−0.25	∞	35.95	1.683	14.62	1.376
	1	53.99	1.620	22.00	1.125
	0	112.92	1.892	112.92	1.892
−0.5	∞	44.20	1.727	20.29	1.407
	1	61.02	1.697	29.92	1.184
	0	99.17	1.931	99.17	1.931
−1	−	79.61	1.993	79.61	1.993

3.3 Eigenvalue M_A (Case (iii)) for $N_C=0$

An obvious example of the eigenvalue relation for the gas ($M_A=F_A(\alpha, \gamma, B_{AW}, B_{AG}, 0)$) is given by $B_{AG}\to\infty$: since the boundary condition (2.31) with s=0 ($N_C=0$) reduces to $g(1)=0$, the Marangoni effect due to the gas concentration vanishes (see (2.35)). In other words, when $B_{AG}\to\infty$, the disturbance of gas concentration itself cannot cause the Marangoni instability,[5] so that an eigenvalue problem for the gas coupled with the product (or the solute) reduces to the one discussed in § 3.1 (or § 3.2).

When $B_{AG}<\infty$, the eigenvalue M_A takes finite values. The critical values M_{AC} and α_C thus obtained are shown in Fig. 5 for various values of B_{AG} and two limiting cases of B_{AW}. It turns out from Fig. 5(a) that M_{AC} changes considerably with the variation of B_{AG}, and that M_{AC} for $B_{AG}>1$ can be estimated mainly by B_{AG} whenever $\gamma>3$. This is because the gas absorbed exists only within a thin surface layer and that it is expended in the process of the reaction. The dependence of M_{AC} on B_{AW} appears only for $\gamma\lesssim 3$, and M_{AC} for $B_{AW}=0$ increases as γ decreases, since M_A for $B_{AW}=0$ takes the form of $M_A\propto\gamma^{-2}$ in the vicinity of $\gamma=0$ (but M_A for $B_{AW}=0$ gives, in the limit of $\gamma\to 0$, an exceptional example, though it is omitted here). In Fig. 5(b), α_C increases monotonically with increase of γ (>3). Then, the curves of α_C for $B_{AG}\geqq 10^4$ approach a single curve expressed as $\alpha_C=\gamma$ for $\gamma>5$. For small values of γ, α_C decreases with decrease of B_{AW}: note that α_C at $\gamma=0$ for $B_{AW}=0$ corresponds to the exceptional example. One of the typical values of M_{AC} in Fig. 5(a) is

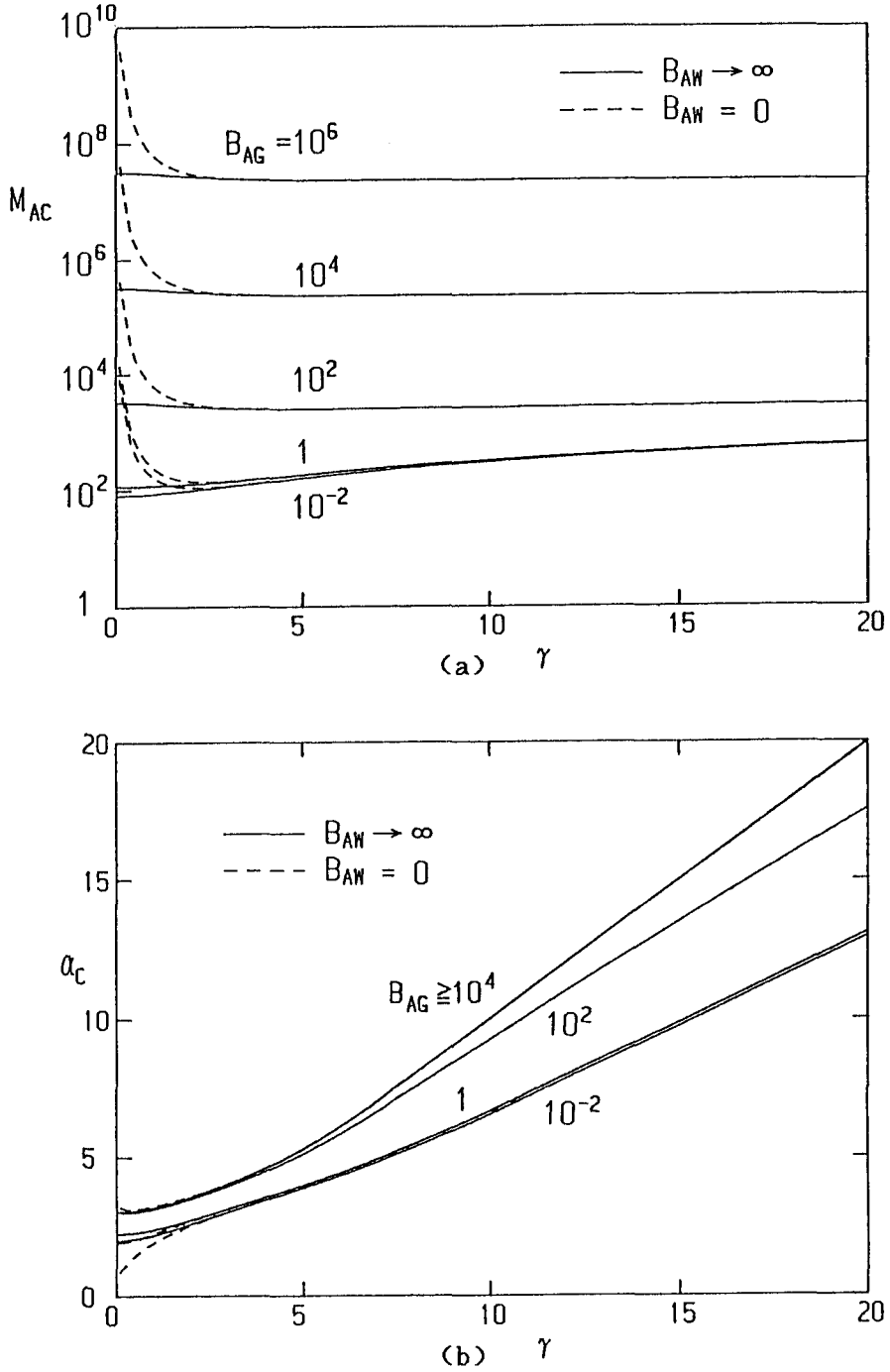

Fig. 5. Critical values M_{AC} and α_C versus γ for various values of B_{AG}: (a) M_{AC} and (b) α_C.

found to be given by $M_{AC}=79.61$ at $\alpha_C=1.993$ when $\gamma=B_{AG}=0$ and $B_{AW}\to\infty$; this agrees with the result for the physical absorption.[10]

3.4 Marangoni instability due to multiple components

Taking account of the results obtained for the three elementary problems, let us now consider a coupled Marangoni instability due to the product and the solute. On setting $M_A=N_C=0$, the general eigenvalue relation (2.45) can be written as

$$F = \frac{M_P}{F_P} + \frac{M_B}{F_B} - 1 = 0, \tag{3.1}$$

where F_P and F_B are of the forms given in (2.46a,b). For the sake of convenience, M_P is taken as a function of α with a parameter M_B and the parameters contained in F_P and F_B. Along this line, the lowest value M_{PC} can be obtained at a critical wavenumber α_C. Since F_P and F_B are bounded, respectively, as $F_P \geqq (M_{PC})_0$ and $F_B \geqq M_{BC}$ (in which $(M_{PC})_0$ denotes the value of M_{PC} for $M_B=0$, and M_{BC} is the critical value of M_B given in § 3.2), the equation (3.1) yields

$$\frac{M_{PC}}{(M_{PC})_0} + \frac{M_B}{M_{BC}} \geqq 1, \tag{3.2}$$

where the equality holds for $M_B=0$ and $M_B=M_{BC}$ (for which $M_{PC}=0$), while the inequality holds for the range of $0<M_B<M_{BC}$ except some special cases to be discussed later. In addition, differentiating (3.1) with respect to α leads, on imposing the condition

$\partial M_P/\partial\alpha=0$, to the equation:

$$\frac{M_{PC}}{F_P{}^2}\frac{\partial F_P}{\partial\alpha}+\frac{M_B}{F_B{}^2}\frac{\partial F_B}{\partial\alpha}=0 \qquad \text{at } \alpha=\alpha_C\ , \tag{3.3}$$

so that $\partial F_P/\partial\alpha$ must take opposite sign to $\partial F_B/\partial\alpha$ in $0<M_B<M_{BC}$ (otherwise it should hold that $\partial F_P/\partial\alpha=\partial F_B/\partial\alpha=0$). Thus, for the general case, both M_{PC} and α_C obtained from (3.1) do not coincide with those given in § 3.1. To see this, examples of M_{PC} and α_C for typical values of L_A are shown in Fig. 6 with setting $\gamma=0.1$, $L_B=1$, $B_{AW}=1$, $B_{AG}=0$ and $\chi=-1$. On changing M_B/M_{BC}, we find in Fig. 6(a) that the left-hand-side of (3.2) takes the maximum 1.098 for $L_A=0.1$, 1.021 for $L_A=1$, and 1.003 for $L_A=10$. At the same time, α_C in Fig. 6(b) changes monotonically as predicted by (3.3), and the variation of α_C versus M_B/M_{BC} is remarkable for smaller values of L_A. Similar results can be obtained for other values of γ, L_B, B_{AW}, B_{AG} and χ, for which the left-hand-side of (3.2) can be evaluated within the range from 1 to about 1.1. In this sense, we can say that the Marangoni effect due to the product and that due to the solute are coupled so as to reinforce each other.

Let us discuss special cases of the eigenvalue relation (3.1). Recalling the results for $\chi=0$ given in § 3.2 (in which the eigenvalue relation for the solute is equivalent to that for the product obtained in § 3.1), and setting $L_B=1$ (for which note the replacement $L_A/L_B\rightarrow L_A$), we can write down (3.1) as $(M_P+M_B)=F_P(\alpha,\gamma,L_A,B_{AW},B_{AG},0)$. Then we can define an effective

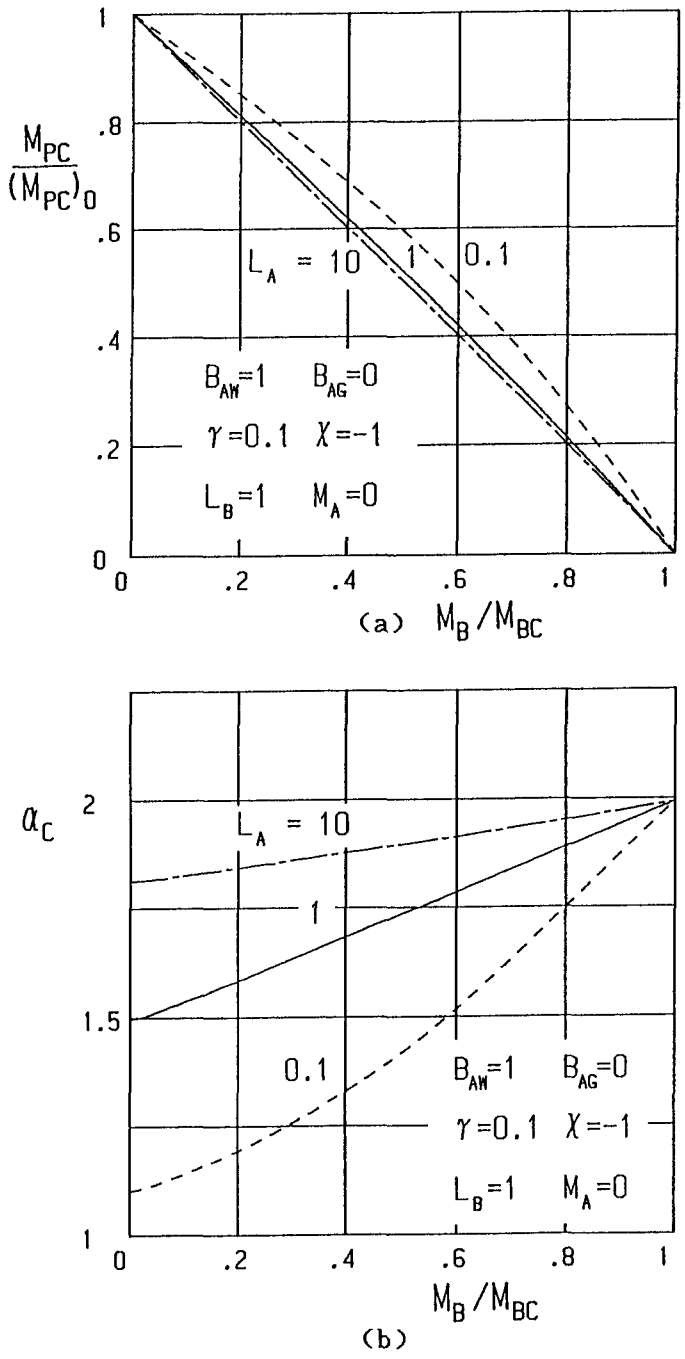

Fig. 6. Examples of the coupled Marangoni instability due to the product and the solute for typical values of L_A: (a) $M_{PC}/(M_{PC})_0$ versus M_B/M_{BC}, and (b) α_C versus M_B/M_{BC}.

Marangoni number as (M_P+M_B) whose critical value is given by $(M_P+M_B)_C=F_P(\alpha_C, \gamma, L_A, B_{AW}, B_{AG}, 0)$. This implies that, as both M_P and M_B are taken to be positive, the Marangoni instability easily occurs when the two Marangoni effects coexist: they reinforce each other even if individual Marangoni effect is weak. The discussion made here is also applicable to the limit of $\gamma \to \infty$, which leads to $(M_P+M_B)_C=79.61$ at $\alpha_C=1.993$ irrespective of L_A, L_B, B_{AW}, B_{AG} and χ.

§ 4. Effects of the Surface Deformation

Following the conjecture made in § 2, let us derive asymptotic forms of neutral stability curves for small wavenumbers. Expanding the solutions (2.40)-(2.44) and $b_1 \sim b_6$ about $\alpha=0$, we get the following expression for (2.35):

$$\frac{2}{3}\frac{\alpha^2}{N_C} = [M_P + L_B M_B(1+\chi)]E - L_B M_B \chi + L_A M_A Q + O(\alpha^2), \quad (4.1)$$

with

$$q = \frac{B_{AG}a^* + \gamma a}{B_{AG}a + \gamma a^*}, \quad (4.2a)$$

$$E = \beta_P \gamma^2 \left(1 - \frac{q}{a} - \frac{a^*}{a} q + \frac{q}{\gamma}\right), \quad (4.2b)$$

$$Q = \frac{a^*}{a} - q, \quad (4.2c)$$

where the term of $O(\alpha^2)$ in (4.1) consists of the terms of order α^2 multiplied by M_P, M_B or M_A and of the higher order terms; the

functions U(y), V(y) and W(y) in (2.42)-(2.44) can be discarded, since the magnitude of the surface deformation at small wavenumbers is much larger than that of the velocity (refer to (2.41)). Equation (4.1) thus implies the tangential stress balance at the deformed free surface for small wavenumbers. The function E given by (4.2b) is plotted against γ in Fig.7. We find that E depends upon B_{AW} and B_{AG} only for $\gamma \lesssim 5$ and its variation with respect to B_{AW} and B_{AG} appears most typically at $\gamma=0$: note that the value at $\gamma=0$ for $B_{AW}=0$ is given as E=2 for $0<B_{AG}$ and E=1 for $B_{AG}=0$, while that for $B_{AW}\to\infty$ and $B_{AG}=0$ as E=3. Then, E approaches unity in the limit of $\gamma\to\infty$, so that it is found that the values of E fall within $1\leqq E\leqq 3$ with changing γ, B_{AW} and B_{AG}. On the other hand, the function Q given by (4.2c) is shown in Fig.8. We find here that Q for $B_{AG}=0$ and $B_{AG}=1$ takes positive values for $B_{AW}\to\infty$, while negative values for $B_{AW}=0$. This means that Q changes its sign at a certain value of B_{AW}, for which the relation $B_{AW}=\gamma$, giving Q=0, is obtained from (4.2c) (see the curves for $B_{AW}=1$, which take negative values for $\gamma>B_{AW}$). Since Q vanishes for $\gamma>3$, it seems that the term L_AM_AQ in (4.1) may be dropped out for larger values of γ. For the other case given by $B_{AG}\to\infty$, Q is always zero, then the disturbance of gas concentration does not cause the Marangoni effect.

Using (4.1), asymptotic forms of the eigenvalues for three elementary problems can be written as

$$M_P = \frac{2}{3E}\frac{\alpha^2}{N_C} + O(\alpha^4), \tag{4.3}$$

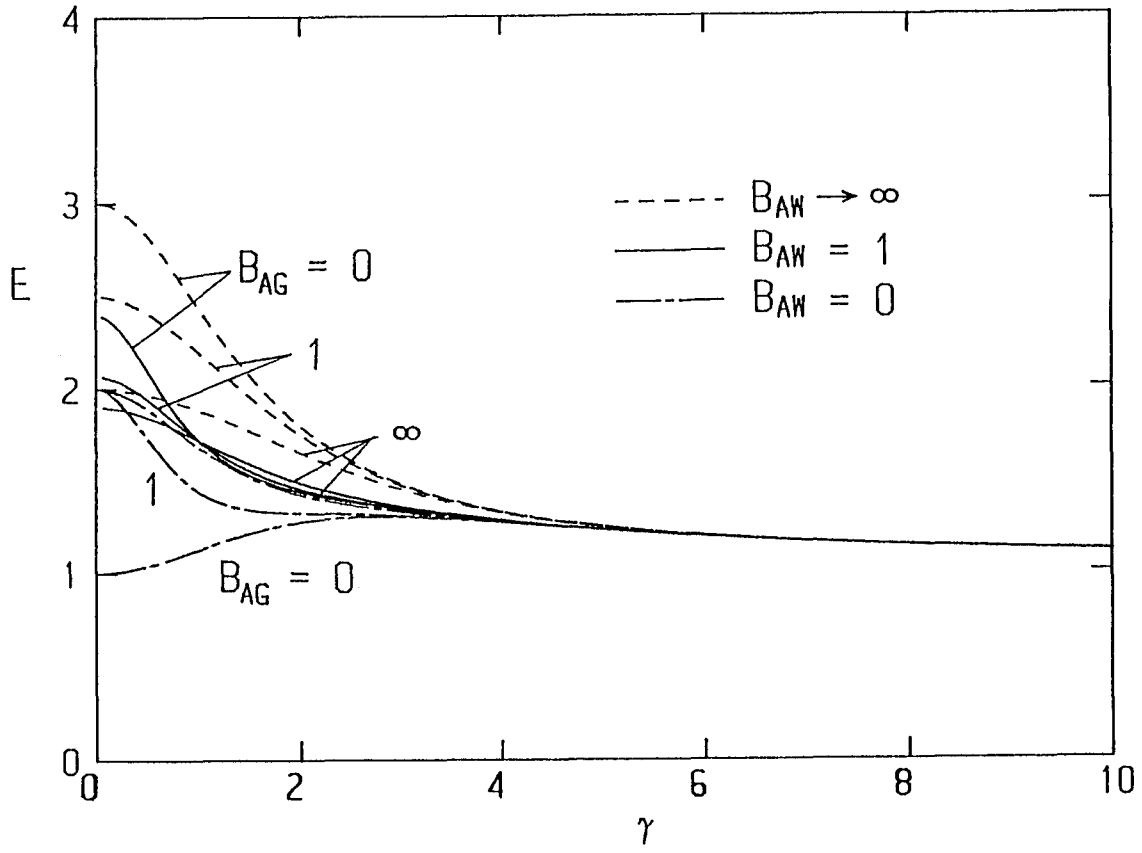

Fig. 7. The function E versus γ.

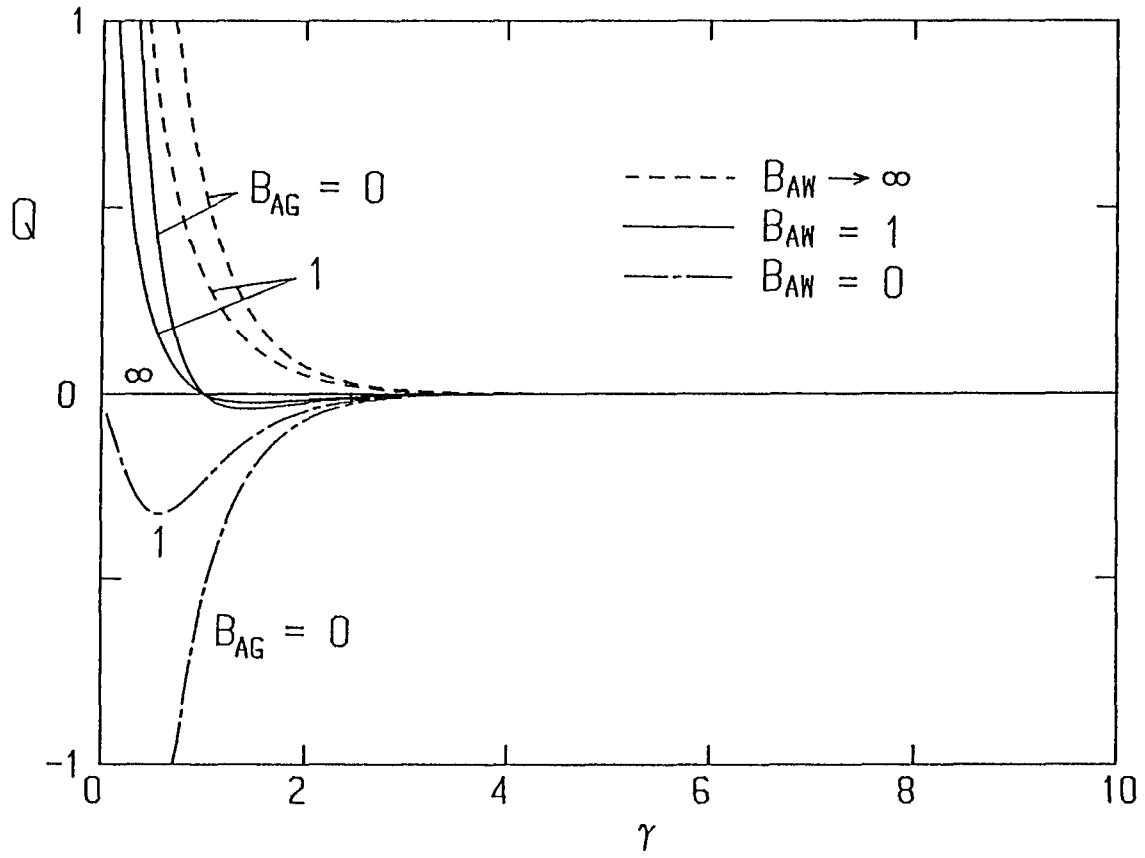

Fig. 8. The function Q versus γ.

$$M_B = \frac{2}{3}\,\frac{1}{(1+\chi)E-\chi}\,\frac{\alpha^2}{N_C} + O(\alpha^4), \qquad (4.4)^*$$

$$M_A = \frac{2}{3Q}\,\frac{\alpha^2}{N_C} + O(\alpha^4). \qquad (4.5)$$

In deriving (4.4) and (4.5), L_B and L_A in (4.1) are set to be unity by renormalizing the velocity, i.e., N_C is redefined.

---

* As for the case of $N_C=0$, the asymptotic form of M_B at small wavenumbers is expressed, for $\gamma >> 1$, as

$$M_B = \frac{80}{\alpha^2}, \qquad (4.6)$$

and, for $\gamma << 1$, as

$$M_B = \frac{560}{\alpha^2[(1+\chi)J-7\chi]}, \qquad (4.7)$$

with

$$J = \frac{1}{2B_{AW}+3}\left[\frac{L_B}{L_A}\,\frac{B_{AW}(53B_{AW}+11B_{AW}B_{AG}+25B_{AG}+105)}{3(B_{AG}+B_{AW}B_{AG}+B_{AW})} + 11B_{AW}+14\right]. \qquad (4.8)$$

When $\chi=-1$, (4.7) reduces to (4.6). If one makes replacement $M_B \to M_P$ and $L_A/L_B \to L_A$, (4.6) and (4.7) with $\chi=0$ give the asymptotic form of the eigenvalue discussed in § 3.1. In contrast to these, the asymptotic form for $\alpha >> 1$ is expressed as $M_B = 8\alpha^2$ irrespective of the parameters involved.

Equation (4.3) agrees, in the limit of $\gamma \to \infty$, with the asymptotic form obtained in refs. 9, 11 and 12. When $\chi=0$, the right-hand-side of (4.4) is equal to that of (4.3), while when $\chi=-1$, (4.4) agrees with (4.3) in the limit of $\gamma \to \infty$. We then notice that (4.4) is positive for $-1 \leqq \chi \leqq 0$ and is similar to (4.3). Therefore, it follows from (4.3) and (4.4) that effects of the surface deformation arise remarkably for the disturbances of small wavenumbers, and that the critical Marangoni number is always given in the limit of zero wavenumber. This makes a striking contrast to the results obtained for the flat free surface. To illustrate this result, the eigenvalue relation given by (2.46b) is plotted in the (α, M_B) plane of Fig. 9, in which the neutral stability curves for small wavenumbers are considerably affected by the surface deformation, as predicted just by the asymptotic form (4.4).

As noted above, M_A in (4.5) changes its sign, depending upon whether $Q>0$ or $Q<0$: note that (4.5) becomes invalid when $Q=0$. This means that when $Q>0$, the equation (4.5) leads also to the critical Marangoni number at zero wavenumber, while when $Q<0$, it leads to a negative critical value at a non-zero wavenumber. The latter result seems to be very interesting in contrast to the former one and the results obtained above for M_P and M_B, though the instability due to the gas may occur only for the special case given by $B_{AG}<\infty$ and $B_{AW}<\gamma \lesssim 3$.

Finally, let us consider the coupled Marangoni instability due to the product and the solute with effects of the surface

deformation. On setting $M_A=\chi=0$, the equation (4.1) yields $M_P+L_BM_B=0$ at $\alpha=0$, so that the state given by $M_P>0$ and $M_B>0$ is always unstable. For other cases of χ, similar results can be obtained.

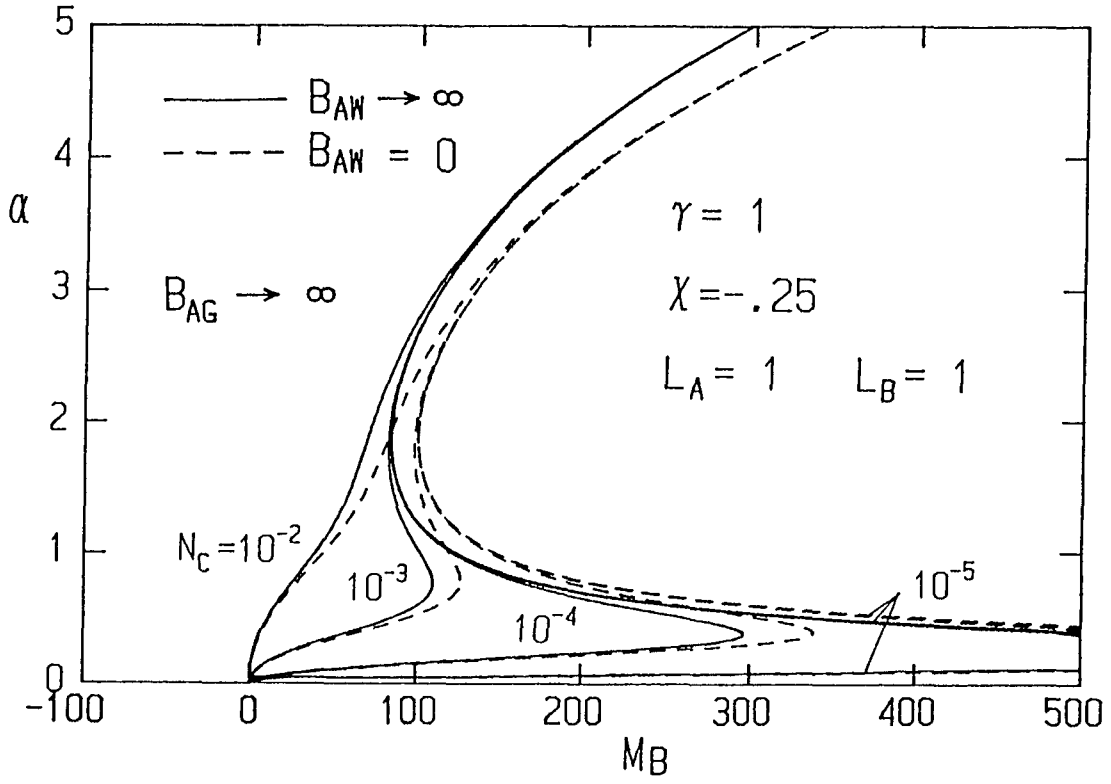

Fig. 9. Typical examples of the neutral stability curves of M_B with effects of the surface deformation.

Appendix

The functions U(y), V(y) and W(y) in (2.42)-(2.44) are expressed as follows:

$$U(y) = (\mathcal{L} - \gamma^2)^{-1}\left(f \frac{d\bar{C}_A}{dy}\right)$$

$$= \frac{1}{4a}\{[B_{AW}Y - \gamma y + (B_{AW} - \gamma b)\frac{\alpha+\gamma}{\alpha\gamma}]\sinh(\alpha+\gamma)y$$

$$- [B_{AW}Y + \gamma y - (B_{AW} + \gamma b)\frac{\alpha-\gamma}{\alpha\gamma}]\sinh(\alpha-\gamma)y$$

$$- [B_{AW}y - \gamma Y + (B_{AW}b - \gamma)\frac{\alpha+\gamma}{\alpha\gamma}]\cosh(\alpha+\gamma)y$$

$$+ [B_{AW}y + \gamma Y - (B_{AW}b + \gamma)\frac{\alpha-\gamma}{\alpha\gamma}]\cosh(\alpha-\gamma)y\}, \quad (A.1)$$

$$V(y) = \mathcal{L}^{-1}f$$

$$= \frac{y}{4}[\frac{3}{\alpha}\cosh\alpha y - y\sinh\alpha y + b(y\cosh\alpha y - \frac{1}{\alpha}\sinh\alpha y)], \quad (A.2)$$

$$W(y) = \mathcal{L}^{-1}\left(f \frac{d\bar{C}_A}{dy}\right)$$

$$= \frac{\alpha}{2a}\{[B_{AW}Y - \gamma y + (B_{AW} - \gamma b)\frac{2(\alpha+\gamma)}{\gamma^2 + 2\alpha\gamma}]\frac{\sinh(\alpha+\gamma)y}{\gamma+2\alpha}$$

$$+ [B_{AW}Y + \gamma y + (B_{AW} + \gamma b)\frac{2(\alpha-\gamma)}{\gamma^2 - 2\alpha\gamma}]\frac{\sinh(\alpha-\gamma)y}{\gamma-2\alpha}$$

$$- [B_{AW}y - \gamma Y + (B_{AW}b - \gamma)\frac{2(\alpha+\gamma)}{\gamma^2 + 2\alpha\gamma}]\frac{\cosh(\alpha+\gamma)y}{\gamma+2\alpha}$$

$$- [B_{AW}y + \gamma Y + (B_{AW}b + \gamma)\frac{2(\alpha-\gamma)}{\gamma^2 - 2\alpha\gamma}]\frac{\cosh(\alpha-\gamma)y}{\gamma - 2\alpha}), \tag{A.3}$$

with

$$b = \coth\alpha - \frac{1}{\alpha}, \quad \text{and} \quad Y = by + \frac{1}{\alpha}. \tag{A.4}$$

List of Principal Symbols

A, gas component;

B, solute component;

B_{AG}, B_{AW}, gas Biot number (transfer coefficient of gas), respectively, across free surface and plane wall;

C_A, gas concentration;

C_{AG}, a constant of gas concentration in gas phase;

C_{As}, equilibrium value of gas concentration at free surface;

C_B, solute concentration, a constant C_{B0} plus deviation C_{B1};

C_{B1s}, equilibrium value of solute concentration at free surface;

C_P, product concentration;

C_{Ps}, equilibrium value of product concentration at free surface;

D_A, D_B, D_P, diffusivity, respectively, of gas, solute, and product;

d, mean level of free surface (thickness of liquid layer);

F, eigenvalue relation; F_A, F_B, F_P, eigenvalue relation for each component (gas, solute, and product);

K, rate constant for a first order irreversible reaction;

k=k(T), rate constant of reaction as function of temperature;

k_{AG}, k_{AW}, transfer coefficient of gas, respectively, across free surface and plane wall;

k_{BG}, transfer coefficient of solute across free surface;

L_A, diffusivity ratio to gas;

L_B, diffusivity ratio to solute;

M_A, gas Marangoni number; its critical value, M_{AC};

M_B, solute Marangoni number; its critical value, M_{BC};

M_P, product Marangoni number; its critical value, M_{PC};

m, n, stoichiometric factors;

N_C, Crispation number;

n, unit normal vector;

P, product component;

P_r, Prandtl number;

p, pressure in liquid;

p_G, constant pressure of gas phase;

r, representative rate of production;

r_A, r_B, r_P, rate of production, respectively, for gas, solute, and product;

S, curvature of free surface;

T, temperature;

T_0, mean temperature of liquid;

$v=(v_1, v_2, v_3)$, velocity;

$x=(x_1, x_2, x_3)$, variables in Cartesian coordinates;

α, wavenumber; its critical value, α_C;

γ, reaction parameter;

ζ', free surface deformation;

μ, viscosity of liquid;

ν, kinematic viscosity of liquid;

ρ, density of liquid;

σ, surface tension coefficient; its constant value corresponding to a steady static state, σ_0;

$\tau_{i,j}$, viscous stress tensor;

χ, solute flux parameter;

References

1) T. K. Sherwood, R. L. Pigford and C. R. Wilke: Mass Transfer, (McGRAW-HILL, 1975) Chap. 5.

2) N. Imaishi and K. Fujinawa: Kagaku Kogaku Ronbunsyu (Collected Papers on Chemical Engineering) 4 (1978) 490 [in Japanese].

3) N. Imaishi: Dr. Thesis, Tohoku University, 1981 [in Japanese].

4) L. D. Landau and E. M. Lifshitz: Fluid Mechanics (Pergamon Press, London, 1966) Chapters 6 and 7.

5) T. Funada, M. Sakata and M. Nishide: Memoirs of the Wakayama Technical College (1980) Vol. 15, p. 7 [in Japanese].

6) M. Sakata and T. Funada: Memoirs of the Wakayama Technical College (1981) Vol. 16, p. 17 [in Japanese].

7) The Chemical Society of Japan, ed.: Kagaku Binran, Kiso-hen (Handbook of Chemistry, Fundamentals) (Maruzen, 1975) Chap. 6 [in Japanese].

8) J. R. A. Pearson: J. Fluid Mech. 4 (1958) 489.

9) M. Takashima: J. Phys. Soc. Jpn. 50 (1981) 2745.

10) C. V. Sternling and L. E. Scriven: AIChE J. 5 (1959) 514.

11) L. E. Scriven and C. V. Sternling: J. Fluid Mech. 19 (1964) 321.

12) K. A. Smith: J. Fluid Mech. 24 (1966) 401.

Acknowledgments

The author would like to express his hearty thanks to Professor T. Kakutani for his invaluable comments, kind inspection of the manuscript and continuous encouragements throughout this study. The author would like to extend his gratitude to Professor R. Ito, Professor H. Yosinobu and Professor T. Yoshikawa for their useful comments on this thesis.

The author's thanks are also due to Professor M. Ohji for his encouragements, and to the staff of Wakayama National College of Technology for their supports to achieve the present study.